UNIVERSITY OF CALIFORNIA
RIVERSIDE

Study of Heterogeneity in Multi-Site Functional Connectivity Analysis of Psychiatric Disorders

A Dissertation submitted in partial satisfaction
of the requirements for the degree of

Doctor of Philosophy

in

Bioengineering

by

Alexandra Reardon

June 2021

Dissertation Committee:
Dr. Xiaoping Hu, Chairperson
Dr. Megan Peters
Dr. Katherine Stavropoulos

The Dissertation of Alexandra Reardon is approved:

Committee Chairperson

University of California, Riverside

Acknowledgements

I would like to thank my PI, Dr. Xiaoping Hu for the opportunity to perform research in his lab. I am deeply grateful for his insights, guidance and support throughout the years. Additionally, I would like to express gratitude to my committee members, Dr. Peters and Dr. Stavropoulos for their time and feedback.

A special thanks to Kaiming Li, for his guidance, support, and insights on my research projects throughout the years. I would also like to thank Jason Langley for always being willing to provide help and feedback. And to Jerry Chen for technical support and guidance. I have enjoyed working with all of you and you were invaluable in the making of this dissertation.

Thank you to the members of Dr. Hu's lab whom it was enjoyable to work alongside: Sana Hussein, Abby Barlow, Kaiqing Chen, Lebo Wang, and Zhenhai Zhang. Finally, a special thanks to my friends and family for their support and encouragement.

To my parents. Thank you.

ABSTRACT OF THE DISSERTATION

Study of Heterogeneity in Multi-Site Functional Connectivity Analysis of Psychiatric Disorders

by

Alexandra Reardon

Doctor of Philosophy, Graduate Program in Bioengineering
University of California, Riverside, June 2021
Dr. Xiaoping Hu, Chairperson

Autism Spectrum Disorder (ASD) is a highly heterogeneous developmental disorder with diverse clinical manifestations. Neuroimaging studies have explored functional connectivity (FC) of ASD through resting-state functional MRI (fMRI) studies, however findings have remained inconsistent, thus reflecting the possibility of multiple subtypes. The Autism Brain Imaging Data Exchange (ABIDE) contains neuroimaging data from more than 17 international scanning sites and has become a useful tool in studying the brain-behavior relationships of ASD. However multi-site databases impose site effects that confound FC due to the use of different scanning hardware, models, and parameters. Although there are established methods to mitigate site effects, these strategies often result in reduced effect size in FC features known to be affected in diseased populations.

In this work, we propose a site-wise de-meaning (SWD) strategy in multi-site FC analysis of fMRI and evaluate the performance against two common site effect mitigation methods (Generalized Linear Model and ComBat Harmonization). These methods were tested on two multi-site psychiatric consortium: ABIDE and Bipolar and Schizophrenia Network on Intermediate Phenotypes. Preservation of consistent FC alterations in patients

were evaluated for each method through the calculation of effect size (Hedge's g) between patients and controls. The SWD method demonstrated superior performance in preserving the effect size in FC features associated with neurodevelopmental and psychiatric disorders compared to the original data and commonly used methods. We then aim to identify the relationships between clinical symptoms and FC measures to help clarify the inconsistencies in earlier findings and advance our understanding of ASD subtypes. Canonical correlation analysis was performed on two-hundred and ten ASD subjects from ABIDE to identify significant linear combinations of resting-state connectomic and clinical profiles of ASD. Then, hierarchical clustering defined three ASD subtypes based on distinct brain-behavior relationships.

Overall, we reduce heterogeneity in multi-site fMRI databases and elucidate the heterogeneity of ASD clinical manifestations and connectomic profiles. The reduction of site effects and preservation of FC associated with disorders can lead to a better understanding of brain connectivity in diseased populations, and identification of distinct ASD subtypes may lead to better targeted therapies for individuals.

Contents

List of Figures

List of Tables

Chapter 1

Background and Significance

1.1 Overview

Functional Magnetic Resonance Imaging (fMRI) is a prominent tool used to study the brain non-invasively. FMRI measures the blood oxygen level dependent (BOLD) signal, which is an indirect measure of neural activity in the brain (Logothetis et al., 2004). Resting-state fMRI, which measures the functional architecture of the brain at rest, has been used to increase understanding of neural changes in many disease states, predict clinical symptoms, detect neuromarkers in various patient populations, predict control versus patient groups, and predict treatment response (Van Horn et al., 2009; Yang et al., 2020).

Resting-state fMRI has been used extensively to study both neurodevelopmental disorders and psychiatric disorders, such as Autism Spectrum Disorder (ASD), and Schizophrenia (SZ). ASD and SZ affect about 1.85% and 1% of the population

respectively (Kahn et al., 2015; Maenner et al., 2020). These disorders are clinically heterogeneous and can manifest themselves in many different ways in individuals. Large-scale resting-state fMRI consortiums, such as the Autism Brain Imaging Data Exchange (ABIDE), and the Bipolar and Schizophrenia Network on Intermediate Phenotypes (B-SNIP), have been created to study the brain in patients with these disorders (Di Martino et al., 2014; Tamminga et al., 2013). These databases have elucidated how the functional connectivity (FC), or BOLD signal correlation in spatially distinct regions of the brain, is associated with clinical symptoms; however inconsistent results have been found across studies (see Hull et al., 2016). While there is heterogeneity associated with the FC findings and clinical manifestations of these disorders, there is also heterogeneity imposed by multi-site databases which are known to introduce site-effects due to the use of different scan parameters, protocols, and MRI models (An et al., 2017; Birn et al., 2013; Newton et al., 2012). In this dissertation we (1) propose a site-wise de-meaning algorithm to reduce site-effects in multi-site FC analysis and evaluate it alongside current methods (2) correlate symptoms of ASD with FC findings to define three subtypes of ASD, thus proposing distinct connectomic profiles that are associated with different clinical manifestations of the disorder.

1.2 ASD: Background

ASD is a common neurodevelopmental disorder characterized by social and communication deficits and restricted and repetitive behaviors (RRBs) (American Psychiatric, 2013). ASD affects approximately 1 in 59 individuals and has increased in

prevalence by 15% since 2014 (Baio et al., 2018). ASD is diagnosed according to the Diagnostic and Statistical Manual for Mental Health Disorders, 5th edition; Persistent social interaction and communication deficits and RRBs must be present for an ASD diagnosis (American Psychiatric, 2013). Social communication impairment include deficits in nonverbal communication behaviors such as abnormalities in eye contact and body language, misunderstanding gestures or facial expressions, and a lack or minimal use of facial expressions. ASD patients often have difficulty understanding social-emotional reciprocity, difficulty holding a conversation, and failure to initiate or respond to social interactions. Individuals with ASD often have minimal social relationships and difficulties working with peers in a school or work environment. RRBs include but are not limited to repetitive motor movements, insistence on sameness, and highly restricted interests. This can include difficulty deviating from routine, wanting to wear the same clothes every day, and fixation on certain topics of interest. Common examples of repetitive movements are body rocking, teeth grinding, and hand flapping (Lewis et al., 2009). These are often a form of self-soothing behavior, however can sometimes range to self-injurious behaviors such as head banging or self-biting.

Another common symptom of ASD is hypersensitivity to sensory input such as sound, textures, or visual stimuli (American Psychiatric, 2013). This can cause extreme discomfort and sensitivity to stimuli such as loud noises, bright lights, and certain fabrics. There are also a wide range of cognitive abilities exhibited in ASD; While intellectual disabilities (generally considered to be an IQ score of below 70) affect approximately 1% of the general population, 38% of individuals with ASD also have an intellectual disability,

24% of individuals were considered to be on the borderline range in terms of intellectual ability, and 38% were considered to be average or above average (Baio, 2012). Neuropsychological tests used to test cognitive processes in ASD as compared to healthy controls (HCs) have reported deficits in planning, selective inhibitory impairment, the inability to generate ideas and behaviors spontaneously, and impairments with cognitive flexibility (Poljac et al., 2012)

There are multiple symptoms associated with ASD and the severity of any of these symptoms can vary from requiring support to requiring substantial support. In order to receive an ASD diagnosis the symptoms exhibited must not be better explained by an intellectual disability. ASD is generally considered to vary on a spectrum of symptom severity, however it is highly heterogeneous in its clinical symptoms and can manifest itself in various different ways in different in people.

ASD is often comorbid with a number of other psychiatric disorders such as epilepsy, depression, anxiety, attention deficit/hyperactivity disorder (ADHD), bipolar disorder, intellectual disabilities, and gastrointestinal disorders (Mohammadi et al., 2019). ASD co-occurs with one or more other developmental disorder in more than 70% of people according to diagnostic interviews (Stadnick et al., 2017). The most common comorbidities are intellectual disabilities, ADHD, and epilepsy (Supekar et al., 2017). The extreme biological and clinical heterogeneity, as well as the common comorbidities that have the potential to mask ASD makes it a very difficult disorder to diagnose. There is no definitive laboratory test or objective diagnostic biomarker to diagnose ASD, but rather a medical professional looks at the patient's developmental history and conducts a structured

assessment to look for signs and symptoms of ASD. The Autism Diagnostic Observation Schedule (ADOS), and Autism Diagnostic Interview-Revised (ADI-R) are considered to be the gold standard ASD assessment measures due to their highest sensitivity and specificity (Falkmer et al., 2013). In the ADOS assessment, a trained clinician observes the participant during a series of semi-structured or structured tasks to assess symptoms relevant to ASD (Reaven et al., 2008). In the ADI-R assessment, the individual in question is not involved, but rather a trained clinician interviews the individual's parents or caregivers to assess developmental history and clinical signs of ASD (Reaven et al., 2008). A combination of both ADOS and ADI-R resulted in a diagnostic accuracy of 80.8% for ASD (Falkmer et al., 2013).

1.3 Theories of ASD

While the cause of ASD is unknown, there are several theoretical risk factors. Boys are four times more likely to be diagnosed with ASD than girls (Maenner et al., 2020). There is evidence that ASD is genetic; twin studies estimate the heritability of ASD to be between 64% and 91% (Tick et al., 2016). Advanced maternal and paternal age have also been known to increase the risk of ASD diagnosis by 38% and 22% respectively (Ratajczak, 2011). Certain medications used during pregnancy, especially Valproic acid which is used to treat epilepsy, has resulted in an increase in the child's risk of ASD (Ratajczak, 2011). Environmental and diet factors have also been shown to increase the risk of ASD; exposure to high levels of mercury increases the rate of ASD by 61%, and nutritional deficiencies can lead to changes in neuronal function that can have detrimental

effects on learning and behavior (Ratajczak, 2011). While there is no known cure for ASD, certain medications and therapies can reduce the severity of symptoms. The most effective biological therapies with proven benefits are Risperidone, an antipsychotic for treating disruptive behaviors, and Aripiprazole, an antipsychotic with benefits for improving the irritability associated with symptoms of ASD (Medavarapu et al., 2019). Studies have found that these medications significantly reduce symptoms of hyperactivity, disruptive behaviors, stereotyped behavior, and irritability in those with ASD. However, there are potential adverse effects of these medications which include but are not limited to weight gain, fatigue, and vomiting. Behavioral therapies such as Applied Behavioral Analysis, Discrete Trail Training, and Verbal Behavioral Intervention, have been shown to have proven benefits in reducing the severity of symptoms in ASD (Medavarapu et al., 2019). These therapies teach appropriate behaviors, adaptive behaviors, and verbal and communication skills.

There are several other theories of ASD such as the dopamine hypothesis, the empathizing-systemizing theory, and the theory of mind hypothesis. The dopamine hypothesis suggests that ASD traits arise from aberrant midbrain dopaminergic signaling (Pavăl, 2017). The midbrain dopaminergic system includes the mesocorticolimbic (MCL) circuit and the nigrostriatal (NS) circuit. The MCL is implicated in behaviors related to reward and motivation, while the NS is involved in goal-directed behavior (Chevallier et al., 2012; Haber, 2014). It is therefore believed that MCL dysfunction in ASD results in reduced social interactions and experiences, as social interactions are not perceived as rewarding. Therefore, ASD individuals are less likely to seek out social interactions, which

can lead to underdeveloped social skills and abilities. It is also believed that the dopamine hypothesis results in RRBs of ASD because the NS circuit regulates stereotyped behaviors, and a dysfunction in this circuit could lead to cycles of repeated behaviors (Lewis et al., 2009). The empathizing-systemizing theory of ASD hypothesizes that features of ASD lie on a dimension of empathizing and systemizing (Baron-Cohen, 2002). It is believed that the social and communication impairments of ASD can be explained by a lower ability to empathize (Baron-Cohen et al., 1999; Baron-Cohen et al., 2001a), while RRBs of ASD can be explained by a high ability to systemize (Baron-Cohen et al., 2001b; Jolliffe et al., 1997).

The theory of mind hypothesis posits that individuals with ASD are unable to infer the emotions or intentions of others, therefore affecting the ability to interact in conventional ways in social settings (Brewer et al., 2017). Theory of mind is often studied using the false-belief task, which is a test that determines if a child is able to differentiate between thoughts that they have, with those others might have (Brewer et al., 2017). Social understanding and theory of mind is also investigated using cartoon animation mental states test, and inferences of mental states using photographs. In all of these assessments, those with ASD have been shown to perform significantly worse than controls (Baron-Cohen et al., 1997; Castelli et al., 2002). While there are clear clinical differences between those HCs and those with ASD, the exact mechanism underlying these symptoms remains unknown.

1.4 Neuroimaging of ASD: Structural MRI and Diffusion Tensor Imaging

Neuroimaging studies have allowed new insights into neuroanatomy and physiology in ASD in recent decades. MRI is beneficial to allow for the underlying brain structure and function to be studied non-invasively, in-vivo, with high contrast sensitivity, high spatial resolution, and without radiation exposure (Chen et al., 2011). Structural MRI studies have investigated the differences in brain morphology between ASD and HC individuals for the past 20 years (Chen et al., 2011). It has been found that children with ASD demonstrate 5-10% abnormal enlargement in grey-matter and white-matter brain volumes compared to HCs (Amaral et al., 2008; Courchesne et al., 2001; Sparks et al., 2002). Egaas et al., found that juveniles with ASD tend to have significantly smaller average size of the corpus callosum than HCs (Egaas et al., 1995), while increased amygdala volumes in children with ASD have been reported (Schumann et al., 2004; Sparks et al., 2002). Longitudinal MRI studies have discovered abnormal brain growth trajectory in ASD as compared to HCs (Schumann et al., 2010). More specifically, the cerebrum in children with ASD has been found to be enlarged by 2.5 years of age, while significant decreases have been observed over time in gray matter volume and cortical thickness over time compared to HCs (Hardan et al., 2009).

Diffusion Tensor Imaging (DTI) is another neuroimaging technique that assesses white matter tract integrity by quantifying water diffusion in voxels (Feldman et al., 2010). Water diffusion is typically measured through fractional anisotropy (FA), which measures the degree of diffusion through white matter tracts (Feldman et al., 2010). Studies have reported decreased FA in ASD compared to HCs in the corpus callosum (Alexander et al.,

2007), frontal lobe short range fibers, and brain regions implicated in theory of mind tasks (Barnea-Goraly et al., 2004). This reduced FA in ASD compared to HCs suggests abnormalities in the microstructure of these regions, such as aberrant myelination, axonal number, diameter, and orientation (Beaulieu, 2002).

1.5 Neuroimaging of ASD: Task-fMRI

Task-fMRI examines the regions that are functionally involved during certain tasks. The functional activation of ASD vs HCs in task-fMRI has been explored through theory of mind tasks, false-belief tasks, and semantic processing (Harris et al., 2006; Just et al., 2004; Kana et al., 2015; Knaus et al., 2008; Nijhof et al., 2018). A theory of mind task-fMRI in which participants watched a video of two "interacting" shapes identified hypoconnectivity in ASD in frontal and posterior regions of interest (ROIs) compared to HCs (Kana et al., 2015). A false-belief task in which participants watched a video of various instances of false-beliefs, observed less activation in ASD in the right anterior middle temporal pole, which is a region that has been implicated in social cognition, emotion recognition, and mentalizing (Nijhof et al., 2018). Semantic processing tasks have reported mixed results, with some studies finding reduced activation in Broca's area (Harris et al., 2006; Just et al., 2004; Kana et al., 2015), an area involved in semantic encoding and retrieval (Blumenfeld et al., 2006), and Knaus et al. reporting increased activation in Broca's area during a semantic processing task (Knaus et al., 2008). The mixed results reported in this area could be due to studies involving different ages of participants; the studies that reported reduced activation involved adults, while the study that reported

increased activation involved adolescents (Knaus et al., 2008). The aberrant activation during these theory of mind, false-belief, and semantic processing tasks could underlie the social cognition, mentalizing, and communication difficulties experienced by those with ASD.

The cortical underconnectivity hypothesis of ASD theorizes that impairments in communication, language, attention and social interactions may arise from decreased connectivity in functionally distinct brain regions (Belmonte et al., 2004; Just et al., 2004; Just et al., 2012). This lower synchronization was reported in frontal and posterior brain regions in ASD in a language comprehension task (Just et al., 2004), visuospatial cognition task (Damarla et al., 2010), theory of mind (Kana et al., 2015; Mason et al., 2008; Mizuno et al., 2011), deictic shifting (Mizuno et al., 2011), inhibition control (Kana et al., 2007), and sentence comprehension (Kana et al., 2006). It is believed that the decreased activation observed in ASD between these long-range cortical areas during tasks involved in language, cognition, and theory of mind, result in the communication, social, and cognitive deficits commonly observed in ASD (Just et al., 2012).

1.6 Neuroimaging of ASD: Resting-State fMRI

Resting-state fMRI measures the modulations in BOLD signal over time while the participant is “at rest”, meaning they are instructed to either close their eyes or stare at a fixation cross and not think about anything in particular (O'Connor et al., 2019). This allows the spatial and temporal activity of neural systems in the brain to be monitored across multiple resting state networks rapidly and non-invasively (O'Connor et al., 2019).

Resting-state fMRI is advantageous over task-fMRI in that data acquisition is less complex, and can be performed on those unable to participate in a task-fMRI, such as in infants/toddlers, sedated, paralyzed, or cognitively impaired patients (O'Connor et al., 2019). Several studies have investigated resting-state FC in participants with ASD as compared with HCs, however inconsistent and mixed results are frequently reported (Doyle-Thomas et al., 2015; Hull et al., 2016; Monk et al., 2009; Washington et al., 2014).

Many resting-state fMRI studies support the hypoconnectivity theory of ASD (see Hull et al., 2016). The Default Mode Network (DMN) is the most commonly implicated resting state network in ASD, and is the network that is active while a person is awake and alert, however it is not active during goal-oriented behavior (Broyd et al., 2009). The DMN consists of both frontal and posterior brain regions including the posterior cingulate cortex, precuneus, medial prefrontal cortex, and parietal cortex (Broyd et al., 2009). Hypoconnectivity in the DMN has been widely reported in ASD, particularly between frontal regions and posterior parietal regions of the DMN (Assaf et al., 2010; Cherkassky et al., 2006; Jung et al., 2014; Kennedy et al., 2008; Kennedy et al., 2006; Starck et al., 2013; Weng et al., 2010; Wiggins et al., 2011). Multiple studies have also reported that the degree of this DMN hypoconnectivity is correlated with the severity of social impairments (Assaf et al., 2010; Weng et al., 2010). Hypoconnectivity has also been reported in other networks in ASD such as between the salience network (insula), and the medial temporal lobe network (von dem Hagen et al., 2013; Ypma et al., 2016), and also in limbic-related regions (Gotts et al., 2012).

While hypoconnectivity has been widely reported in ASD, a number of resting-state fMRI studies also report hyperconnectivity in ASD (see Hull et al., 2016). Hyperconnectivity has been reported between the striatum and the right superior temporal gyrus, insular cortex, and pons, as well as between the pons and insular cortex in ASD (Di Martino et al., 2011). Increased connectivity has also been reported in frontostriatal connections (Delmonte et al., 2013), in the primary motor cortex (Nebel et al., 2014), and between the right posterior temporoparietal junction and the right ventral occipital-temporal cortex (Chien et al., 2015). Hyperconnectivity between primary sensory and subcortical networks has been associated with overall ASD symptom severity (Cerliani et al., 2015). Increased connectivity within the DMN has also been reported (Anderson, 2014; Redcay et al., 2013).

Some studies have also reported both increased and decreased connectivity of the DMN in ASD (Doyle-Thomas et al., 2015; Monk et al., 2009; Washington et al., 2014). For example, Monk et al. found hyperconnectivity between the posterior cingulate cortex and temporal lobes and right parahippocampal gyrus, and hypoconnectivity between the posterior cingulate cortex and superior frontal gyrus in ASD (Monk et al., 2009). The hypoconnectivity of posterior cingulate cortex and temporal lobe was associated with social impairments, while the hyperconnectivity of the posterior cingulate cortex and right parahippocampal gyrus was correlated with more severe RRBs (Monk et al., 2009). Washington et al. reported global hypoconnectivity and local hyperconnectivity within the DMN (Washington et al., 2014), while Doyle-Thomas et al. reported both hyperconnectivity and hypoconnectivity of the posterior cingulate cortex and other regions

of the DMN (Doyle-Thomas et al., 2015). The inconsistencies in the literature in fMRI findings could be a result of the variability of clinical and functional manifestations in ASD.

1.7 Subtypes of ASD

The heterogeneous nature of ASD, in terms of clinical symptoms, severity and inconsistent FC findings points to the possibility of multiple subtypes of ASD. Multiple studies have investigated the possibility of subtypes in ASD, however they defined subtypes based on different facets of ASD and have led to inconsistent numbers and definitions of subtypes (Easson et al., 2019; Feczko et al., 2018; Georgiades et al., 2013; Hong et al., 2018; Hrdlicka et al., 2005). Georgiades et al. used factor analysis to define three subtypes of ASD based on social communication defects and RRBs (Georgiades et al., 2013). Feczko et al. defined three ASD subtypes based on seven cognitive domains: spatial working memory, response inhibition, temporal discounting of reward, attentional vigilance, facial recognition, facial affect processing, and vocal affect processing (Feczko et al., 2018). Hong et al. defined three subtypes of ASD based on neuroanatomical profiles and found that the subtypes differed in cortical thickness, intensity contrast, cortical surface area, and geodesic stances between two points (Hong et al., 2018). Hrdlicka et al. also defined three subtypes of ASD based on structural MRI and found that subtypes differed in terms of size of substructures of the corpus callosum, amygdala, hippocampus, and caudate nucleus (Hrdlicka et al., 2005). Easson et al. defined two ASD subtypes based on resting-state fMRI and found that one subtype was defined by increased within network

connectivity and decreased between network connectivity, while the other was defined by decreased within network connectivity and increased between network connectivity (Easson et al., 2019). Furthermore, clinical symptom patterns were investigated between these two subtypes, however the subtypes did not differ in clinical symptoms or severity. The recent work that subtyped ASD based on resting state FC and their clinical profiles treated the two dimensions independently (Easson et al., 2019). However, current literature has shown that FC profiles and ASD symptoms co-occur (Assaf et al., 2010; Cerliani et al., 2015; Lynch et al., 2013; Monk et al., 2009). In order to subtype ASD, a large amount of ASD data must be utilized in order to capture the heterogeneity of the disorder. Data sharing initiatives such as ABIDE allow for the study and subtyping of ASD by aggregating phenotypic, clinical and neuroimaging data.

1.8 ABIDE

Multi-site consortiums are becoming increasingly common for psychiatric and developmental disorders; they increase statistical power, allow for geographic variability, capture a wide scope of symptoms, behaviors and neuromarkers that are present in such disorders (Lombardo et al., 2019; Van Horn et al., 2009). Pooled multi-site neuroimaging databases exist for ADHD (ADHD-200), SZ (SchizConnect, B-SNIP), Bipolar Disorder (B-SNIP), Major Depressive Disorder (SRPBS Multisite Disorder Database), and ASD (ABIDE). The ABIDE I is a consortium of neuroimaging data acquired from 17 international sites and contains structural MRI data, resting-state fMRI data, DTI data, clinical assessments, and phenotypic information of 539 ASD subjects and 573 age-

matched healthy controls between the ages of 6 and 64 years old (Di Martino et al., 2014). Although these big databases are beneficial for studying large sample sizes of patients, there are also several limitations in using multi-site consortiums.

ABIDE data are highly heterogeneous in terms of both clinical and imaging features. On the clinical side, there are different trained professionals gathering clinical information at each site, different clinical assessments used (i.e. ADOS, ADI-R, Vineland Adaptive Behavioral Scale), and different cut-off Full-Scale IQ scores. IQs were measured with various different classification scales and versions of each scale at each site. Additionally, different sample sizes were obtained at each site, and each site used individuals of different ages.

In terms of imaging heterogeneity, the data was acquired with different MRI scanner vendors, different scanner models, different imaging parameters (i.e. repetition time (TR), echo time (TE), voxel size, and acquisition time), and different sample sizes across sites. Differing imaging parameters and scanner vendors have been known to have an effect on scan reliability and resting-state results (An et al., 2017; Badhwar et al., 2019; Birn et al., 2013; Jahanian et al., 2019; Newton et al., 2012; Noble et al., 2017). This variability across sites could result in erroneous imaging markers and decrease the power to detect changes in the brain related to ASD (Yu et al., 2018).

1.9 Effects of Parameters on Resting-State fMRI Data

Acquisition time, voxel size, TR, and TE are all scanning parameters that are known to have an effect on resting-state fMRI (Birn et al., 2013; Huotari et al., 2019; Jahanian et

al., 2019; Noble et al., 2017; Rane et al., 2014; White et al., 2014). Noble et al. reported that a five minute resting-state scan results in poor test-retest reliability of whole brain connectivity (Noble et al., 2017). Birn et al. determined that increasing resting state fMRI scans from 5 to 13 minutes greatly improved the test-retest reliability (Birn et al., 2013). However, White et al. reported that at 5-and-a-half-minute scan lengths, component group maps of brain networks stabilized in school-aged children (White et al., 2014). Additionally, increasing TR led to drastic scan time reductions which enables more widespread use of fMRI studies in clinical practices (Jahanian et al., 2019). Newton et al. reported that decreasing voxel size dimensions increased FC correlations in resting state scan (Newton et al., 2012), while Rane et al. determined that a short TE of 15ms correlated less with group level results than scans acquired at a higher TE of 35ms (Rane et al., 2014).

Other factors such as preprocessing pipelines, technical imaging approaches, temporal SNR, scanner manufacturer, and head motion can also affect resting-state fMRI results (An et al., 2017; Aurich et al., 2015; Borchardt et al., 2016; Braun et al., 2012; DeDora et al., 2016; Gargouri et al., 2018; Huotari et al., 2019; Liang et al., 2012; Satterthwaite et al., 2012; Wu et al., 2011). Different preprocessing strategies are known to significantly change graph theoretical measurements (Aurich et al., 2015), smoothing has been found to increase FC estimates (Wu et al., 2011), slice timing applied at a TR of 2s has been found to significantly increase amplitude of low frequency fluctuations (Wu et al., 2011), and filtering has been shown to improve local information transfer among nodes (i.e. local efficiency) (Aurich et al., 2015; Borchardt et al., 2016; Braun et al., 2012; Gargouri et al., 2018; Liang et al., 2012). Huotari et al. determined that different spin

acquisition approaches yield different connectivity results (Huotari et al., 2019). Temporal SNR, which is a measure of timeseries signal stability, was found to be inversely correlated with the degree to which an fMRI accurately captures true BOLD fluctuation (DeDora et al., 2016). Studies have found that scanners manufactured by Siemens were associated with higher consistency than Philips (An et al., 2017; Badhwar et al., 2019). In addition, individual subject in-scanner head motion has also been found to affect FC measures (Satterthwaite et al., 2012; Van Dijk et al., 2012); Head motion was found to increase within-network connectivity in specific seed based brain networks, and increase correlation for nodes that are closer together but diminished connectivity of voxels that are farther apart (Satterthwaite et al., 2012; Van Dijk et al., 2012). There are many confounding factors associated with multi-site pooling in neuroimaging data, however this limitation can be overcome by harmonizing multi-site consortiums to increase comparability when using multi-site data.

1.10 Multi-Site Harmonization: Previous Work

Multi-site harmonization has been performed using three main methods: (1) A travelling-subject dataset to remove measurement bias associated with different sites (Yamashita et al., 2019), (2) Generalized linear model (GLM) harmonization to adjust FC values for site differences (Rao et al., 2017), and (3) Combining Batches (ComBat) Harmonization. ComBat was originally used to correct for batch effects in genomic studies but has been extended for structural MRI harmonization and resting-state fMRI harmonization (Fortin et al., 2018; Johnson et al., 2007; Yu et al., 2018). In the travelling-

subject study, they utilized a cohort of subjects that travelled to each site and received resting-state scans and quantified the sampling bias and engineering measurement bias (Yamashita et al., 2019). This harmonization technique removed only the measurement bias from FC measures which improved signal-to-noise ratios by 40% and reduced measurement bias by 29% (Yamashita et al., 2019). However, utilizing a travelling-cohort is costly, time consuming, and was not used at many established multi-site consortiums (i.e., ABIDE and B-SNIP), and therefore a post-collection harmonization technique is necessary.

GLM and ComBat report the ability to harmonize multi-site neuroimaging data on resting state data post-acquisition (Rao et al., 2017; Yu et al., 2018). GLM harmonization has been used to adjust FC values for site differences, however this method results in decreased effect size in FC features known to be affected in diseased populations (Rao et al., 2017). ComBat extends the GLM method by using site-specific scaling factors and an empirical Bayesian criteria to improve the estimation of site parameters (Yu et al., 2018). This was able to successfully remove site effects on a total of 240 subjects that were scanned on one of four different scanners with homogenized scanning parameters. However it is unclear if ComBat harmonized fMRI data preserves the functional brain networks associated with psychological disorders (Yu et al., 2018). Also, it has yet to be determined if this method accurately accounts for FC effects imposed by inhomogeneous scanning parameters.

ASD is heterogeneous in terms of clinical manifestations and neuroimaging findings. While the ABIDE data are useful in studying large sample sizes of ASD, this

multi-site consortium further contributes to heterogeneity in studying ASD. It is therefore crucial to explore the individual variability of ASD as well as the variability imposed by multi-site disorder databases in making this disorder, as well as many others, less elusive.

1.11 Overview of Studies

ASD is a heterogeneous disorder both in terms of clinical and FC variability. This variability could arise from individual manifestation of ASD in different patients, along with different site and scanning factors. We aim to address heterogeneity in multi-site databases by mitigating site-effects in multi-site imaging databases while preserving the functional networks associated with neurodevelopmental and psychiatric disorders. We aim to address heterogeneity within ASD by subtyping ASD based on brain-behavior relationships.

In the first study, we propose a site-wise demeaning (SWD) strategy and evaluate it along with two common site-effect mitigation methods (GLM, and ComBat) by comparing the effect size of consistent FC alterations in group analysis (ASD vs controls, and SZ vs controls) in literature. We first establish the consistent FC differences between case groups and control groups in literature, then apply site-effect mitigation methods (GLM, ComBat, SWD) to multi-site FC data, and finally compare the effect size of established FC findings of the three site-effect mitigation methods.

In the second study, we used 210 ASD participants from ABIDE to define three ASD subtypes. Canonical correlation analysis was used to correlate linear combinations of FC features with linear combinations of clinical features, which were used as the

dimensions for subtyping. Hierarchical clustering was then used to identify three distinct subtypes of ASD. The subtypes differed significantly in terms of clinical and FC features and an SVM classifier was used to verify subtype assignment.

References

Alexander, A. L., Lee, J. E., Lazar, M., Boudos, R., DuBray, M. B., Oakes, T. R., . . . Lainhart, J. E. (2007). Diffusion tensor imaging of the corpus callosum in Autism. *Neuroimage, 34*(1), 61-73. doi:10.1016/j.neuroimage.2006.08.032

Amaral, D. G., Schumann, C. M., & Nordahl, C. W. (2008). Neuroanatomy of autism. *Trends Neurosci., 31*(3), 137-145. doi:10.1016/j.tins.2007.12.005

American Psychiatric, A. (2013). *Diagnostic and Statistical Manual of Mental Disorders (DSM-5®)*: American Psychiatric Pub.

An, H. S., Moon, W.-J., Ryu, J.-K., Park, J. Y., Yun, W. S., Choi, J. W., . . . Park, J.-Y. (2017). Inter-vender and test-retest reliabilities of resting-state functional magnetic resonance imaging: Implications for multi-center imaging studies. *Magn. Reson. Imaging, 44*, 125-130. doi:10.1016/j.mri.2017.09.001

Anderson, J. S. (2014). Cortical Underconnectivity Hypothesis in Autism: Evidence from Functional Connectivity MRI. In V. B. Patel, V. R. Preedy, & C. R. Martin (Eds.), *Comprehensive Guide to Autism* (pp. 1457-1471). New York, NY: Springer New York.

Assaf, M., Jagannathan, K., Calhoun, V. D., Miller, L., Stevens, M. C., Sahl, R., . . . Pearlson, G. D. (2010). Abnormal functional connectivity of default mode sub-networks in autism spectrum disorder patients. *Neuroimage, 53*(1), 247-256. doi:10.1016/j.neuroimage.2010.05.067

Aurich, N. K., Alves Filho, J. O., Marques da Silva, A. M., & Franco, A. R. (2015). Evaluating the reliability of different preprocessing steps to estimate graph theoretical measures in resting state fMRI data. *Front. Neurosci., 9*, 48. doi:10.3389/fnins.2015.00048

Badhwar, A., Collin-Verreault, Y., Orban, P., Urchs, S., Chouinard, I., Vogel, J., . . . Bellec, P. (2019). Multivariate consistency of resting-state fMRI connectivity maps acquired on a single individual over 2.5 years, 13 sites and 3 vendors. *bioRxiv*. doi:10.1101/497743

Baio, J. (2012). Prevalence of Autism Spectrum Disorders — Autism and Developmental Disabilities Monitoring Network, 14 Sites, United States, 2008.

Baio, J., Wiggins, L., Christensen, D. L., Maenner, M. J., Daniels, J., Warren, Z., . . . Dowling, N. F. (2018). Prevalence of Autism Spectrum Disorder Among Children Aged 8 Years - Autism and Developmental Disabilities Monitoring Network, 11

Sites, United States, 2014. *MMWR Surveill. Summ., 67*(6), 1-23. doi:10.15585/mmwr.ss6706a1

Barnea-Goraly, N., Kwon, H., Menon, V., Eliez, S., Lotspeich, L., & Reiss, A. L. (2004). White matter structure in autism: preliminary evidence from diffusion tensor imaging. *Biol. Psychiatry, 55*(3), 323-326. doi:10.1016/j.biopsych.2003.10.022

Baron-Cohen, S. (2002). The extreme male brain theory of autism. *Trends Cogn. Sci., 6*(6), 248-254. doi:10.1016/s1364-6613(02)01904-6

Baron-Cohen, S., Jolliffe, T., Mortimore, C., & Robertson, M. (1997). Another advanced test of theory of mind: evidence from very high functioning adults with autism or asperger syndrome. *J. Child Psychol. Psychiatry, 38*(7), 813-822. doi:10.1111/j.1469-7610.1997.tb01599.x

Baron-Cohen, S., O'Riordan, M., Jones, R., Stone, V., & Plaisted, K. (1999). A new test of social sensitivity: Detection of faux pas in normal children and children with Asperger syndrome. *J. Autism Dev. Disord., 29*(5), 407-418.

Baron-Cohen, S., Wheelwright, S., Hill, J., Raste, Y., & Plumb, I. (2001a). The `` Reading the Mind in the Eyes " Test Revised Version : A Study with Normal Adults, and Adults with Asperger Syndrome or High-functioning Autism. *J. Child Psychol. Psychiatry, 42*(2), 241-251.

Baron-Cohen, S., Wheelwright, S., Spong, A., Scahill, V., & Lawson, J. (2001b). Are intuitive physics and intuitive psychology independent? A test with children with Asperger Syndrome. *undefined*.

Beaulieu, C. (2002). The basis of anisotropic water diffusion in the nervous system - a technical review. *NMR Biomed., 15*(7-8), 435-455. doi:10.1002/nbm.782

Belmonte, M. K., Allen, G., Beckel-Mitchener, A., Boulanger, L. M., Carper, R. A., & Webb, S. J. (2004). Autism and abnormal development of brain connectivity. *J. Neurosci., 24*(42), 9228-9231. doi:10.1523/JNEUROSCI.3340-04.2004

Birn, R. M., Molloy, E. K., Patriat, R., Parker, T., Meier, T. B., Kirk, G. R., . . . Prabhakaran, V. (2013). The effect of scan length on the reliability of resting-state fMRI connectivity estimates. *Neuroimage, 83*, 550-558. doi:10.1016/j.neuroimage.2013.05.099

Blumenfeld, H. K., Booth, J. R., & Burman, D. D. (2006). Differential prefrontal-temporal neural correlates of semantic processing in children. *Brain Lang., 99*(3), 226-235. doi:10.1016/j.bandl.2005.07.004

Borchardt, V., Lord, A. R., Li, M., van der Meer, J., Heinze, H.-J., Bogerts, B., . . . Walter, M. (2016). Preprocessing strategy influences graph-based exploration of altered functional networks in major depression. *Hum. Brain Mapp., 37*(4), 1422-1442. doi:10.1002/hbm.23111

Braun, U., Plichta, M. M., Esslinger, C., Sauer, C., Haddad, L., Grimm, O., . . . Meyer-Lindenberg, A. (2012). Test-retest reliability of resting-state connectivity network characteristics using fMRI and graph theoretical measures. *Neuroimage, 59*(2), 1404-1412. doi:10.1016/j.neuroimage.2011.08.044

Brewer, N., Young, R. L., & Barnett, E. (2017). Measuring Theory of Mind in Adults with Autism Spectrum Disorder. *J. Autism Dev. Disord., 47*(7), 1927-1941. doi:10.1007/s10803-017-3080-x

Broyd, S. J., Demanuele, C., Debener, S., Helps, S. K., James, C. J., & Sonuga-Barke, E. J. S. (2009). Default-mode brain dysfunction in mental disorders: a systematic review. *Neurosci. Biobehav. Rev., 33*(3), 279-296. doi:10.1016/j.neubiorev.2008.09.002

Castelli, F., Frith, C., Happé, F., & Frith, U. (2002). Autism, Asperger syndrome and brain mechanisms for the attribution of mental states to animated shapes. *Brain, 125*(Pt 8), 1839-1849. doi:10.1093/brain/awf189

Cerliani, L., Mennes, M., Thomas, R. M., Di Martino, A., Thioux, M., & Keysers, C. (2015). Increased Functional Connectivity Between Subcortical and Cortical Resting-State Networks in Autism Spectrum Disorder. *JAMA Psychiatry, 72*(8), 767-777. doi:10.1001/jamapsychiatry.2015.0101

Chen, R., Jiao, Y., & Herskovits, E. H. (2011). Structural MRI in autism spectrum disorder. *Pediatr. Res., 69*(5 Pt 2), 63R-68R. doi:10.1203/PDR.0b013e318212c2b3

Cherkassky, V. L., Kana, R. K., Keller, T. A., & Just, M. A. (2006). Functional connectivity in a baseline resting-state network in autism. *Neuroreport, 17*(16), 1687-1690. doi:10.1097/01.wnr.0000239956.45448.4c

Chevallier, C., Kohls, G., Troiani, V., Brodkin, E. S., & Schultz, R. T. (2012). The social motivation theory of autism. *Trends Cogn. Sci., 16*(4), 231-239. doi:10.1016/j.tics.2012.02.007

Chien, H.-Y., Lin, H.-Y., Lai, M.-C., Gau, S. S.-F., & Tseng, W.-Y. I. (2015). Hyperconnectivity of the Right Posterior Temporo-parietal Junction Predicts Social Difficulties in Boys with Autism Spectrum Disorder. *Autism Res., 8*(4), 427-441. doi:10.1002/aur.1457

Courchesne, E., Karns, C. M., Davis, H. R., Ziccardi, R., Carper, R. A., Tigue, Z. D., . . . Courchesne, R. Y. (2001). Unusual brain growth patterns in early life in patients with autistic disorder: an MRI study. *Neurology, 57*(2), 245-254. doi:10.1212/wnl.57.2.245

Damarla, S. R., Keller, T. A., Kana, R. K., Cherkassky, V. L., Williams, D. L., Minshew, N. J., & Just, M. A. (2010). Cortical underconnectivity coupled with preserved visuospatial cognition in autism: Evidence from an fMRI study of an embedded figures task. *Autism Res., 3*(5), 273-279. doi:10.1002/aur.153

DeDora, D. J., Nedic, S., Katti, P., Arnab, S., Wald, L. L., Takahashi, A., . . . Mujica-Parodi, L. R. (2016). Signal Fluctuation Sensitivity: An Improved Metric for Optimizing Detection of Resting-State fMRI Networks. *Front. Neurosci., 10*, 180. doi:10.3389/fnins.2016.00180

Delmonte, S., Gallagher, L., O'Hanlon, E., McGrath, J., & Balsters, J. H. (2013). Functional and structural connectivity of frontostriatal circuitry in Autism Spectrum Disorder. *Front. Hum. Neurosci., 7*, 430. doi:10.3389/fnhum.2013.00430

Di Martino, A., Kelly, C., Grzadzinski, R., Zuo, X.-N., Mennes, M., Mairena, M. A., . . . Milham, M. P. (2011). Aberrant striatal functional connectivity in children with autism. *Biol. Psychiatry, 69*(9), 847-856. doi:10.1016/j.biopsych.2010.10.029

Di Martino, A., Yan, C. G., Li, Q., Denio, E., Castellanos, F. X., Alaerts, K., . . . Milham, M. P. (2014). The autism brain imaging data exchange: towards a large-scale evaluation of the intrinsic brain architecture in autism. *Mol. Psychiatry, 19*(6), 659-667. doi:10.1038/mp.2013.78

Doyle-Thomas, K. A. R., Lee, W., Foster, N. E. V., Tryfon, A., Ouimet, T., Hyde, K. L., . . . NeuroDevNet, A. S. D. I. G. (2015). Atypical functional brain connectivity during rest in autism spectrum disorders. *Ann. Neurol., 77*(5), 866-876. doi:10.1002/ana.24391

Easson, A. K., Fatima, Z., & McIntosh, A. R. (2019). Functional connectivity-based subtypes of individuals with and without autism spectrum disorder. *Netw Neurosci, 3*(2), 344-362. doi:10.1162/netn_a_00067

Egaas, B., Courchesne, E., & Saitoh, O. (1995). Reduced size of corpus callosum in autism. *Arch. Neurol., 52*(8), 794-801. doi:10.1001/archneur.1995.00540320070014

Falkmer, T., Anderson, K., Falkmer, M., & Horlin, C. (2013). Diagnostic procedures in autism spectrum disorders: a systematic literature review. *Eur. Child Adolesc. Psychiatry, 22*(6), 329-340. doi:10.1007/s00787-013-0375-0

Feczko, E., Balba, N. M., Miranda-Dominguez, O., Cordova, M., Karalunas, S. L., Irwin, L., . . . Fair, D. A. (2018). Subtyping cognitive profiles in Autism Spectrum Disorder using a Functional Random Forest algorithm. *Neuroimage, 172*, 674-688. doi:10.1016/j.neuroimage.2017.12.044

Feldman, H. M., Yeatman, J. D., Lee, E. S., Barde, L. H. F., & Gaman-Bean, S. (2010). Diffusion tensor imaging: a review for pediatric researchers and clinicians. *J. Dev. Behav. Pediatr., 31*(4), 346-356. doi:10.1097/DBP.0b013e3181dcaa8b

Fortin, J.-P., Cullen, N., Sheline, Y. I., Taylor, W. D., Aselcioglu, I., Cook, P. A., . . . Shinohara, R. T. (2018). Harmonization of cortical thickness measurements across scanners and sites. *Neuroimage, 167*, 104-120. doi:10.1016/j.neuroimage.2017.11.024

Gargouri, F., Kallel, F., Delphine, S., Ben Hamida, A., Lehéricy, S., & Valabregue, R. (2018). The Influence of Preprocessing Steps on Graph Theory Measures Derived from Resting State fMRI. *Front. Comput. Neurosci., 12*, 8. doi:10.3389/fncom.2018.00008

Georgiades, S., Szatmari, P., Boyle, M., Hanna, S., Duku, E., Zwaigenbaum, L., . . . Pathways in, A. S. D. S. T. (2013). Investigating phenotypic heterogeneity in children with autism spectrum disorder: a factor mixture modeling approach: ASD factor mixture model. *J. Child Psychol. Psychiatry, 54*(2), 206-215. doi:10.1111/j.1469-7610.2012.02588.x

Gotts, S. J., Simmons, W. K., Milbury, L. A., Wallace, G. L., Cox, R. W., & Martin, A. (2012). Fractionation of social brain circuits in autism spectrum disorders. *Brain, 135*(Pt 9), 2711-2725. doi:10.1093/brain/aws160

Haber, S. N. (2014). The place of dopamine in the cortico-basal ganglia circuit. *Neuroscience, 282*, 248-257. doi:10.1016/j.neuroscience.2014.10.008

Hardan, A. Y., Libove, R. A., Keshavan, M. S., Melhem, N. M., & Minshew, N. J. (2009). A preliminary longitudinal magnetic resonance imaging study of brain volume and cortical thickness in autism. *Biol. Psychiatry, 66*(4), 320-326. doi:10.1016/j.biopsych.2009.04.024

Harris, G. J., Chabris, C. F., Clark, J., Urban, T., Aharon, I., Steele, S., . . . Tager-Flusberg, H. (2006). Brain activation during semantic processing in autism

spectrum disorders via functional magnetic resonance imaging. *Brain Cogn., 61*(1), 54-68. doi:10.1016/j.bandc.2005.12.015

Hong, S.-J., Valk, S. L., Di Martino, A., Milham, M. P., & Bernhardt, B. C. (2018). Multidimensional Neuroanatomical Subtyping of Autism Spectrum Disorder. *Cereb. Cortex, 28*(10), 3578-3588. doi:10.1093/cercor/bhx229

Hrdlicka, M., Dudova, I., Beranova, I., Lisy, J., Belsan, T., Neuwirth, J., . . . Urbanek, T. (2005). Subtypes of autism by cluster analysis based on structural MRI data. *Eur. Child Adolesc. Psychiatry, 14*(3), 138-144. doi:10.1007/s00787-005-0453-z

Hull, J. V., Dokovna, L. B., Jacokes, Z. J., Torgerson, C. M., Irimia, A., & Van Horn, J. D. (2016). Resting-State Functional Connectivity in Autism Spectrum Disorders: A Review. *Front. Psychiatry, 7*, 205. doi:10.3389/fpsyt.2016.00205

Huotari, N., Raitamaa, L., Helakari, H., Kananen, J., Raatikainen, V., Rasila, A., . . . Korhonen, V. O. (2019). Sampling Rate Effects on Resting State fMRI Metrics. *Front. Neurosci., 13*, 279. doi:10.3389/fnins.2019.00279

Jahanian, H., Holdsworth, S., Christen, T., Wu, H., Zhu, K., Kerr, A. B., . . . Zaharchuk, G. (2019). Advantages of short repetition time resting-state functional MRI enabled by simultaneous multi-slice imaging. *J. Neurosci. Methods, 311*, 122-132. doi:10.1016/j.jneumeth.2018.09.033

Johnson, W. E., Li, C., & Rabinovic, A. (2007). Adjusting batch effects in microarray expression data using empirical Bayes methods. *Biostatistics, 8*(1), 118-127. doi:10.1093/biostatistics/kxj037

Jolliffe, T., & Baron-Cohen, S. (1997). Are people with autism and Asperger syndrome faster than normal on the Embedded Figures Test? *J. Child Psychol. Psychiatry, 38*(5), 527-534. doi:10.1111/j.1469-7610.1997.tb01539.x

Jung, M., Kosaka, H., Saito, D. N., Ishitobi, M., Morita, T., Inohara, K., . . . Iidaka, T. (2014). Default mode network in young male adults with autism spectrum disorder: relationship with autism spectrum traits. *Mol. Autism, 5*, 35. doi:10.1186/2040-2392-5-35

Just, M. A., Cherkassky, V. L., Keller, T. A., & Minshew, N. J. (2004). Cortical activation and synchronization during sentence comprehension in high-functioning autism: evidence of underconnectivity. *Brain, 127*(Pt 8), 1811-1821. doi:10.1093/brain/awh199

Just, M. A., Keller, T. A., Malave, V. L., Kana, R. K., & Varma, S. (2012). Autism as a neural systems disorder: a theory of frontal-posterior underconnectivity. *Neurosci. Biobehav. Rev., 36*(4), 1292-1313. doi:10.1016/j.neubiorev.2012.02.007

Kahn, R. S., Sommer, I. E., Murray, R. M., Meyer-Lindenberg, A., Weinberger, D. R., Cannon, T. D., . . . Insel, T. R. (2015). Schizophrenia. *Nat Rev Dis Primers, 1*, 15067. doi:10.1038/nrdp.2015.67

Kana, R. K., Keller, T. A., Cherkassky, V. L., Minshew, N. J., & Just, M. A. (2006). Sentence comprehension in autism: thinking in pictures with decreased functional connectivity. *Brain, 129*(Pt 9), 2484-2493. doi:10.1093/brain/awl164

Kana, R. K., Keller, T. A., Minshew, N. J., & Just, M. A. (2007). Inhibitory control in high-functioning autism: decreased activation and underconnectivity in inhibition networks. *Biol. Psychiatry, 62*(3), 198-206. doi:10.1016/j.biopsych.2006.08.004

Kana, R. K., Maximo, J. O., Williams, D. L., Keller, T. A., Schipul, S. E., Cherkassky, V. L., . . . Just, M. A. (2015). Aberrant functioning of the theory-of-mind network in children and adolescents with autism. *Mol. Autism, 6*, 59. doi:10.1186/s13229-015-0052-x

Kennedy, D. P., & Courchesne, E. (2008). The intrinsic functional organization of the brain is altered in autism. *Neuroimage, 39*(4), 1877-1885. doi:10.1016/j.neuroimage.2007.10.052

Kennedy, D. P., Redcay, E., & Courchesne, E. (2006). Failing to deactivate: resting functional abnormalities in autism. *Proc. Natl. Acad. Sci. U. S. A., 103*(21), 8275-8280. doi:10.1073/pnas.0600674103

Knaus, T. A., Silver, A. M., Lindgren, K. A., Hadjikhani, N., & Tager-Flusberg, H. (2008). fMRI activation during a language task in adolescents with ASD. *J. Int. Neuropsychol. Soc., 14*(6), 967-979. doi:10.1017/S1355617708081216

Lee, M. H., Smyser, C. D., & Shimony, J. S. (2013). Resting-state fMRI: a review of methods and clinical applications. *AJNR Am. J. Neuroradiol., 34*(10), 1866-1872. doi:10.3174/ajnr.A3263

Lewis, M., & Kim, S.-J. (2009). The pathophysiology of restricted repetitive behavior. *J. Neurodev. Disord., 1*(2), 114-132. doi:10.1007/s11689-009-9019-6

Liang, X., Wang, J., Yan, C., Shu, N., Xu, K., Gong, G., & He, Y. (2012). Effects of different correlation metrics and preprocessing factors on small-world brain functional networks: a resting-state functional MRI study. *PLoS One, 7*(3), e32766. doi:10.1371/journal.pone.0032766

Logothetis, N. K., & Wandell, B. A. (2004). Interpreting the BOLD signal. *Annu. Rev. Physiol., 66*, 735-769. doi:10.1146/annurev.physiol.66.082602.092845

Lombardo, M. V., Eyler, L., Moore, A., Datko, M., Carter Barnes, C., Cha, D., . . . Pierce, K. (2019). Default mode-visual network hypoconnectivity in an autism subtype with pronounced social visual engagement difficulties. *Elife, 8*. doi:10.7554/eLife.47427

Lynch, C. J., Uddin, L. Q., Supekar, K., Khouzam, A., Phillips, J., & Menon, V. (2013). Default mode network in childhood autism: posteromedial cortex heterogeneity and relationship with social deficits. *Biol. Psychiatry, 74*(3), 212-219. doi:10.1016/j.biopsych.2012.12.013

Maenner, M. J., Shaw, K. A., Baio, J., Washington, A., Patrick, M., DiRienzo, M., . . . PhD. (2020). Prevalence of Autism Spectrum Disorder Among Children Aged 8 Years — Autism and Developmental Disabilities Monitoring Network, 11 Sites, United States, 2016. *MMWR. Surveillance Summaries, 69*(4), 1-12. doi:10.15585/mmwr.ss6904a1

Mason, R. A., Williams, D. L., Kana, R. K., Minshew, N., & Just, M. A. (2008). Theory of Mind disruption and recruitment of the right hemisphere during narrative comprehension in autism. *Neuropsychologia, 46*(1), 269-280. doi:10.1016/j.neuropsychologia.2007.07.018

Medavarapu, S., Marella, L. L., Sangem, A., & Kairam, R. (2019). Where is the Evidence? A Narrative Literature Review of the Treatment Modalities for Autism Spectrum Disorders. *Cureus, 11*(1), e3901. doi:10.7759/cureus.3901

Mizuno, A., Liu, Y., Williams, D. L., Keller, T. A., Minshew, N. J., & Just, M. A. (2011). The neural basis of deictic shifting in linguistic perspective-taking in high-functioning autism. *Brain, 134*(Pt 8), 2422-2435. doi:10.1093/brain/awr151

Mohammadi, M. R., Ahmadi, N., Khaleghi, A., Zarafshan, H., Mostafavi, S.-A., Kamali, K., . . . Ghanizadeh, A. (2019). Prevalence of Autism and its Comorbidities and the Relationship with Maternal Psychopathology: A National Population-Based Study. *Arch. Iran. Med., 22*(10), 546-553.

Monk, C. S., Peltier, S. J., Wiggins, J. L., Weng, S.-J., Carrasco, M., Risi, S., & Lord, C. (2009). Abnormalities of intrinsic functional connectivity in autism spectrum disorders. *Neuroimage, 47*(2), 764-772. doi:10.1016/j.neuroimage.2009.04.069

Nebel, M. B., Joel, S. E., Muschelli, J., Barber, A. D., Caffo, B. S., Pekar, J. J., & Mostofsky, S. H. (2014). Disruption of functional organization within the primary

motor cortex in children with autism. *Hum. Brain Mapp., 35*(2), 567-580. doi:10.1002/hbm.22188

Newton, A. T., Rogers, B. P., Gore, J. C., & Morgan, V. L. (2012). Improving measurement of functional connectivity through decreasing partial volume effects at 7 T. *Neuroimage, 59*(3), 2511-2517. doi:10.1016/j.neuroimage.2011.08.096

Nijhof, A. D., Bardi, L., Brass, M., & Wiersema, J. R. (2018). Brain activity for spontaneous and explicit mentalizing in adults with autism spectrum disorder: An fMRI study. *Neuroimage Clin, 18*, 475-484. doi:10.1016/j.nicl.2018.02.016

Noble, S., Spann, M. N., Tokoglu, F., Shen, X., Constable, R. T., & Scheinost, D. (2017). Influences on the Test-Retest Reliability of Functional Connectivity MRI and its Relationship with Behavioral Utility. *Cereb. Cortex, 27*(11), 5415-5429. doi:10.1093/cercor/bhx230

O'Connor, E. E., & Zeffiro, T. A. (2019). Why is Clinical fMRI in a Resting State? *Front. Neurol., 10*, 420. doi:10.3389/fneur.2019.00420

Pavăl, D. (2017). A Dopamine Hypothesis of Autism Spectrum Disorder. *Dev. Neurosci., 39*(5), 355-360. doi:10.1159/000478725

Poljac, E., & Bekkering, H. (2012). A review of intentional and cognitive control in autism. *Front. Psychol., 3*, 436. doi:10.3389/fpsyg.2012.00436

Rane, S., Mason, E., Hussey, E., Gore, J., Ally, B. A., & Donahue, M. J. (2014). The effect of echo time and post-processing procedure on blood oxygenation level-dependent (BOLD) functional connectivity analysis. *Neuroimage, 95*, 39-47. doi:10.1016/j.neuroimage.2014.03.055

Rao, A., & Joao, M. (2017). Predictive modelling using neuroimaging data in the presence of confounds. *Neuroimage*.

Ratajczak, H. V. (2011). Theoretical aspects of autism: causes--a review. *J. Immunotoxicol., 8*(1), 68-79. doi:10.3109/1547691X.2010.545086

Reaven, J. A., Hepburn, S. L., & Ross, R. G. (2008). Use of the ADOS and ADI-R in children with psychosis: importance of clinical judgment. *Clin. Child Psychol. Psychiatry, 13*(1), 81-94. doi:10.1177/1359104507086343

Redcay, E., Moran, J. M., Mavros, P. L., Tager-Flusberg, H., Gabrieli, J. D. E., & Whitfield-Gabrieli, S. (2013). Intrinsic functional network organization in high-functioning adolescents with autism spectrum disorder. *Front. Hum. Neurosci., 7*, 573. doi:10.3389/fnhum.2013.00573

Satterthwaite, T. D., Wolf, D. H., Loughead, J., Ruparel, K., Elliott, M. A., Hakonarson, H., . . . Gur, R. E. (2012). Impact of in-scanner head motion on multiple measures of functional connectivity: relevance for studies of neurodevelopment in youth. *Neuroimage, 60*(1), 623-632. doi:10.1016/j.neuroimage.2011.12.063

Schumann, C. M., Bloss, C. S., Barnes, C. C., Wideman, G. M., Carper, R. A., Akshoomoff, N., . . . Courchesne, E. (2010). Longitudinal magnetic resonance imaging study of cortical development through early childhood in autism. *J. Neurosci., 30*(12), 4419-4427. doi:10.1523/JNEUROSCI.5714-09.2010

Schumann, C. M., Hamstra, J., Goodlin-Jones, B. L., Lotspeich, L. J., Kwon, H., Buonocore, M. H., . . . Amaral, D. G. (2004). The Amygdala Is Enlarged in Children But Not Adolescents with Autism; the Hippocampus Is Enlarged at All Ages. *J. Neurosci., 24*(28), 6392-6401. doi:10.1523/JNEUROSCI.1297-04.2004

Sparks, B. F., Friedman, S. D., Shaw, D. W., Aylward, E. H., Echelard, D., Artru, A. A., . . . Dager, S. R. (2002). Brain structural abnormalities in young children with autism spectrum disorder. *Neurology, 59*(2), 184-192. doi:10.1212/wnl.59.2.184

Stadnick, N., Chlebowski, C., Baker-Ericzén, M., Dyson, M., Garland, A., & Brookman-Frazee, L. (2017). Psychiatric comorbidity in autism spectrum disorder: Correspondence between mental health clinician report and structured parent interview. *Autism, 21*(7), 841-851. doi:10.1177/1362361316654083

Starck, T., Nikkinen, J., Rahko, J., Remes, J., Hurtig, T., Haapsamo, H., . . . Kiviniemi, V. J. (2013). Resting state fMRI reveals a default mode dissociation between retrosplenial and medial prefrontal subnetworks in ASD despite motion scrubbing. *Front. Hum. Neurosci., 7*, 802. doi:10.3389/fnhum.2013.00802

Supekar, K., Iyer, T., & Menon, V. (2017). The influence of sex and age on prevalence rates of comorbid conditions in autism. *Autism Res., 10*(5), 778-789. doi:10.1002/aur.1741

Tamminga, C. A., Ivleva, E. I., Keshavan, M. S., Pearlson, G. D., Clementz, B. A., Witte, B., . . . Sweeney, J. A. (2013). Clinical phenotypes of psychosis in the Bipolar-Schizophrenia Network on Intermediate Phenotypes (B-SNIP). *Am. J. Psychiatry, 170*(11), 1263-1274. doi:10.1176/appi.ajp.2013.12101339

Tick, B., Bolton, P., Happé, F., Rutter, M., & Rijsdijk, F. (2016). Heritability of autism spectrum disorders: a meta-analysis of twin studies. *J. Child Psychol. Psychiatry, 57*(5), 585-595. doi:10.1111/jcpp.12499

Van Dijk, K. R. A., Sabuncu, M. R., & Buckner, R. L. (2012). The influence of head motion on intrinsic functional connectivity MRI. *Neuroimage, 59*(1), 431-438. doi:10.1016/j.neuroimage.2011.07.044

Van Horn, J. D., & Toga, A. W. (2009). Multisite neuroimaging trials. *Curr. Opin. Neurol., 22*(4), 370-378. doi:10.1097/WCO.0b013e32832d92de

von dem Hagen, E. A. H., Stoyanova, R. S., Baron-Cohen, S., & Calder, A. J. (2013). Reduced functional connectivity within and between 'social' resting state networks in autism spectrum conditions. *Soc. Cogn. Affect. Neurosci., 8*(6), 694-701. doi:10.1093/scan/nss053

Washington, S. D., Gordon, E. M., Brar, J., Warburton, S., Sawyer, A. T., Wolfe, A., . . . VanMeter, J. W. (2014). Dysmaturation of the default mode network in autism. *Hum. Brain Mapp., 35*(4), 1284-1296. doi:10.1002/hbm.22252

Weng, S.-J., Wiggins, J. L., Peltier, S. J., Carrasco, M., Risi, S., Lord, C., & Monk, C. S. (2010). Alterations of resting state functional connectivity in the default network in adolescents with autism spectrum disorders. *Brain Res., 1313*, 202-214. doi:10.1016/j.brainres.2009.11.057

White, T., Muetzel, R., Schmidt, M., Langeslag, S. J. E., Jaddoe, V., Hofman, A., . . . Tiemeier, H. (2014). Time of acquisition and network stability in pediatric resting-state functional magnetic resonance imaging. *Brain Connect., 4*(6), 417-427. doi:10.1089/brain.2013.0195

Wiggins, J. L., Peltier, S. J., Ashinoff, S., Weng, S.-J., Carrasco, M., Welsh, R. C., . . . Monk, C. S. (2011). Using a self-organizing map algorithm to detect age-related changes in functional connectivity during rest in autism spectrum disorders. *Brain Res., 1380*, 187-197. doi:10.1016/j.brainres.2010.10.102

Wu, C. W., Chen, C.-L., Liu, P.-Y., Chao, Y.-P., Biswal, B. B., & Lin, C.-P. (2011). Empirical evaluations of slice-timing, smoothing, and normalization effects in seed-based, resting-state functional magnetic resonance imaging analyses. *Brain Connect., 1*(5), 401-410. doi:10.1089/brain.2011.0018

Yamashita, A., Yahata, N., Itahashi, T., Lisi, G., Yamada, T., Ichikawa, N., . . . Imamizu, H. (2019). Harmonization of resting-state functional MRI data across multiple imaging sites via the separation of site differences into sampling bias and measurement bias. *PLoS Biol., 17*(4), e3000042. doi:10.1371/journal.pbio.3000042

Yang, J., Gohel, S., & Vachha, B. (2020). Current methods and new directions in resting state fMRI. *Clin. Imaging, 65*, 47-53. doi:10.1016/j.clinimag.2020.04.004

Ypma, R. J. F., Moseley, R. L., Holt, R. J., Rughooputh, N., Floris, D. L., Chura, L. R., . . . Rubinov, M. (2016). Default Mode Hypoconnectivity Underlies a Sex-Related Autism Spectrum. *Biol Psychiatry Cogn Neurosci Neuroimaging, 1*(4), 364-371. doi:10.1016/j.bpsc.2016.04.006

Yu, M., Linn, K. A., Cook, P. A., Phillips, M. L., McInnis, M., Fava, M., . . . Sheline, Y. I. (2018). Statistical harmonization corrects site effects in functional connectivity measurements from multi-site fMRI data. *Hum. Brain Mapp., 39*(11), 4213-4227. doi:10.1002/hbm.24241

Chapter 2

Improved Between-Group Effect Size for Multi-Site Functional Connectivity Data via Site-Wise De-Meaning

2.1 Abstract:

Multi-site functional MRI (fMRI) databases are becoming increasingly prevalent in the study of neurodevelopmental and psychiatric disorders. However, multi-site databases are known to introduce site-effects that may confound neurobiological measures such as functional connectivity (FC). Although studies have been conducted to mitigate site-effects, these methods often result in reduced effect size in FC features known to be affected in diseased populations. We present a site-wise de-meaning (SWD) strategy in multi-site FC analysis and compare its performance with two common site-effect mitigation methods, i.e., generalized linear model (GLM), and Combining Bathces

(ComBat) Harmonization. For SWD, after FC was calculated and Fisher z-transformed, the site-wise FC mean was removed from each subject before group-level statistical analysis. These methods were tested on two multi-site psychiatric consortiums (Autism Brain Imaging Data Exchange (ABIDE) and Bipolar and Schizophrenia Network on Intermediate Phenotypes (B-SNIP)). Preservation of consistent FC alterations in patients were evaluated for each method through the effect sizes (Hedge's g) of patients vs. controls. For the B-SNIP dataset, SWD improved the effect size between schizophrenic and control subjects by 4.5% - 7.9%, while GLM and ComBat decreased the effect size by 22.5% – 42.6%. For the ABIDE dataset, SWD improved the effect size between autistic and control subjects by 2.9% - 5.3%, while GLM and ComBat decreased the effect size by up to 11.4%. The SWD method demonstrated superior performance in preserving the effect size in FC features associated with neurodevelopmental and psychiatric disorders compared to the original data and commonly used methods.

2.2 Introduction

Neuroimaging has become a powerful tool in studying psychiatric disorders (Peter et al., 2018). Functional magnetic resonance imaging (fMRI) allows for the study of aberrant functional connectivity (FC), predictions of normal individuals versus patients, early identification of neurological diseases, neuromarkers, and responses to treatment (Van Horn et al., 2009). Many traditional fMRI studies were limited by statistical power, since large-scale data is difficult to obtain at a single imaging site due to limited diseased population in one geographical location, limited time, and limited funds (Van Horn et al., 2009). Multi-site neuroimaging consortiums are becoming increasingly common in attempts to capture heterogeneity associated with various disorders, as well as to increase geographic variability, sample size, and statistical power (Van Horn et al., 2009).

While there are many benefits to multi-site consortiums, there are significant challenges in combining the data for analysis. FMRI data from different sites may contain scanner and site variability, leading to conflicting results and inferior reliability (An et al., 2017; Badhwar et al., 2019; Birn et al., 2013; Newton et al., 2012; Rane et al., 2014; Van Horn et al., 2009). Scanner variability can arise from different scanning vendors, scanner technology, and field inhomogeneities (Van Horn et al., 2009). Sites using the same scanner vendors and models have been found to introduce different field inhomogeneities that have affected the way the data was interpreted (Van Horn et al., 2009). Additionally, different scanner manufacturers are known to have different levels of test-retest reliability. It has been reported that Siemen's scanners have improved consistency than Philips's scanners (An et al., 2017; Badhwar et al., 2019). In many multi-site consortiums,

individual imaging sites utilized different scanning parameters, including repetition time, echo time, acquisition time, voxel size, flip angle, field of view, and slice thickness in collecting fMRI data. The use of different scanning parameters has been known to influence resting-state fMRI results (Birn et al., 2013; Newton et al., 2012; Rane et al., 2014). For example, increasing the acquisition time of scans from five minutes to thirteen minutes has been proven to greatly improve the reliability and similarity of functional correlations in resting state scans (Birn et al., 2013). Newton et al., reported that decreasing voxel size dimensions increased FC correlations in resting state scans (Newton et al., 2012), while Rane et al. demonstrated that a short TE (TE = 15ms) in scans led to results less correlated with group results than scans acquired at a higher TE (TE = 35ms and TE = 55ms) (Rane et al., 2014).

Efforts to reduce site variability have been made through homogenizing scanning protocols and/or through site-to-site quality assurance via standardized brain imaging phantoms (Yu et al., 2018). While these methods mitigate some of the variability associated with site-effects, in existing multi-site consortiums where data were not originally purposed for aggregation, homogenized scanning protocols and imaging phantoms were not available. One study quantified the sampling bias and engineering measurement bias of a travelling subject cohort who received resting-state scans at multiple imaging sites (Yamashita et al., 2019). This method was able to remove only the measurement bias, therefore improving signal-to-noise ratio. However, utilizing a travelling-cohort is costly, time consuming, and may be impractical with many established

multi-site consortiums, and therefore a post-acquisition method to mitigate site-effects is desirable.

Attempts to reduce multi-site consortium variability after acquisition include generalized linear model (GLM) and Combining Batches (ComBat) harmonization (Rao et al., 2017; Yamashita et al., 2019; Yu et al., 2018). GLM modifies FC values to account for site differences, but important FC features associated with patient groups may be compromised after this method (Rao et al., 2017; Yamashita et al., 2019). ComBat utilizes site-specific scaling factors and an empirical Bayesian criterion to shift samples to the grand mean and pooled variance across sites (Yu et al., 2018). It has demonstrated effectiveness in small samples of resting-state fMRI data using homogenized scanning parameters. However, it is unclear if ComBat harmonized fMRI data preserves the functional networks associated with psychiatric disorders or can accurately account for FC effects imposed by heterogeneous scan parameters (Yu et al., 2018). ComBat also centers the FC data of each site to the overall, grand mean of all sites, thus resulting in harmonized FC features that lose their original physical meaning (Da-Ano et al., 2020)

Although some multi-site consortiums may use phantoms or homogenous scanning parameters, there is always the possibility that sites will decide to aggregate FC data after image acquisition. There is a great need for a site-effect mitigation method that can be applied post-acquisition, on heterogeneous scanning parameters, and that preserves functional networks associated with psychiatric disorders. Examples of such multi-site database are the Autism Brain Imaging Data Exchange (ABIDE) and the Bipolar and Schizophrenia Network on Intermediate Phenotypes (B-SNIP) (Di Martino et al., 2014;

Tamminga et al., 2013). ABIDE is a consortium of neuroimaging data from Autism Spectrum Disorder (ASD) subjects and healthy controls (HC) from 17 international sites, while B-SNIP is a consortium of Schizophrenia (SZ), Schizoaffective disorder (SA), Bipolar disorder subjects and HCs from 5 different imaging sites (Tamminga et al., 2013). Both databases include sites that utilize different resting-state scanning parameters, protocols, and scanner models.

Here, we describe a site-wise de-meaning (SWD) strategy for multi-site FC analysis of fMRI data and compare its performance with two common site-effect mitigation methods (generalized linear model (GLM), and ComBat Harmonization). We (1) establish the consistent FC differences between disease groups and control groups in literature, (2) apply site-effect mitigation methods (GLM, ComBat, SWD) to multi-site FC data, and (3) compare the effect size of established FC findings of the three site-effect mitigation methods.

2.3 Materials and Methods

2.3.1 Datasets

i. B-SNIP

Resting-state fMRI data of 317 subjects from 4 sites in B-SNIP with a Diagnostic and Statistical Manual, 4th Edition (DSM-IV) SZ diagnosis (n = 149) and the corresponding HCs (n = 168) from the same sites were included in this study (Tamminga et al., 2013). Demographic information including site, sample size, sex, and age is shown in Table 2.1.

Table 2.1. Demographic information for the SZ and HC subjects from B-SNIP

Site	N	% SZ	% Male	Age (yr) Mean ± std
Baltimore	188	71.3	52.8	38.7 ± 12.7
Boston	52	65.4	50.0	34.7 ± 11.5
Dallas	143	59.4	44.1	39.6 ± 11.4
Hartford	129	705	51.9	33.9 ± 11.3

ii. ABIDE

Resting-state fMRI data from 850 subjects in ABIDE I with an ASD DSM-IV-TR diagnosis (n = 355) and the corresponding HCs (n = 495) from the same sites were used in this study (Di Martino et al., 2014; First et al., 2004). Demographic information including site, sample size, sex, age, and mean Full Scale IQ (FIQ) is shown in Table 2.2.

Table 2.2. Demographic information for the ASD and HC subjects from ABIDE

Site	N	% ASD	% Male	Age (yr) Mean ± std
Caltech	23	47.8	78.3	27.1 ± 5.8
CMU	32	40.6	78.1	26.8 ± 9.8
KKI	44	25.0	77.3	10.1 ± 1.2
Leuven	62	46.8	88.7	18.1 ± 5.0
Ludwig	34	5.9	88.2	25.3 ± 10.3
NYU	122	43.4	73.0	13.8 ± 5.8
Olin	36	55.6	86.1	16.8 ± 3.5
SBL	17	11.8	100	32.7 ± 7.0
SDSU	24	12.5	70.8	14.1 ± 1.9
Trinity	35	28.6	100	16.8 ± 3.5
UCLA	102	54.9	88.2	13.1 ± 2.5
UMich	129	41.1	81.4	14.2 ± 3.3
UPitt	56	51.8	85.7	18.8 ± 6.9
USM	100	57.0	100	22.1 ± 7.7
Yale	34	17.7	70.6	13.1 ± 2.8

Abbreviations: California Institute of Technology (Caltech), Carnegie Mellon University (CMU), Full Scale IQ (FIQ), Kennedy Krieger Institute (KKI), Ludwig Maximilians University Munich (Ludwig), New York University Langone Medical Center (NYU), Olin, Institute of Living at Hartford Hospital (Olin), San Diego State University (SDSU), Social Brain Lab (SBL), Trinity Centre for Health Sciences (Trinity), University of California, Los Angeles (UCLA), University of Leuven (Leuven), University of Michigan (UMich), University of Pittsburgh School of Medicine (UPitt), University of Utah School of Medicine (USM), and Yale Child Study Center (Yale).

2.3.2 Image Acquisition

Imaging data used in this analysis were collected on 3T MRI scanners. Scan parameters for the resting-state fMRI protocols from B-SNIP are summarized in Table 2.3 and scan parameters from ABIDE are summarized in Table 2.4. For each subject, a T_1-weighted structural image was collected and used for registration to the MNI152 space. Full details for acquisition parameters, informed consent, and site-specific protocols can be found at http://fcon_1000.projects.nitrc.org/indi/abide/abide_I.html for ABIDE and http://b-snip.org/ for B-SNIP (Di Martino et al., 2014; Tamminga et al., 2013).

Table 2.3. Resting-state fMRI scan parameters for subjects in B-SNIP

Site	Scanner	TR (ms)	TE (ms)	Acq. Time	Voxel Size	Number of slices	Flip Angle (degree)
Baltimore	Siemens Trio Tim	2210	30	5 min	3.4x3.4x3	36	70
Boston	GE Signa HDX	3000	27	5 min	3.4x3.4x4	30	60
Dallas	Philips	1500	27	5 min	3.4x3.4x4	29	60
Hartford	Siemens Allegra	1500	27	5 min	3.4x3.4x5	29	70

Abbreviations: Acquisition Time (Acq. Time), Echo Time (TE), Repetition Time (TR)

Table 2.4. Resting-state fMRI scan parameters for subjects in ABIDE

Site	Scanner	TR (ms)	TE (ms)	Acq. Time (min)	Voxel Size (mm)	Number of slices	Flip Angle (deg)
Caltech	Siemens Trio	2000	30	5:04	3.5 x 3.5 x 3.5	34	75
CMU	Siemens Verio	2000	30	8:06	3 x 3 x 3	28	73
KKI	Philips Achieva	2500	30	6:40	3.59 x 3.59 x 4	47	75
Leuven	Philips Intera	1667	33	7:06	3 x 3x 4	32	90
Ludwig	Siemens Verio	3000	30	6:06	3 x 3 x 4	28	80
NYU	Siemens Allegra	2000	15	6:00	3.75 x 3.75 x 3.8	33	90
Olin	Siemens Allegra	1500	27	5:15	2.75 x 2.75 x 2.72	29	60
SBL	Philips Intera	2200	30	7:28	3.44 x 3.44 x 3.4	38	80
SDSU	GE MR750	2000	30	6:10	3.13 x 3.13 x 4.5	34	90
Trinity	Philips Achieva	2000	28	5:06	3 x 3 x 3.5	38	90
UCLA	Siemens Trio	3000	28	6:06	3 x 3 x 4	34	90
UMich	GE Signa	2000	30	10:00	3.44 x 3.44 x 3	40	90
UPitt	Siemens Allegra	1500	25	5:06	3.1 x 3.1 x 4	29	70
USM	Siemens Trio	2000	28	8:06	3.4 x 3.4 x 3	40	90
Yale	Siemens Trio	2000	25	6:50	3.4 x 3.4 x 4	34	60

Abbreviations: Acquisition time (Acq. Time), California Institute of Technology (Caltech), Carnegie Mellon University (CMU), degree (deg), Echo time (TE), Field of view (FOV), Kennedy Krieger Institute (KKI), Ludwig Maximilians University Munich (Ludwig), New York University Langone Medical Center (NYU), Olin, Institute of Living at Hartford Hospital (Olin), Repetition time (TR), San Diego State University (SDSU), Social Brain Lab (SBL), Trinity Centre for Health Sciences (Trinity), University of California, Los Angeles (UCLA), University of Leuven (Leuven), University of Michigan (UMich), University of Pittsburgh School of Medicine (UPitt), University of Utah School of Medicine (USM), Yale Child Study Center (Yale).

2.3.3 Preprocessing

The resting-state fMRI data was preprocessed using the Connectome Computation System pipeline (Zuo et al., 2013). Steps included slice time correction, motion correction, skull stripping, global mean intensity normalization, nuisance signal regression, band pass filtering (0.01-0.1 Hz), and registration of the resting-state fMRI image to the T1-weighted image, followed by a transformation to standard space (Zuo et al., 2013). The resting state fMRI data was then parcellated into 200 regions of interest (ROIs) (Craddock et al., 2012).

2.3.4 Functional Connectivity Matrices and Parcellation

Pearson's correlation coefficient was used to ascertain the FC of each region of interest (ROI) pair, resulting in a 200×200 FC matrix for each subject. Each correlation coefficient was Fisher z-transformed, then linear regression was used to regress out age, sex, and site covariates to ensure that these confounding variables did not affect results.

2.3.5 Established FC Differences in Diagnostic Groups

The most common resting-state FC findings between patient and control groups was determined by performing a literature review in PubMed to identify relevant studies published within the last 15 years for FC differences between SZ and HCs (keywords: SZ, FC, resting-state, functional MRI) and for FC differences between ASD and HCs (keywords: ASD, FC, resting-state, functional MRI).

2.3.6 Comparison of Methods

We compared the effect size of FC differences between patients and for the following methods: (1) GLM, (2) ComBat (Johnson et al., 2007), and (3) SWD.

i. **GLM**

After Fisher z-transforming the FC data, multiple linear regression with terms for age, sex, and site was performed in MATLAB. The regression model can be written as

$$y_{ijv} = \alpha_v + X_{ij}^T \beta_v + \varepsilon_{ijv}$$

where α_v is the average connectivity value for a particular connectivity value (v), X_{ij}^T is the design matrix for the covariates (age, sex, site) for every site (i), and subject (j), and β_v is the vector of regression coefficients corresponding to X_{ij}^T. The removal of site-effects is done by subtracting the estimated site-effects

$$y_{ijv}^{GLM} = y_{ijv} - \alpha_v - X_{ij}^T \beta_v$$

ii. **ComBat**

FC values were Fisher z-transformed and a multivariate linear mixed effects regression with terms for biological variables and scanner were used to model FC (Yu et al., 2018). The ComBat harmonization model can be written as:

$$y_{ijv} = \alpha_v + X_{ij}^T \beta_v + \gamma_{iv} + \delta_{iv} \varepsilon_{ijv}$$

where α_v is the average connectivity value for a particular connectivity value (v), $X^T{}_{ij}$ is a design matrix for the covariates of interest (age, sex, and diagnostic group) for every subject (j), β_v is a vector of regression coefficients corresponding to $X^T{}_{ij}$, γ_{iv} and δ_{iv} are the additive (or location parameter) and multiplicative (or scale parameter), respectively,

of site-effects of site i for connectivity value v (Yu et al., 2018). ComBat was performed in MATLAB and the adjusted FC values are given by:

$$y_{ijv}^{ComBat} = \frac{y_{ijv} - \widehat{\alpha_v} - X_{ij}^T \widehat{\beta_v} - \gamma_{iv}^*}{\delta_{iv}^*} + \widehat{\alpha_v} + X_{ij}^T \widehat{\beta_v}$$

where γ_{iv}^* and δ_{iv}^* are the empirical Bayes estimate of the additive (or location parameter) and multiplicative (or scale parameter), respectively, of site-effects of site i for connectivity value v (Yu et al., 2018). Age and sex effects were then regressed out of the ComBat harmonized FC data.

iii. ***SWD***

The Fisher z-transformed data with age and sex regressed out is referred to in the algorithm as FC. A single overall mean value for each site was determined by averaging all FC values for every subject in each site. The mean value was then subtracted from each FC feature for every subject.

Algorithm

Input: Fisher z-transformed functional connectivity data (*FC)*, number of subjects (*N)*, number of FC values (*n)*, site means *(SM)*
Output: SWD FC data (*FC_{SWD})*
 	
For: i = 1:*N*
  For: j = 1:*n*
  FC_{SWD}(i, j) = *FC*(i, j) – *SM*(i)
  End
End

2.3.7 Effect Size

To evaluate how each method affects FC measures, Hedge's g was used to calculate the effect size of consistent FC alterations in group analysis (ASD vs HCs and SZ vs HCs) for (1) original data with sex and age regressed out, (2) GLM, (3) ComBat harmonized data, and (4) SWD. It is suggested that 0.2 is considered to be a small effect size, 0.5 represents a medium effect size and 0.8 represents a large effect size (Hedges et al., 1985).

2.4 Results

2.4.1 Consistent FC Alterations

i. HC vs SZ Literature Review Findings

Hypoconnectivity, specifically in the medial prefrontal cortex (MPFC), as well as between the MPFC and the anterior cingulate cortex (ACC) (Figure 2.1), was the most common resting state finding in SZ. Further information regarding the literature findings on hypoconnectivity within MPFC and between MPFC and ACC can be found in Table 2.5 and 2.6, respectively.

Table 2.5. Resting state fMRI studies finding within MPFC hypoconnectivity in SZ participants.

Author	**n (HC/SZ)**	**Age mean(std) (HC/SZ)**	**N female (HC / SZ)**	**Analysis Method**	**B-SNIP**	**SZ participant info**
Bluhm et al. (2007)	17 / 17	30.94(12.60) / 33.54(13.77)	3 / 3	Seed	No	15 paranoid SZ / 2 undifferentiated SZ
Chen et al. (2017)	20 / 20	41.6(13.6)/ 40.3(13.8)	13 / 11	Local FCD	No	SZ only
Cole et al. (2011)	22 / 23	37.18(7.59)/ 36.54(9.36)	6 / 5	Seed	No	SZ only
Du et al. (2016)	82 / 82	37.7(10.8)/ 38.0(14.0)	19 / 17	ROI	No	SZ only
Fang et al. (2018)	22 / 20	24.3(4.8)/ 24.2(4.8)	10 / 13	Seed/ROI (Effective Connectivity)	No	FES
Guo et al. (2014)	50 / 49	23.48(2.49)/ 22.69(4.62)	27 / 19	Network Homogeneity	No	SZ only
He et al. (2013)	113 /115	26.61(8.9)/ 25.36(8.2)	56 / 62	fALFF	No	FES
Huang et al. (2010)	66 / 66	24.5(8.6)/ 24.2(8.4)	36 / 36	ALFF	No	FES (Treatment naïve)
Su Lui et al. (2010)	34 / 34	25.0(8.0)/ 24.6(8.5)	21 /21	ICA	No	FES (Treatment naïve)
Meda et al. (2012)	324 /296	35.2(13.4)/ 34.9(12.2)	144 / 97	ICA	Yes	SZ only

Mingoia et al. (2012)	25 / 25	29.1(8.6)/ 30(7.3)	10 / 8	pICA	No	SZ only
Mwansisya et al. (2013)	33 /41	24.52(6.33)/ 23.88(5.85)	17 / 16	Seed	No	FES
Ongür et al. (2010)	15 / 14	37.9(9.5)/ 42.3(9.5)	6 / 6	ICA	No	SZ and SA
Su et al. (2013)	25 / 25	42.5(9.9)/ 42.5(9.9)	13 /13	Seed	No	SZ only

Abbreviations: Amplitude of Low Frequency Fluctuations (ALFF), Blood Oxygenation Level Dependent (BOLD), First Episode Schizophrenia (FES), Fractional Amplitude of Low Frequency Fluctuations (fALFF), Functional Connectivity Density (FCD, Independent Component Analysis (ICA), Probabilistic ICA (pICA)

Table 2.6. Resting state fMRI studies finding MPFC to ACC hypoconnectivity in SZ participants.

Author	**n (HC/SZ)**	**Age mean(std) (HC/SZ)**	**N Female (HC/ASD)**	**Analysis Method**	**B-SNIP**	**SZ participant info**
Alonso-Solís et al. (2015)	20 / 19	37.75(7.4) /40.05(8.9)	7 / 6	Seed	No	Auditory hallucinating SZ participants
Anticevic et al. (2015)	56 / 73	31.25 (10.3) / 32.99 (10.9)	32 / 24	Seed	No	SZ only
Camchong et al. (2009)	29 / 29	41.1(10.6) / 41.3(9.28)	11 / 11	ICA/ ROI	No	SZ only
Fang et al. (2018)	22 / 20	24.3(4.8) / 24.2(4.8)	10 / 13	Seed/ROI (Effective Connectivity)	No	FES
Holt et al. (2011)	17 / 18	40(12.5) / 35.9(13.7)	6 / 6	Seed	No	SZ only
Hoptman et al. (2014)	31 / 33	38.6(9) / 38.2 (10.4)	9 / 6	Seed	No	SZ and SA
Jang et al. (2011)	16 /16	22.06(1.65) / 21.32(5.65)	7 /7	Seed	No	Genetic high risk for SZ
Kyriakopoulos et al. (2012)	20 / 25	16.3(2.1) / 16.1(2.5)	8 /11	Seed	No	EOS
Li et al. (2019)	2567/2588	31.17 /31	1168 / 1092	ICA	No	SZ only Meta-Analysis
S. Lui et al. (2015)	59 / 37	38(17) / 36(14)	33 / 15	ALFF	Yes	SZ only
Meda et al. (2014)	324 /296	35.2(13.4) / 34.9(12.2)	144 / 97	ICA	Yes	SZ only

Penner et al. (2016)	24 / 24	23.8(4.3) / 23.2(4.2)	12 / 3	Seed	No	SZ only
Zhou et al. (2015)	10 / 91	33.3(10.5) / 33.9(7.7)	55 / 40	Seed	No	SZ only

Abbreviations: Amplitude Low Frequency Fluctuations (ALFF), Early onset Schizophrenia (EOS), First Episode Schizophrenia (FES), Independent Component Analysis (ICA), Schizoaffective Disorder (SA), Schizophrenia (SZ).

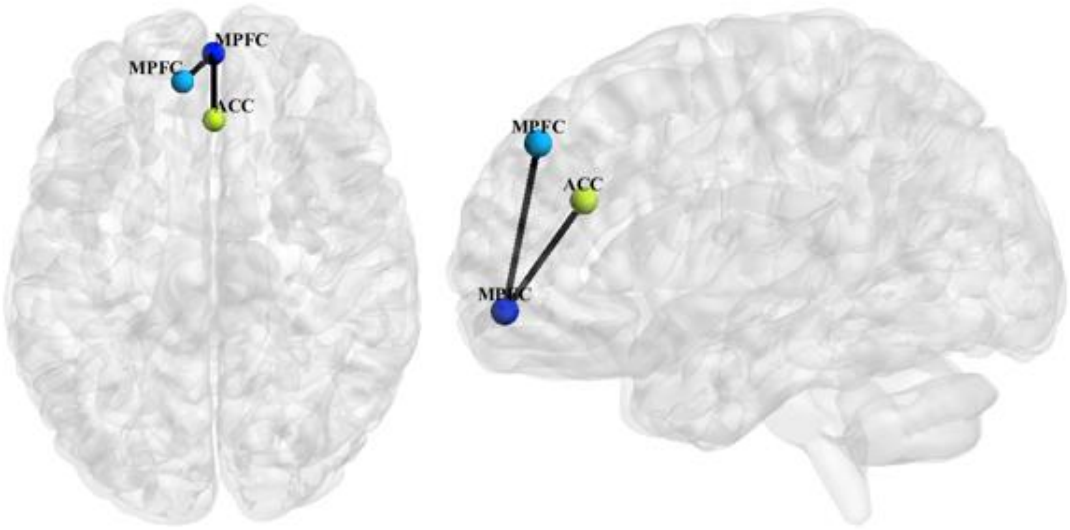

Figure 2.1. FC features associated with SZ. Medial Prefrontal Cortex (MPFC), Anterior Cingulate Cortex (ACC).

ii. ASD Findings

The hypoconnectivity hypothesis of ASD posits that behavioral features of ASD arise from reduced neural connections in the brain (Just et al., 2012). The most common resting state fMRI finding regarding ASD FC was anterior-posterior DMN hypoconnectivity (see Hull et al., 2016). More specifically, our literature review resulted in eighteen studies reporting hypoconnectivity between the posterior cingulate cortex (PCC)/precuneus and the MPFC (Figure 2.2; Table 2.7). Hypoconnectivity between the MPFC in the frontal lobe and MTG of the temporal lobe was the second most common finding in the ASD literature (Figure 2.2; Table 2.8).

Table 2.7. Resting state fMRI studies of the primary FC feature of ASD finding MPFC to PCC hypoconnectivity compared to HCs.

Author	**N (HC/ASD)**	**Age mean(std) (HC/ASD)**	**N female (HC/ASD)**	**Analysis Method**	**ABIDE**	**ASD participant info**
Abbott et al. (2016)	38 / 37	13.0(2.6) / 13.9(2.6)	8 / 5	iFC	No	ASD only
Assaf et al. (2010)	15 / 15	17.1(3.6) / 15.7(3.0)	2 /1	ICA	No	HFA
Cherkassky et al. (2006)	57 / 57	24(9.0) / 24(10.6)	5 / 4	ROI	No	HFA
Doyle-Thomas et al. (2015)	44 / 71	12.2(3.8) / 12.3(3.1)	0 / 0	Seed	No	ASD
Eilam-Stock et al. (2014)	15 / 17	27.1(8.2) / 26.1(6.5)	NA	Seed	No	HFA(12), ASP(5)
Falahpour et al. (2016)	76 / 76	64(12) / 62(14)	12/9	iFC	Yes	ASD
Falahpour et al. (2016)	32 / 32	13.5(2.7) / 14.3(2.4)	5 / 4	SD-iFC	No	ASD
Joshi et al. (2017)	16 / 15	21.9(3.5) / 21.6(3.7)	0 / 0	Seed	No	HFA
Jung et al. (2014)	21 / 19	24.8(4.3) / 25.3(6.9)	0 / 0	Seed	No	HFA
Jones et al. (2010)	20 / 17	17.1(2.1) / 16.1(2.6)	0 / 0	Seed	No	HFA
Lee et al. (2016)	517 / 458	16.5(7.3) / 16.2(7.4)	90 / 54	FCD	Yes	ASD/ ASP/ PDD-NOS
Liu et al. (2020)	548 / 506	16.86(7.55) / 16.59(8.05)	95 / 60	Seed	Yes	ASD/ ASP/ PDD-NOS
Long et al. (2016)	64 / 64	Child Cohort: 9.3(1.5)/9.6 (1.0)	10 / 10	Seed	Yes	ASD/ ASP/ PDD-NOS

		Adolescent Cohort: 14.5(1.9)/13.7(1.8) Adult Cohort: 25.5(4.2)/25.4(5.9)				
Maximo et al. (2013)	29 / 29	13.5(2.2) / 13.8(2.4)	7 / 4	ReHo	No	HFA
Monk et al. (2009)	12 / 12	27(6.1) / 26(5.9)	2 / 1	Seed	No	ASD (7) / ASP(3) and PDD-NOS(3)
Murdaugh et al. (2012)	14 / 13	22.6(4.2) / 21.4(3.9)	0 / 0	Seed	No	HFA
Washington et al. (2014)	24 /24	10.08(3.17) / 10.88(2.27)	3 / 3	ICA/ ROI	No	ASD only
Weng et al. (2010)	15 /16	16(1.44) / 15(1.45)	2 / 1	Seed	No	ASP(2), PDD-NOS(8), ASD(6)
Yerys et al. (2015)	22 /22	11.37(1.56) / 11.41(1.51)	4 / 4	Seed	No	ASD

Abbreviations: Asperger's (ASP), Functional Connectivity Density (FCD), High Functioning Autism (HFA), Independent Component Analysis (ICA), Intrinsic Functional Connectivity (iFC), Pervasive Development Disorder-Not Otherwise Specified (PDD-NOS), Region of Interest (ROI), Regional Homogeneity (ReHo), Standard deviation of the sliding window correlation (SD-iFC)

Table 2.8. Resting state fMRI studies for the secondary FC feature of ASD finding MPFC – MTG hypoconnectivity for ASD participants.

Author	**N (HC/ASD)**	**Age mean(std) (HC/ASD)**	**N female (HC/ASD)**	**Analysis Method**	**ABIDE**	**ASD participant info**
Borràs-Ferrís et al. (2019)	74 / 74	Child Cohort 10.63(0.86) Adolescent Cohort: 14.35(1.77)	0 / 0	ROI	Yes	ASD only
Cheng et al. (2015)	509 / 418	16.4(7.08)/ 17.17(7.97)	85 / 51	ROI	Yes	ASD/ASP/ PDD-NOS
von dem Hagen et al. (2013)	24 / 15	25(6) / 30(8)	0 / 0	Seed/ ICA	No	HFA(2) / ASP(13)
Hahamy et al. (2015)	73 / 68	25.82(0.79) / 26.6(0.77)	14 / 6	Seed	Yes	HFA
Iidaka (2015)	328 / 312	12.9(3.0) / 13.2(3.1)	61/ 39	ROI	Yes	ASD
Liu et al. (2020)	548 / 506	16.86(7.55) / 16.59(8.05)	95 / 60	Seed	Yes	ASD/ ASP/ PDD-NOS
Murdaugh et al. (2012)	14 / 13	22.6(4.2) / 21.4(3.9)	0 / 0	Seed	No	HFA
Paakki et al. (2010)	27 / 28	14.49(1.51) /14.58(1.62)	9 / 8	ReHo	No	ASD (9)/ASP(19)

Abbreviations: Asperger's (ASP), High Functioning Autism (HFA), Independent Component Analysis (ICA), Pervasive Development Disorder-Not Otherwise Specified (PDD-NOS), Region of Interest (ROI), Regional Homogeneity (ReHo)

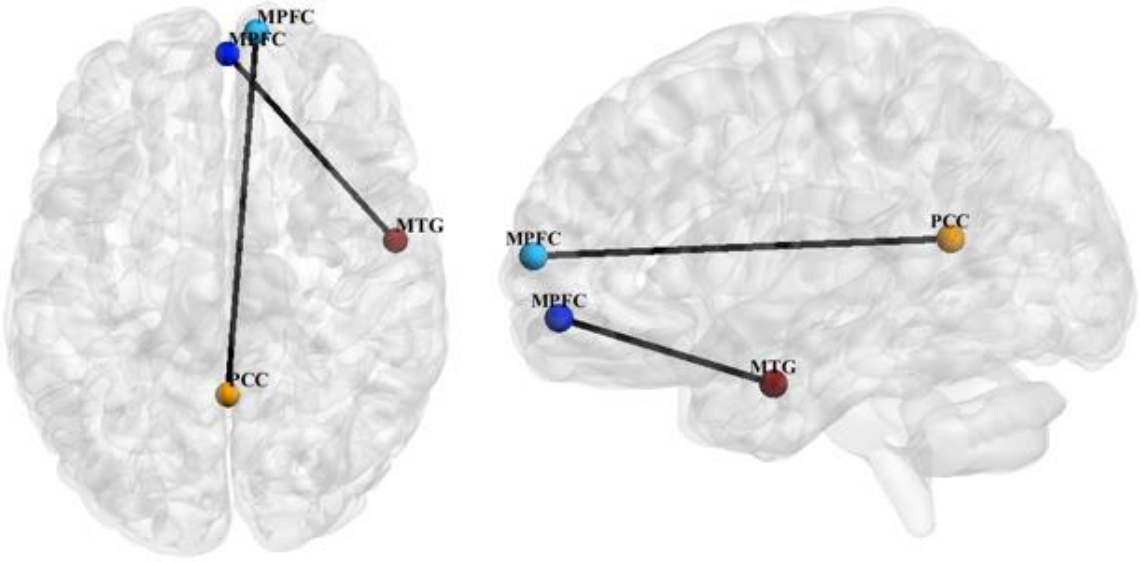

Figure 2.2. FC features associated with ASD. Medial prefrontal cortex (MPFC), Posterior Cingulate Cortex (PCC), Medial Temporal Gyrus (MTG).

2.4.2 Effect Size

i. SZ

Hedge's g was used to calculate the effect size of SZ vs HCs for the primary and secondary FCs depicted in Figure 2.1 for (1) the original data, (2) GLM, (3) ComBat, and (4) SWD. For the primary FC feature, a seed region for the MPFC (center of mass MNI coordinates 1.4, 55.9, -7.2; volumes: 193), and a seed region for the ACC (center of mass MNI coordinates 1.6, 33.3, 24.3; volumes: 297) was used for the effect size calculation (Figure 2.1). For the secondary FC feature (within MPFC FC), two seed regions in the prefrontal cortex were used, MPFC (center of mass MNI coordinates 1.4, 55.9, -7.2; volumes: 193) and MPFC (center of mass MNI coordinates -9.1, 46.4, 40.6; volumes: 206) to calculate the effect size (Figure 2.1). For the primary FC feature, the effect size

decreased compared to the original data for GLM (42.6% decrease), and ComBat (22.5% decrease), and increased for SWD (4.5% increase) (Table 2.9). For the secondary FC feature (within MPFC FC), the effect size decreased compared to the original data for GLM (40% decrease) and ComBat (23.9% decrease) and increased for SWD (7.9% increase) (Table 2.9).

Table 2.9. Effect size (Hedge's g) comparison between SZ and HCs for the primary FC feature (within MPFC), and for the secondary FC feature (MPFC and ACC) for the original FC data, GLM, ComBat, and SWD.

	Original	**GLM**	**%change**	**ComBat**	**%change**	**SWD**	**%change**
Within MPFC	0.3069	0.1761	-42.6%	0.2379	-22.5%	0.3206	4.5%
MPFC - ACC	0.2046	0.1228	-40.0%	0.1557	-23.9%	0.2207	7.9%

ii. ASD

Hedge's g was used to calculate the effect size of ASD vs HCs for the primary and secondary FC features depicted in Figure .22 for (1) the original data, (2) GLM, (3) ComBat, and (4) SWD. For the primary FC feature, a seed region for the MPFC (center of mass MNI coordinates 10.7, 63.0, 10.0; volumes: 202) and PCC/precuneus (center of mass MNI coordinates: 1.5, -52.8, 14.8; volumes: 231) was used for effect size calculation (Figure 2.2). The effect size decreased compared to the original data for GLM (7.5% decrease) and increased for ComBat (5.1% decrease) and SWD (5.3% increase) for the primary FC feature (Table 2.10). For the secondary FC feature (frontal pole to temporal lobe FC), a seed region in the frontal pole (center of mass MNI coordinates 1.4, 55.9, -7.2; volumes: 193) and temporal lobe (center of mass MNI coordinates 55.1, -3.6, -25.4; volumes: 201) were used to calculate the effect size (Figure 2.2). The effect size decreased

compared to the original data for GLM (11.4% decrease) and ComBat (1.3% decrease), and increased for SWD (2.9% increase) for the secondary FC feature (Table 2.10).

Table 2.10. Effect size (Hedge's g) comparison between ASD and HCs for the primary FC feature (MPFC and PCC/precuneus), and for the secondary FC feature (MPFC and MTG) for the original FC data, GLM, ComBat, and the SWD method. The percent change columns indicate the percent increase/decrease between each method and the original data.

	Original	**GLM**	**%change**	**ComBat**	**%change**	**SWD**	**%change**
MPFC–PCC	0.2634	0.2436	-7.5%	0.2769	5.1%	0.2773	5.3%
MPFC – MTG	0.4892	0.4334	-11.4%	0.4829	-1.3%	0.5034	2.9%

2.5 Discussion

Previously introduced methods to reduce fMRI site-effects associated with multi-site disorders result in the loss of effect size associated with psychiatric or neurodevelopmental disorders. The SWD method reduced site-effects in large sample sizes in multi-site databases with heterogeneous scan parameters, while improving the effect size of FC features associated with ASD and SZ compared to previous site-effect mitigation methods. This simple method is computationally inexpensive, is applicable to multi-site consortiums post-acquisition, and can be applied to various other multi-site fMRI databases.

2.5.1 Preservation of Functional Networks Associated with ASD and SZ

ComBat has been proposed to mitigate site-effects in small sizes, when using homogeneous scanning parameters, however it is unknown if it can accurately account for site-effects imposed by heterogeneous scan parameters and whether it can preserve the functional networks associated with psychiatric disorders (Yu et al., 2018). ComBat also

centers the FC data of each site to an overall grand mean, thus resulting in harmonized FC features that lose their meaning (Da-Ano et al., 2020; Yu et al., 2018). In addition, GLM may diminish the measurable disease effects when applied to FC data (Yamashita et al., 2019). Therefore, a method is needed to reduce site-effects while maintaining the FC effects present in psychiatric and neurodevelopmental disorders.

Hypoconnectivity in SZ has been widely reported and is associated with symptoms of SZ (Cole et al., 2011; Du et al., 2016; Fang et al., 2018; Mwansisya et al., 2013), while DMN anterior-posterior connectivity in ASD has also been widely reported and has been found to be predictive of clinical symptoms of ASD (Assaf et al., 2010; Weng et al., 2010; Yerys et al., 2015). GLM resulted in a reduction of the effect size of these features by up to 42.6% and ComBat resulted in a reduction of the effect size of these features up to 23.9% in patients vs. control subjects. By de-meaning multi-site FC data, we removed site-effects and improved the effect size by 2.9% - 7.9% for patients vs. control subjects in the established FC features in both disorders compared to the original data.

The superior performance of SWD compared to GLM may be due to better generalizability and removal of overall site-effects in site de-meaning. In sites with unequal cohort sizes, GLM may introduce a diagnostic group bias. In addition, while diagnostic group is a covariate used in ComBat, the FC values are shifted to an overall mean, which can result in the loss of important diagnostic group information.

2.5.2 Limitations and Future Work

While there are advantages with SWD, there are several limitations as well. First, while there are many reports of hypoconnectivity in SZ and ASD, there is no conclusive ground

truth fMRI neuromarker for either disorder. In addition, while we postulate that this method could be utilized on multiple multi-site databases with various other disorders, this has only been tested on two multi-site consortiums with two different disorders. Therefore, more extensive testing is needed.

2.6 Conclusion

We introduce a site-size demeaning method for reducing site effects in multi-site studies and compared it with two existing methods. The SWD method improved the effect size across these features in two multi-site disorder databases as compared to the original data and previously used harmonization methods (ComBat and GLM).

2.7 Acknowledgements

The authors thank the contributors to the Autism Brain Imaging Data Exchange, Preprocessed Connectomes Project, and Bipolar and Schizophrenia Network for Intermediate Phenotypes for access to subject data.

2.8 References

Abbott, A. E., Nair, A., Keown, C. L., Datko, M., Jahedi, A., Fishman, I., & Müller, R.-A. (2016). Patterns of Atypical Functional Connectivity and Behavioral Links in Autism Differ Between Default, Salience, and Executive Networks. *Cereb. Cortex, 26*(10), 4034-4045. doi:10.1093/cercor/bhv191

Agcaoglu, O., Wilson, T. W., Wang, Y.-P., Stephen, J., & Calhoun, V. D. (2019). Resting state connectivity differences in eyes open versus eyes closed conditions. *Hum. Brain Mapp., 40*(8), 2488-2498. doi:10.1002/hbm.24539

Alonso-Solís, A., Vives-Gilabert, Y., Grasa, E., Portella, M. J., Rabella, M., Sauras, R. B., . . . Corripio, I. (2015). Resting-state functional connectivity alterations in the default network of schizophrenia patients with persistent auditory verbal hallucinations. *Schizophr. Res., 161*(2-3), 261-268. doi:10.1016/j.schres.2014.10.047

An, H. S., Moon, W.-J., Ryu, J.-K., Park, J. Y., Yun, W. S., Choi, J. W., . . . Park, J.-Y. (2017). Inter-vender and test-retest reliabilities of resting-state functional magnetic resonance imaging: Implications for multi-center imaging studies. *Magn. Reson. Imaging, 44*, 125-130. doi:10.1016/j.mri.2017.09.001

Anticevic, A., Savic, A., Repovs, G., Yang, G., McKay, D. R., Sprooten, E., . . . Glahn, D. C. (2015). Ventral anterior cingulate connectivity distinguished nonpsychotic bipolar illness from psychotic bipolar disorder and schizophrenia. *Schizophr. Bull., 41*(1), 133-143. doi:10.1093/schbul/sbu051

Assaf, M., Jagannathan, K., Calhoun, V. D., Miller, L., Stevens, M. C., Sahl, R., . . . Pearlson, G. D. (2010). Abnormal functional connectivity of default mode sub-networks in autism spectrum disorder patients. *Neuroimage, 53*(1), 247-256. doi:10.1016/j.neuroimage.2010.05.067

Badhwar, A., Collin-Verreault, Y., Orban, P., Urchs, S., Chouinard, I., Vogel, J., . . . Bellec, P. (2019). Multivariate consistency of resting-state fMRI connectivity maps acquired on a single individual over 2.5 years, 13 sites and 3 vendors. *bioRxiv*. doi:10.1101/497743

Birn, R. M., Molloy, E. K., Patriat, R., Parker, T., Meier, T. B., Kirk, G. R., . . . Prabhakaran, V. (2013). The effect of scan length on the reliability of resting-state fMRI connectivity estimates. *Neuroimage, 83*, 550-558. doi:10.1016/j.neuroimage.2013.05.099

Bluhm, R. L., Miller, J., Lanius, R. A., Osuch, E. A., Boksman, K., Neufeld, R. W. J., . . . Williamson, P. (2007). Spontaneous low-frequency fluctuations in the BOLD signal in schizophrenic patients: anomalies in the default network. *Schizophr. Bull., 33*(4), 1004-1012. doi:10.1093/schbul/sbm052

Borràs-Ferrís, L., Pérez-Ramírez, Ú., & Moratal, D. (2019). Link-Level Functional Connectivity Neuroalterations in Autism Spectrum Disorder: A Developmental Resting-State fMRI Study. *Diagnostics (Basel), 9*(1). doi:10.3390/diagnostics9010032

Camchong, J., MacDonald, A. W., III, Bell, C., Mueller, B. A., & Lim, K. O. (2009). Altered functional and anatomical connectivity in schizophrenia. *Schizophr. Bull., 37*(3), 640-650.

Chen, X., Liu, C., He, H., Chang, X., Jiang, Y., Li, Y., . . . Yao, D. (2017). Transdiagnostic differences in the resting-state functional connectivity of the prefrontal cortex in depression and schizophrenia. *J. Affect. Disord., 217*, 118-124. doi:10.1016/j.jad.2017.04.001

Cheng, W., Rolls, E. T., Gu, H., Zhang, J., & Feng, J. (2015). Autism: reduced connectivity between cortical areas involved in face expression, theory of mind, and the sense of self. *Brain, 138*(Pt 5), 1382-1393. doi:10.1093/brain/awv051

Cherkassky, V. L., Kana, R. K., Keller, T. A., & Just, M. A. (2006). Functional connectivity in a baseline resting-state network in autism. *Neuroreport, 17*(16), 1687-1690. doi:10.1097/01.wnr.0000239956.45448.4c

Cole, M. W., Anticevic, A., Repovs, G., & Barch, D. (2011). Variable global dysconnectivity and individual differences in schizophrenia. *Biol. Psychiatry, 70*(1), 43-50. doi:10.1016/j.biopsych.2011.02.010

Craddock, R. C., James, G. A., Holtzheimer, P. E., 3rd, Hu, X. P., & Mayberg, H. S. (2012). A whole brain fMRI atlas generated via spatially constrained spectral clustering. *Hum. Brain Mapp., 33*(8), 1914-1928. doi:10.1002/hbm.21333

Da-Ano, R., Masson, I., Lucia, F., Doré, M., Robin, P., Alfieri, J., . . . Hatt, M. (2020). Performance comparison of modified ComBat for harmonization of radiomic features for multicenter studies. *Sci. Rep., 10*(1), 10248. doi:10.1038/s41598-020-66110-w

Di Martino, A., Yan, C. G., Li, Q., Denio, E., Castellanos, F. X., Alaerts, K., . . . Milham, M. P. (2014). The autism brain imaging data exchange: towards a large-scale evaluation of the intrinsic brain architecture in autism. *Mol. Psychiatry, 19*(6), 659-667. doi:10.1038/mp.2013.78

Doyle-Thomas, K. A. R., Lee, W., Foster, N. E. V., Tryfon, A., Ouimet, T., Hyde, K. L., . . . NeuroDevNet, A. S. D. I. G. (2015). Atypical functional brain connectivity during rest in autism spectrum disorders. *Ann. Neurol., 77*(5), 866-876. doi:10.1002/ana.24391

Du, Y., Pearlson, G. D., Yu, Q., He, H., Lin, D., Sui, J., . . . Calhoun, V. D. (2016). Interaction among subsystems within default mode network diminished in schizophrenia patients: A dynamic connectivity approach. *Schizophr. Res., 170*(1), 55-65. doi:10.1016/j.schres.2015.11.021

Eilam-Stock, T., Xu, P., Cao, M., Gu, X., Van Dam, N. T., Anagnostou, E., . . . Fan, J. (2014). Abnormal autonomic and associated brain activities during rest in autism spectrum disorder. *Brain, 137*(Pt 1), 153-171. doi:10.1093/brain/awt294

Falahpour, M., Thompson, W. K., Abbott, A. E., Jahedi, A., Mulvey, M. E., Datko, M., . . . Müller, R.-A. (2016). Underconnected, But Not Broken? Dynamic Functional Connectivity MRI Shows Underconnectivity in Autism Is Linked to Increased Intra-Individual Variability Across Time. *Brain Connect., 6*(5), 403-414. doi:10.1089/brain.2015.0389

Fang, X., Wang, Y., Cheng, L., Zhang, Y., Zhou, Y., Wu, S., . . . Jiang, T. (2018). Prefrontal dysconnectivity links to working memory deficit in first-episode schizophrenia. *Brain Imaging Behav., 12*(2), 335-344. doi:10.1007/s11682-017-9692-0

First, M. B., & Gibbon, M. (2004). The Structured Clinical Interview for DSM-IV Axis I Disorders (SCID-I) and the Structured Clinical Interview for DSM-IV Axis II Disorders (SCID-II). In M. J. Hilsenroth (Ed.), *Comprehensive handbook of psychological assessment, Vol* (Vol. 2, pp. 134-143). Hoboken, NJ, US: John Wiley & Sons Inc, xvi.

Guo, W., Yao, D., Jiang, J., Su, Q., Zhang, Z., Zhang, J., . . . Xiao, C. (2014). Abnormal default-mode network homogeneity in first-episode, drug-naive schizophrenia at rest. *Prog. Neuropsychopharmacol. Biol. Psychiatry, 49*, 16-20. doi:10.1016/j.pnpbp.2013.10.021

Hahamy, A., Behrmann, M., & Malach, R. (2015). The idiosyncratic brain: distortion of spontaneous connectivity patterns in autism spectrum disorder. *Nat. Neurosci., 18*(2), 302-309. doi:10.1038/nn.3919

He, Z., Deng, W., Li, M., Chen, Z., Jiang, L., Wang, Q., . . . Li, T. (2013). Aberrant intrinsic brain activity and cognitive deficit in first-episode treatment-naive patients with schizophrenia. *Psychol. Med., 43*(4), 769-780. doi:10.1017/S0033291712001638

Hedges, L. V., & Olkin, I. (1985). Statistical Methods for Meta-Analysis (San Diego, CA: Academic).

Hill, K., Mann, L., Laws, K. R., Stephenson, C. M. E., Nimmo-Smith, I., & McKenna, P. J. (2004). Hypofrontality in schizophrenia: a meta-analysis of functional imaging studies. *Acta Psychiatr. Scand., 110*(4), 243-256. doi:10.1111/j.1600-0447.2004.00376.x

Holt, D. J., Cassidy, B. S., Andrews-Hanna, J. R., Lee, S. M., Coombs, G., Goff, D. C., . . . Moran, J. M. (2011). An anterior-to-posterior shift in midline cortical activity in schizophrenia during self-reflection. *Biol. Psychiatry, 69*(5), 415-423. doi:10.1016/j.biopsych.2010.10.003

Hoptman, M. J., Antonius, D., Mauro, C. J., Parker, E. M., & Javitt, D. C. (2014). Cortical thinning, functional connectivity, and mood-related impulsivity in schizophrenia: relationship to aggressive attitudes and behavior. *Am. J. Psychiatry, 171*(9), 939-948. doi:10.1176/appi.ajp.2014.13111553

Huang, X.-Q., Lui, S., Deng, W., Chan, R. C. K., Wu, Q.-Z., Jiang, L.-J., . . . Gong, Q.-Y. (2010). Localization of cerebral functional deficits in treatment-naive, first-episode schizophrenia using resting-state fMRI. *Neuroimage, 49*(4), 2901-2906. doi:10.1016/j.neuroimage.2009.11.072

Hull, J. V., Dokovna, L. B., Jacokes, Z. J., Torgerson, C. M., Irimia, A., & Van Horn, J. D. (2016). Resting-State Functional Connectivity in Autism Spectrum Disorders: A Review. *Front. Psychiatry, 7*, 205. doi:10.3389/fpsyt.2016.00205

Iidaka, T. (2015). Resting state functional magnetic resonance imaging and neural network classified autism and control. *Cortex, 63*, 55-67. doi:10.1016/j.cortex.2014.08.011

Jang, J. H., Jung, W. H., Choi, J.-S., Choi, C.-H., Kang, D.-H., Shin, N. Y., . . . Kwon, J. S. (2011). Reduced prefrontal functional connectivity in the default mode network is related to greater psychopathology in subjects with high genetic loading for schizophrenia. *Schizophr. Res., 127*(1-3), 58-65. doi:10.1016/j.schres.2010.12.022

Johnson, W. E., Li, C., & Rabinovic, A. (2007). Adjusting batch effects in microarray expression data using empirical Bayes methods. *Biostatistics, 8*(1), 118-127. doi:10.1093/biostatistics/kxj037

Jones, T. B., Bandettini, P. A., Kenworthy, L., Case, L. K., Milleville, S. C., Martin, A., & Birn, R. M. (2010). Sources of group differences in functional connectivity: an

investigation applied to autism spectrum disorder. *Neuroimage, 49*(1), 401-414. doi:10.1016/j.neuroimage.2009.07.051

Joshi, G., Arnold Anteraper, S., Patil, K. R., Semwal, M., Goldin, R. L., Furtak, S. L., . . . Whitfield-Gabrieli, S. (2017). Integration and Segregation of Default Mode Network Resting-State Functional Connectivity in Transition-Age Males with High-Functioning Autism Spectrum Disorder: A Proof-of-Concept Study. *Brain Connect., 7*(9), 558-573. doi:10.1089/brain.2016.0483

Jung, M., Kosaka, H., Saito, D. N., Ishitobi, M., Morita, T., Inohara, K., . . . Iidaka, T. (2014). Default mode network in young male adults with autism spectrum disorder: relationship with autism spectrum traits. *Mol. Autism, 5*, 35. doi:10.1186/2040-2392-5-35

Just, M. A., Keller, T. A., Malave, V. L., Kana, R. K., & Varma, S. (2012). Autism as a neural systems disorder: a theory of frontal-posterior underconnectivity. *Neurosci. Biobehav. Rev., 36*(4), 1292-1313. doi:10.1016/j.neubiorev.2012.02.007

Karbasforoushan, H., & Woodward, N. D. (2012). Resting-state networks in schizophrenia. *Curr. Top. Med. Chem., 12*(21), 2404-2414. doi:10.2174/156802612805289863

Kyriakopoulos, M., Dima, D., Roiser, J. P., Corrigall, R., Barker, G. J., & Frangou, S. (2012). Abnormal functional activation and connectivity in the working memory network in early-onset schizophrenia. *J. Am. Acad. Child Adolesc. Psychiatry, 51*(9), 911-920.e912. doi:10.1016/j.jaac.2012.06.020

Lee, J. M., Kyeong, S., Kim, E., & Cheon, K.-A. (2016). Abnormalities of Inter- and Intra-Hemispheric Functional Connectivity in Autism Spectrum Disorders: A Study Using the Autism Brain Imaging Data Exchange Database. *Front. Neurosci., 10*, 191. doi:10.3389/fnins.2016.00191

Li, S., Hu, N., Zhang, W., Tao, B., Dai, J., Gong, Y., . . . Lui, S. (2019). Dysconnectivity of Multiple Brain Networks in Schizophrenia: A Meta-Analysis of Resting-State Functional Connectivity. *Front. Psychiatry, 10*, 482. doi:10.3389/fpsyt.2019.00482

Liu, Y., Xu, L., Li, J., Yu, J., & Yu, X. (2020). Attentional Connectivity-based Prediction of Autism Using Heterogeneous rs-fMRI Data from CC200 Atlas. *Exp. Neurobiol., 29*(1), 27-37. doi:10.5607/en.2020.29.1.27

Long, Z., Duan, X., Mantini, D., & Chen, H. (2016). Alteration of functional connectivity in autism spectrum disorder: effect of age and anatomical distance. *Sci. Rep., 6*, 26527. doi:10.1038/srep26527

Lui, S., Li, T., Deng, W., Jiang, L., Wu, Q., Tang, H., . . . Gong, Q. (2010). Short-term effects of antipsychotic treatment on cerebral function in drug-naive first-episode schizophrenia revealed by "resting state" functional magnetic resonance imaging. *Arch. Gen. Psychiatry, 67*(8), 783-792. doi:10.1001/archgenpsychiatry.2010.84

Lui, S., Yao, L., Xiao, Y., Keedy, S. K., Reilly, J. L., Keefe, R. S., . . . Sweeney, J. A. (2015). Resting-state brain function in schizophrenia and psychotic bipolar probands and their first-degree relatives. *Psychol. Med., 45*(1), 97-108. doi:10.1017/S003329171400110X

Maximo, J. O., Keown, C. L., Nair, A., & Müller, R.-A. (2013). Approaches to local connectivity in autism using resting state functional connectivity MRI. *Front. Hum. Neurosci., 7*, 605. doi:10.3389/fnhum.2013.00605

Meda, S. A., Gill, A., Stevens, M. C., Lorenzoni, R. P., Glahn, D. C., Calhoun, V. D., . . . Pearlson, G. D. (2012). Differences in resting-state functional magnetic resonance imaging functional network connectivity between schizophrenia and psychotic bipolar probands and their unaffected first-degree relatives. *Biol. Psychiatry, 71*(10), 881-889. doi:10.1016/j.biopsych.2012.01.025

Meda, S. A., Ruaño, G., Windemuth, A., O'Neil, K., Berwise, C., Dunn, S. M., . . . Pearlson, G. D. (2014). Multivariate analysis reveals genetic associations of the resting default mode network in psychotic bipolar disorder and schizophrenia. *Proc. Natl. Acad. Sci. U. S. A., 111*(19), E2066-2075. doi:10.1073/pnas.1313093111

Mingoia, G., Wagner, G., Langbein, K., Maitra, R., Smesny, S., Dietzek, M., . . . Nenadic, I. (2012). Default mode network activity in schizophrenia studied at resting state using probabilistic ICA. *Schizophr. Res., 138*(2-3), 143-149. doi:10.1016/j.schres.2012.01.036

Monk, C. S., Peltier, S. J., Wiggins, J. L., Weng, S.-J., Carrasco, M., Risi, S., & Lord, C. (2009). Abnormalities of intrinsic functional connectivity in autism spectrum disorders. *Neuroimage, 47*(2), 764-772. doi:10.1016/j.neuroimage.2009.04.069

Murdaugh, D. L., Shinkareva, S. V., Deshpande, H. R., Wang, J., Pennick, M. R., & Kana, R. K. (2012). Differential deactivation during mentalizing and classification of autism based on default mode network connectivity. *PLoS One, 7*(11), e50064. doi:10.1371/journal.pone.0050064

Mwansisya, T. E., Wang, Z., Tao, H., Zhang, H., Hu, A., Guo, S., & Liu, Z. (2013). The diminished interhemispheric connectivity correlates with negative symptoms and cognitive impairment in first-episode schizophrenia. *Schizophr. Res., 150*(1), 144-150. doi:10.1016/j.schres.2013.07.018

Newton, A. T., Rogers, B. P., Gore, J. C., & Morgan, V. L. (2012). Improving measurement of functional connectivity through decreasing partial volume effects at 7 T. *Neuroimage, 59*(3), 2511-2517. doi:10.1016/j.neuroimage.2011.08.096

Ongür, D., Lundy, M., Greenhouse, I., Shinn, A. K., Menon, V., Cohen, B. M., & Renshaw, P. F. (2010). Default mode network abnormalities in bipolar disorder and schizophrenia. *Psychiatry Res., 183*(1), 59-68. doi:10.1016/j.pscychresns.2010.04.008

Paakki, J.-J., Rahko, J., Long, X., Moilanen, I., Tervonen, O., Nikkinen, J., . . . Kiviniemi, V. (2010). Alterations in regional homogeneity of resting-state brain activity in autism spectrum disorders. *Brain Res., 1321*, 169-179. doi:10.1016/j.brainres.2009.12.081

Penner, J., Ford, K. A., Taylor, R., Schaefer, B., Théberge, J., Neufeld, R. W. J., . . . Williamson, P. C. (2016). Medial Prefrontal and Anterior Insular Connectivity in Early Schizophrenia and Major Depressive Disorder: A Resting Functional MRI Evaluation of Large-Scale Brain Network Models. *Front. Hum. Neurosci., 10*, 132. doi:10.3389/fnhum.2016.00132

Peter, F., Andrea, S., & Nancy, A. (2018). Forty years of structural brain imaging in mental disorders: is it clinically useful or not? *Dialogues Clin. Neurosci., 20*(3), 179-186.

Rane, S., Mason, E., Hussey, E., Gore, J., Ally, B. A., & Donahue, M. J. (2014). The effect of echo time and post-processing procedure on blood oxygenation level-dependent (BOLD) functional connectivity analysis. *Neuroimage, 95*, 39-47. doi:10.1016/j.neuroimage.2014.03.055

Rao, A., & Joao, M. (2017). Predictive modelling using neuroimaging data in the presence of confounds. *Neuroimage*.

Su, T.-W., Lan, T.-H., Hsu, T.-W., Biswal, B. B., Tsai, P.-J., Lin, W.-C., & Lin, C.-P. (2013). Reduced neuro-integration from the dorsolateral prefrontal cortex to the whole brain and executive dysfunction in schizophrenia patients and their relatives. *Schizophr. Res., 148*(1-3), 50-58. doi:10.1016/j.schres.2013.05.005

Tamminga, C. A., Ivleva, E. I., Keshavan, M. S., Pearlson, G. D., Clementz, B. A., Witte, B., . . . Sweeney, J. A. (2013). Clinical phenotypes of psychosis in the Bipolar-Schizophrenia Network on Intermediate Phenotypes (B-SNIP). *Am. J. Psychiatry, 170*(11), 1263-1274. doi:10.1176/appi.ajp.2013.12101339

Van Horn, J. D., & Toga, A. W. (2009). Multisite neuroimaging trials. *Curr. Opin. Neurol., 22*(4), 370-378. doi:10.1097/WCO.0b013e32832d92de

von dem Hagen, E. A. H., Stoyanova, R. S., Baron-Cohen, S., & Calder, A. J. (2013). Reduced functional connectivity within and between 'social' resting state networks in autism spectrum conditions. *Soc. Cogn. Affect. Neurosci., 8*(6), 694-701. doi:10.1093/scan/nss053

Washington, S. D., Gordon, E. M., Brar, J., Warburton, S., Sawyer, A. T., Wolfe, A., . . . VanMeter, J. W. (2014). Dysmaturation of the default mode network in autism. *Hum. Brain Mapp., 35*(4), 1284-1296. doi:10.1002/hbm.22252

Weng, S.-J., Wiggins, J. L., Peltier, S. J., Carrasco, M., Risi, S., Lord, C., & Monk, C. S. (2010). Alterations of resting state functional connectivity in the default network in adolescents with autism spectrum disorders. *Brain Res., 1313*, 202-214. doi:10.1016/j.brainres.2009.11.057

Yamashita, A., Yahata, N., Itahashi, T., Lisi, G., Yamada, T., Ichikawa, N., . . . Imamizu, H. (2019). Harmonization of resting-state functional MRI data across multiple imaging sites via the separation of site differences into sampling bias and measurement bias. *PLoS Biol., 17*(4), e3000042. doi:10.1371/journal.pbio.3000042

Yerys, B. E., Gordon, E. M., Abrams, D. N., Satterthwaite, T. D., Weinblatt, R., Jankowski, K. F., . . . Vaidya, C. J. (2015). Default mode network segregation and social deficits in autism spectrum disorder: Evidence from non-medicated children. *NeuroImage: Clinical, 9*, 223-232. doi:10.1016/j.nicl.2015.07.018

Yu, M., Linn, K. A., Cook, P. A., Phillips, M. L., McInnis, M., Fava, M., . . . Sheline, Y. I. (2018). Statistical harmonization corrects site effects in functional connectivity measurements from multi-site fMRI data. *Hum. Brain Mapp., 39*(11), 4213-4227. doi:10.1002/hbm.24241

Zhou, Y., Ma, X., Wang, D., Qin, W., Zhu, J., Zhuo, C., & Yu, C. (2015). The selective impairment of resting-state functional connectivity of the lateral subregion of the frontal pole in schizophrenia. *PLoS One, 10*(3), e0119176. doi:10.1371/journal.pone.0119176

Zuo, X.-N., Xu, T., Jiang, L., Yang, Z., Cao, X.-Y., He, Y., . . . Milham, M. P. (2013). Toward reliable characterization of functional homogeneity in the human brain: preprocessing, scan duration, imaging resolution and computational space. *Neuroimage, 65*, 374-386. doi:10.1016/j.neuroimage.2012.10.017

Chapter 3

Subtyping Autism Spectrum Disorder via Joint Modeling of Clinical and Connectomic Profiles

3.1 Abstract

Autism Spectrum Disorder (ASD) is a highly heterogeneous developmental disorder with diverse clinical manifestations. Neuroimaging studies have explored functional connectivity (FC) of ASD through resting-state functional MRI studies, however the findings have remained inconsistent, thus reflecting the possibility of multiple subtypes. Identification of the relationship between clinical symptoms and FC measures may help clarify the inconsistencies in earlier findings and advance our understanding of ASD subtypes. Canonical correlation analysis was performed on two-hundred and ten ASD subjects from the Autism Brain Imaging Data Exchange to identify significant linear combinations of resting-state connectomic and clinical profiles of ASD. Then, hierarchical

clustering defined ASD subtypes based on distinct brain-behavior relationships. Finally, a support vector machine classifier was used to verify that subtypes were comprised of subjects with distinct clinical and connectivity features. Three ASD subtypes were identified. Subtype 1 exhibited increased intra-network FC, increased IQ scores and restricted and repetitive behaviors. Subtype 2 was characterized by decreased whole-brain FC and more severe ADI-R and SRS symptoms. Subtype 3 demonstrated mixed FC, low IQ scores, as well as social motivation and verbal deficits. To verify subtype assignment, a multi-class support vector machine using connectomic and clinical profiles yielded an average accuracy of 71.3% and 65.2% respectively for subtype classification, which is significantly higher than chance (33.3%). The present study demonstrates that combining connectomic and behavioral measures is a powerful approach for disease subtyping and suggests that there are ASD subtypes with distinct connectomic and clinical profiles.

3.2 Introduction

Autism Spectrum Disorder (ASD) is a heterogeneous disorder characterized by deficits in social communication and social interaction, as well as restricted and repetitive behaviors (RRBs) (American Psychiatric, 2013). The symptoms and severities of ASD vary widely; social communication deficits range from nonverbal ASD to difficulty interacting and relating to others, while RRBs range from self-stimming behaviors to intense and restricted focus (American Psychiatric, 2013). In addition, there is variation in cognitive impairments implicated in the disorder; ASD is comorbid with intellectual disabilities 50-80% of the time (Simonoff et al., 2008), while approximately 44% of individuals with ASD have IQ scores in the average to above average range (Maenner et al., 2020). The underlying brain connectivity associated with the deficits in ASD behavior and cognition is not fully understood.

Resting-state functional connectivity (FC) patterns are predictive of clinical symptoms in ASD (Plitt et al., 2015). The default mode network (DMN) is the most highly implicated network in ASD and plays a role in social functions, mentalizing, and theory of mind (Padmanabhan et al., 2017). To date, no consistent pattern of aberrant FC in ASD has emerged in the literature (see Hull et al., 2016). Studies reporting hyperconnectivity across brain networks, including the DMN, have suggested hyperconnectivity is associated with RRB severity (Dupong et al., 2020; McKinnon et al., 2019; Monk et al., 2009; Uddin et al., 2013a). However, other studies have indicated that hypoconnectivity across brain regions is predictive of RRB severity (Assaf et al., 2010; Weng et al., 2010). In addition, several studies have found anterior-posterior hypoconnectivity involving regions of the

DMN in ASD, and the degree of hypoconnectivity was predictive of severity of social impairments (Assaf et al., 2010; Weng et al., 2010; Yerys et al., 2015).

The heterogeneity of FC patterns in ASD has led to the development of several competing neurodevelopmental models of ASD. These theories include the hypoconnectivity hypothesis (Just et al., 2012), aberrant within- and between-network connectivity (Lynch et al., 2013; Monk et al., 2009; Yerys et al., 2015), abnormal local and long distance connections (Anderson et al., 2011; Belmonte et al., 2004), and age-related changes in connectivity (Uddin et al., 2013b). The heterogeneity in clinical presentation and neurodevelopmental models of ASD may indicate that there are ASD subtypes with distinct clinical and FC patterns.

A few studies have explored ASD subtypes based on 1) structural MRI (Hong et al., 2018; Hrdlicka et al., 2005), 2) cognitive lab tasks (Feczko et al., 2018), 3) common symptoms of ASD (Georgiades et al., 2013), and 4) resting-state functional MRI (fMRI) (Easson et al., 2019). The recent work that subtyped ASD based on resting-state FC and their clinical profiles treated the two dimensions independently (Easson et al., 2019). However, current literature has shown that FC profiles and ASD symptoms co-occur (Assaf et al., 2010; Lynch et al., 2013; Monk et al., 2009). Here, we present an alternative approach to subtype ASD using canonical correlation analysis (CCA) to examine dimensions of connectomic patterns and associated clinical profiles, aiming to elucidate the complex and heterogeneous nature of ASD.

CCA is a multivariate statistical method to identify correlations between two sets of variables (Hotelling, 1992). It has been used to identify linear combinations of

connectivity features that were correlated with a linear combination of clinical features in psychiatric disorders (Drysdale et al., 2017; Xia et al., 2018). Xia et al. linked dimensions of psychopathology with specific FC profiles, and Drysdale et al. identified linear combinations of connectivity features with major depressive disorder symptoms using CCA (Drysdale et al., 2017; Xia et al., 2018). Inspired by the above studies, we applied CCA to identify the association of brain-behavior profiles and then used hierarchical clustering to define subtypes with specific patterns of FC and clinical symptoms. Finally, we use a multiclass support vector machine (SVM) classifier with 5-fold cross validation to verify subtype assignment by predicting which subtype each subject belongs to using their FC and clinical profiles.

3.3 Materials and Methods

3.3.1 Dataset

Resting-state fMRI data and corresponding phenotypic information from the Autism Brain Imaging Data Exchange (ABIDE), an open-access consortium of neuroimaging data from more than 24 international scanning sites (Di Martino et al., 2014), were used in this analysis. Two hundred and ten ASD subjects from seven sites (ETH Zurich, Georgetown University, Kennedy Krieger Institute, New York University Langone Medical Center Sample 1, New York University Langone Medical Center Sample 2, San Diego State University, and Trinity Center for Health Sciences) with resting-state fMRI data, T1-weighted structural scans, and clinical assessments containing IQ scores, Autism Diagnostic Interview- Revised (ADI-R) assessments, and Social Responsiveness Scale

(SRS) scores were chosen for analysis. Demographic information including scanning sites, age, sex, and mean values of IQ (full scale IQ (FIQ), verbal IQ (VIQ), performance IQ (PIQ), ADI-R (social, verbal, and RRB), and SRS (awareness, cognition, communication, motivation and mannerisms) are shown in Table 3.1. Further information regarding subject medication status and comorbidities can be found in Table A1.

Table 3.1. Subject Demographic Information

Site	N	Age (years) mean ± sd	Male n (%)	IQ mean ± sd	ADI-R mean ± sd	SRS mean ± sd
ETH	10	20.5 ± 3.9	10 (100)	110.4 ± 13.2	11.8 ± 7.0	17.9 ± 11.5
GU	32	10.9 ± 1.5	29 (90.6)	119.8 ± 15.0	13.3 ±7.3	16.6 ± 8.9
KKI	49	10.3 ± 1.5	35 (71.4)	107.3 ± 15.5	13.5 ± 7.0	18.8 ± 9.3
NYU 1	44	9.5 ± 5.3	39 (88.6)	102.0 ± 17.6	12.2 ± 7.2	17.3 ± 10.0
NYU 2	23	6.7 ± 1.0	20 (87.0)	106.4 ± 15.7	13.1 ± 6.9	18.2 ± 9.3
SDSU	31	12.9 ± 3.2	25 (80.7)	99.7 ± 16.4	12.8 ± 6.6	20.8 ± 9.8
TCD	21	14.8 ± 3.3	21 (100)	107.7 ±15.4	12.0 ± 5.9	19.6 ± 9.3

Abbreviations: ETH Zurich (ETH), Georgetown University (GU), Kennedy Krieger Institute (KKI), New York University Langone Medical Center Sample 1 (NYU 1), New York University Langone Medical Center Sample 2 (NYU 2), San Diego State University (SDSU), and Trinity Center for Health Sciences (TCD), Intelligence Quotient (IQ), Autism Diagnostic Interview- Revised (ADI-R), Social Responsiveness Scale (SRS).

The ADI-R contains social, verbal, and RRB subscales. Each subscale consists of individual questions that are rated on a scale of 0-3, where a score of 0 means the behavior is not present and a score of 3 means the behavior is severely present. For each subscale, the numbers are summed and the participant is given a single score (Lord et al., 1994). The SRS contains 65 questions measuring behavior in the following social domains: awareness, cognition, communication, motivation, and mannerism. Each subscale consists of items that are scored from 1 to 4, where a score of 1 means the symptom is not present and a score of 4 means the symptom is severely present. The scores for each of the social

subscales are summed, and a single score is given to each participant for each subscale (Booker et al., 2011).

3.3.2 Image Acquisition

Imaging data used in this analysis were collected on 3T MRI scanners. Scan parameters for the resting-state fMRI protocols are summarized in Table 3.2. For each subject, a T_1-weighted structural image was collected and used for registration to MNI152 space. Full details for acquisition parameters, informed consent, and site-specific protocols can be found at http://fcon_1000.projects.nitrc.org/indi/abide/abide_I.html.

Table 3.2. Resting-state fMRI Scan Parameters

Site	Flip angle (deg)	TE (ms)	TR (ms)	# TRs	xy (mm)	z (mm)	FOV (mm^2)
ETH	90	25	2000	120	3	3	240 × 240
GU	90	30	2000	154	3	2.5	192 × 192
KKI	75	30	2500	151	3	3	256 × 256
NYU 1	82	30	2000	180	3	3	240 × 240
NYU 2	90	15	2000	180	3	4	240 × 240
SDSU	90	30	2000	180	3.4	3.4	220 × 220
TCD	90	27	2000	210	3	3.2	240 × 240

Abbreviations: ETH Zurich (ETH), Georgetown University (GU), Kennedy Krieger Institute (KKI), New York University Langone Medical Center Sample 1 (NYU 1), New York University Langone Medical Center Sample 2 (NYU 2), San Diego State University (SDSU), and Trinity Center for Health Sciences (TCD), degrees (deg), Echo Time (TE), Repetition Time (TR), Field of View (FOV).

3.3.3 Preprocessing

The resting-state fMRI data was preprocessed using the Connectome Computation System (CCS) pipeline (Zuo et al., 2013), and was parcellated into 200 regions of interest

(ROIs) through a spectrally constrained clustering algorithm (Craddock et al., 2012). The CCS preprocessing pipeline included slice time correction, motion correction, skull stripping, global mean intensity normalization, nuisance signal regression, band pass filtering (0.01-0.1 Hz), and registration of the resting-state fMRI image to the T_1-weighted image, followed by a transformation to standard space (Zuo et al., 2013).

3.3.4 Functional Connectivity Matrices and Parcellation

Pearson's correlation coefficient was used to ascertain the FC of each ROI pair, resulting in a 200×200 FC matrix for each subject (Figure 3.1b). Each correlation coefficient was Fisher z-transformed, then linear regression was used to regress out age, sex, and site covariates to ensure that confounding variables did not affect CCA results. Cortical ROIs from the resultant residual matrices were then grouped into networks using a seven network liberal parcellation mask from Thomas Yeo (Yeo et al., 2011).

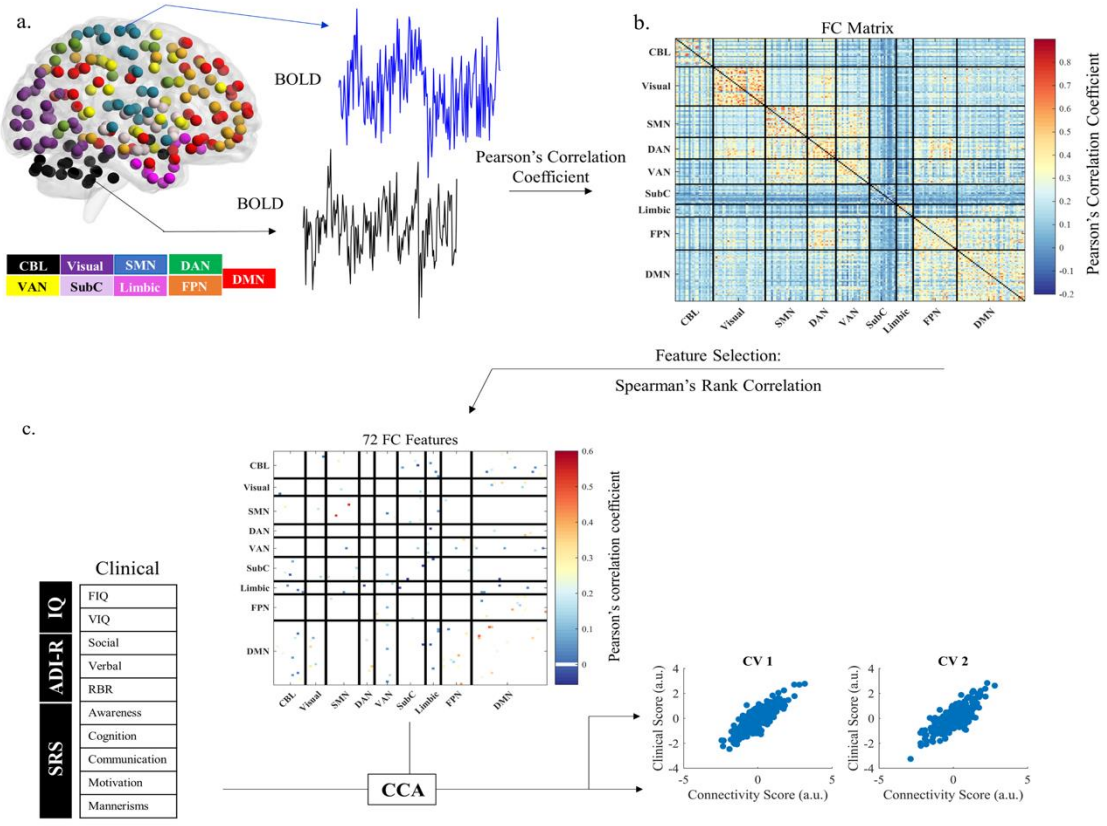

Figure 3.1. Data analysis and CCA schematic. (a) After preprocessing, blood oxygenation level dependent (BOLD) signal time series were extracted from the 200 ROIs. (b) Pearson's correlation coefficient was then used to correlate each ROI time series to construct a 200×200 FC matrix for each subject. (c) Feature selection was performed using Spearman's rank correlation coefficient to isolate the FC features that are most highly correlated with clinical features and the resulting FC and clinical profiles are used in CCA. (d) CCA then identified linear combinations of FC and clinical features and maximized their correlation. Network Assignment: Cerebellum (CBL), Somatomotor Network (SMN), Dorsal Attention Network (DAN), Ventral Attention Network (VAN), Subcortical (SubC) ROIs, Frontoparietal Network (FPN), Default Mode Network (DMN), Canonical Variate (CV).

3.3.5 Feature Selection

The FC matrices contain 19,900 (200 × 199/2) unique connectivity features for every subject. To identify non-redundant and relevant connectivity features that will lead to

meaningful ASD subtypes based on correlated clinical and connectivity features, we selected a subset of connectivity features using Spearman's rank correlation coefficients. The top 100 FC features that were most highly correlated with one or more of the 11 clinical features were selected using MATLAB's *corr* function. The variance inflation factor (VIF) was used to assess the degree of multicollinearity among the 11 clinical and 100 FC variables to ensure the absence of multicollinearity prior to CCA. A VIF of less than 5-10 is generally considered to be absent of multicollinearity (Gareth et al., 2013). We removed highly correlated variables to ensure a VIF of less than 5, thus confirming that variables in each of the datasets are not collinear. The neuroanatomical distribution of the nodes of the remaining FC features were depicted in Figure 3.2 using BrainNet Viewer (Xia et al., 2013).

3.3.6 Canonical Correlation Analysis (CCA)

CCA is an unsupervised learning technique that assigns loadings to two sets of variables in order to maximize their correlation (Hotelling, 1992). Here, we used CCA to identify linear combinations of FC and clinical features to define a low dimensional representation of the selected features in subjects with ASD. The input data consisted of 72 unique FC features and 10 clinical variables. Each resulting linear combination ("canonical variate") represents a weighted set of FC features that are related to a weighted set of clinical features (Figure 3.1c). Bartlett's chi square test was used to evaluate canonical correlations and the corresponding p-value (the right tail significance level for χ^2) was used to test for the significance of canonical correlations (Sánchez, 1982). The

connectivity patterns from the first two canonical variates (CV) were used as the dimensions for which subjects were projected onto for subtyping.

3.3.7 Hierarchical Clustering

We applied hierarchical clustering to define distinct subtypes of ASD with linked FC and clinical profiles along the first two CV dimensions. The optimal number of clusters was determined using the Calinski-Harabsz method, which maximizes the between-subtype to within-subtype variance while maintaining a sufficient number of subjects in each subtype to be able to sustain high statistical power to detect subtype differences. To identify subtypes, a dissimilarity matrix describing the Euclidean distance between each pair of subjects was calculated using MATLAB's *pdist* function, then the *linkage* function was used to iteratively link pairs of subjects in close proximity using the Ward's minimum variance method.

3.3.8 FC and Clinical Differences between Subtypes

A Kruskal-Wallis one-way ANOVA with false-discovery rate (FDR) correction was used to identify FC differences between the three subtypes. The assumptions were checked to ensure the distributions had the same shape prior to performing the Kruskal-Wallis ANOVA. To determine the unique resting-state FC patterns associated with each ASD subtype, Wilcoxon rank-sum tests were used to test for differences between the resting-state profiles of each subtype compared to the other two. The z-value of the FC features that significantly differed ($P < 0.05$, FDR corrected) between subtypes indicate strength in

connectivity compared to the other subtypes. To identify FC features that differed most between subtypes, Bonferroni correction was applied for the number of FC features tested ($P < 0.0007$).

To determine whether subtypes of ASD defined by resting-state FC patterns were associated with specific clinical features, Kruskal-Wallis one-way ANOVAs and post-hoc multiple comparisons Tukey Analysis were used to investigate the clinical differences between the subtypes. A Kruskal-Wallis one-way ANOVA was also used to ensure that there were no significant between-subtype differences in age, and a chi-square goodness of fit test was used to ensure there were no significant between-subtype differences in comorbidity status, medication status, sex, or scan site.

3.3.9 Subtype Verification

To ensure distinct FC biomarkers and clinical features were associated with each subtype, an SVM classifier was used on FC profiles and clinical profiles independently to determine if subjects could be accurately classified through each domain. A one-versus-all multiclass SVM classifier with a linear kernel function was used on the 72 FC and 10 clinical features identified through feature selection. Classifier training was performed using *libsvm* toolbox (a library for support vector machines) and the ***multisvm*** function in MATLAB (Chang et al., 2011; Cody, 2012). Five-fold cross validation was used to validate the trained model. The performance of classification was evaluated using sensitivity, specificity, f1-measure, and macro-average f1 measure.

3.4 Results

3.4.1 Feature Selection

Spearman's rank correlation identified 100 FC features that were most highly correlated with ASD symptoms ($P < 5.15 \times 10^{-4}$). Each of the 11 clinical features were highly correlated with at least one of the 100 FC features ensuring the use of all variables in CCA. Multicollinear features were removed for both clinical and FC datasets to ensure the absence of multicollinearity prior to CCA; one clinical feature (PIQ) was removed from the clinical dataset and 28 FC features were removed from the FC dataset. The resulting 10 clinical and 72 FC features with a VIF of less than 5 were used in CCA. The majority of the FC features were from the DMN (25 FC features), followed by the visual network (18 FC features), frontoparietal network (FPN) (11 FC features), subcortical (SubC) regions (11 FC features), somatomotor network (SMN) (9 FC features), cerebellar (CBL) regions (9 FC features), ventral attention network (VAN) (9 FC features), limbic network (5 FC features), and the dorsal attention network (DAN) (2 FC features). The neuroanatomical distribution of the nodes associated with the 72 FC features were viewed using BrainNetViewer (Xia et al., 2013) (Figure 3.2; Table A2).

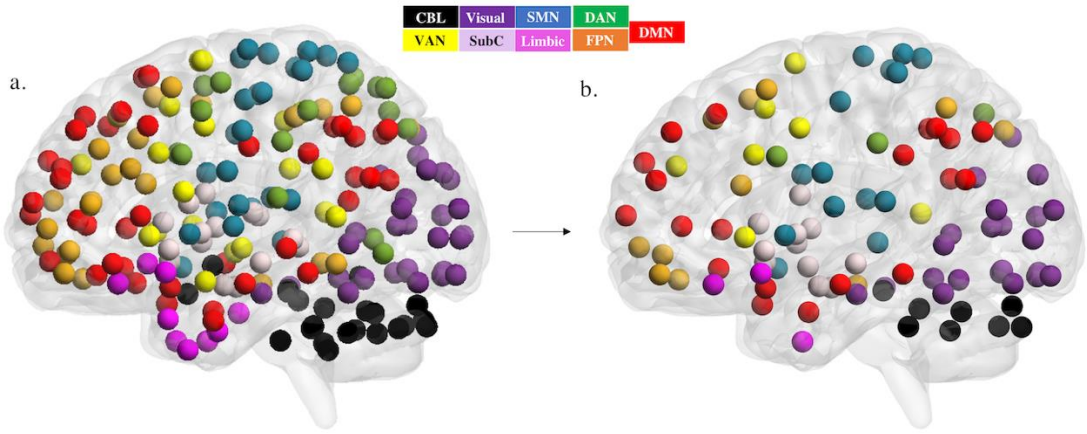

Figure 3.2. The neuroanatomical distributions of the FC features identified using Spearman's rank correlation coefficient. (a) Neuroanatomical distribution of all 200 ROIs prior to dimension reduction. (b) Neuroanatomical distributions associated with the 72 FC features identified during Spearman's rank correlation coefficients ($P < 5.15 \cdot 10^{-4}$) with the highest correlation to clinical features, followed by removal of variables (VIF < 5) to ensure the absence of multicollinearity. See Table A2 for the full names and MNI coordinates of ROIs in b. Network Assignment: Cerebellum (CBL), Somatomotor Network (SMN), Dorsal Attention Network (DAN), Ventral Attention Network (VAN), Subcortical (SubC) ROIs, Frontoparietal Network (FPN), Default Mode Network (DMN).

3.4.2 Linked Connectivity and Clinical Features

CCA identified CVs that represented linear combinations of brain connectivity and clinical features. The first CV ($P < 0.001$, R = 0.75) was defined by FCs predominantly involving the DMN (including within DMN FC) and SubC/limbic network (Figure 3.3a-c; Tables A3-4). This combination of connectivity features was correlated with a combination of social cognition (standardized loading: 0.66) and verbal features (standardized loading: 0.35) of ASD. The proportion of variance explained by the clinical and FC features for the first CV, indicated by the squared canonical correlation was 56.9% ($R^2_{CV1} = 0.569$). The second CV ($P < 0.001$, R = 0.74) was defined by predominantly intra

network DMN FC, SubC/limbic network, and CBL FC (Figure 3.3d-f; Tables A5-6). This combination of connectivity features was correlated with a combination of social motivation (standardized loading: -0.70), verbal (standardized loading: -0.56), social awareness (standardized loading: 0.48), and RRB (standardized loading: 0.47) symptoms of ASD. The proportion of variance explained by the clinical and FC features for the second CV was 55.1% (R^2_{CV2} = 0.551).

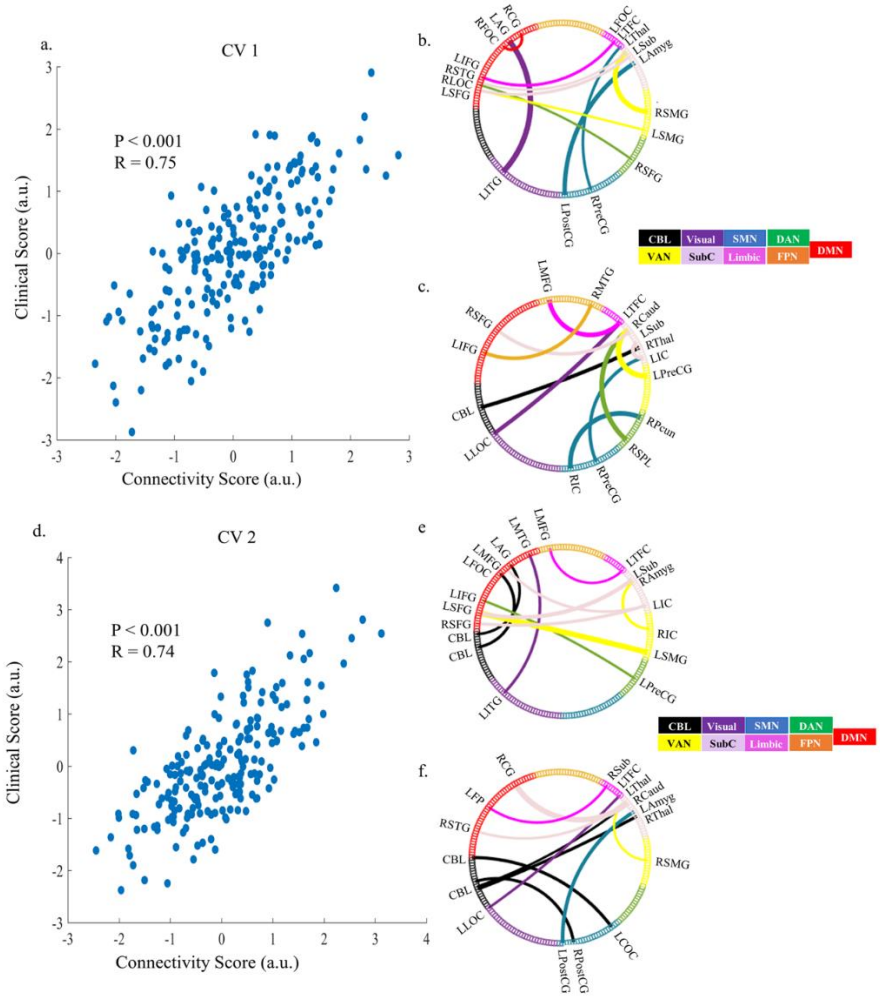

Figure 3.3. Significant Canonical Variates (CVs). (a) Scatter plots depicting the linear combination of FC and clinical features for the first CV. Standardized clinical loading scores of the clinical features with the highest loadings: SRS-cognition (0.66) and ADI-R verbal scores (0.35). (b) Circle plot depicting the top ten positive loading connections contributing to the first CV. (c) Circle plot depicting the top ten negative connections contributing to the first CV. ROI network membership is denoted by the colored legend. See Tables A3-4 for MNI coordinates for ROIs in b and c. (d) Scatter plots showing the linear combination of FC and clinical features for the second CV. Standardized clinical loadings scores of the clinical features with the highest loadings: SRS-motivation (-0.70), ADI-R verbal (-0.56), SRS-awareness (0.48), and ADI-R RRB (0.47). (e) Circle plot depicting the top ten positive loading connections contributing to the second CV. (f) Circle plot depicting the top ten negative connections contributing to the second CV. See Tables A5-6 for MNI coordinates for ROIs in e and f. Abbreviations: Left Inferior Temporal Gyrus (LITG), Right/Left Postcentral Gyrus (R/L PostCG), Right/Left Precentral Gyrus (R/L PreCG), Right/Left Superior Frontal Gyrus (R/L SFG), Right/Left Supramarginal Gyrus (R/L SMG), Right/Left Amygdala (R/L Amyg), Right/Left Subcallosal Gyrus (R/L Sub), Right Thalamus (RThal), Left Temporal Fusiform Cortex (LTFC), Right/Left Frontal Orbital Cortex (R/L FOC), Right Cingulate Gyrus (RCG), Left Angular Gyrus (LAG), Left Inferior Frontal Gyrus (LIFG), Right Superior Temporal Gyrus (RSTG), Right/Left Lateral Occipital Cortex (R/L LOC), Cerebellum (CBL), Right/Left Insular Cortex (R/L IC), Right Superior Parietal Lobule (RSPL), Right Precuneus Cortex (RPcun), Right Caudate (RCaud), Right Middle Temporal Gyrus (RMTG), Left Middle Frontal Gyrus (LMFG), Left Central Opercular Cortex (LCOC), Left Frontal Pole (LFP).

3.4.3 Hierarchical Clustering

The Calinski-Harabasz criterion resulted in three as the optimal number of subtypes. Hierarchical clustering with Euclidean distance identified three subtypes of ASD along the first two CV dimensions; there are 47 subjects in subtype 1 (22.4%), 55 subjects in subtype 2 (26.2%) and 108 subjects in subtype 3 (51.4%) (Figure 3.4). There were no significant between-subtype differences in age, site, sex, medication status, or comorbidities.

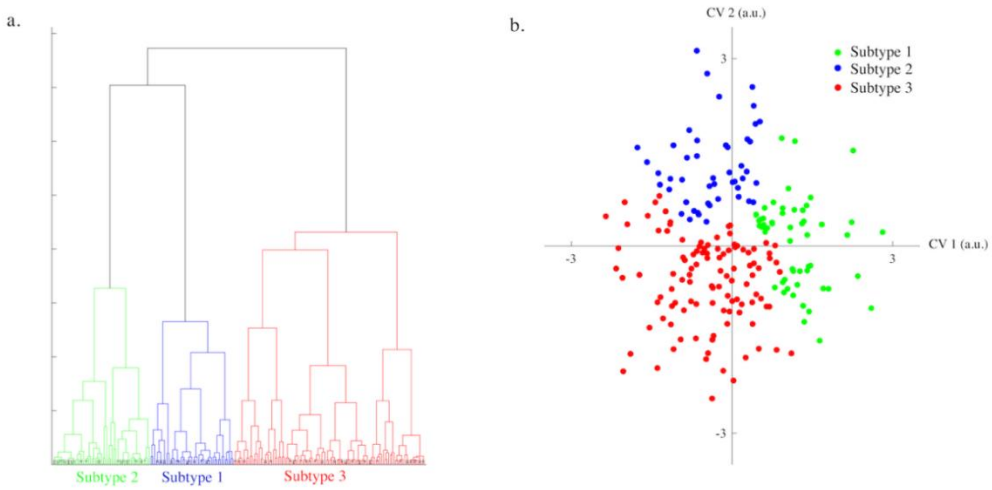

Figure 3.4. Hierarchical Clustering. (a) Dendrogram of hierarchical clustering with Ward's minimum variance showing the three-cluster solution. The height of the links in the dendrogram represent the distance between the clusters. (b) Hierarchical clustering identified three distinct clusters along the first two CVs.

3.4.4 Clinical and FC Features Define Three ASD Subtypes

Kruskal-Wallis one-way ANOVAs and post-hoc multiple comparisons Tukey Analysis were used to determine the clinical differences between subtypes. This analysis identified that all ten of the clinical features significantly differed across subtypes: FIQ (P = 0.01, χ^2

= 9.2), VIQ ($P = 0.01$, $\chi^2 = 9.3$), ADI-R social ($P < 0.001$, $\chi^2 = 19.7$), verbal ($P < 0.001$, $\chi^2 = 35.0$), RRB ($P < 0.001$, $\chi^2 = 29.8$), SRS awareness ($P < 0.001$, $\chi^2 = 26.2$), cognition ($P < 0.001$, $\chi^2 = 52.8$), communication ($P < 0.001$, $\chi^2 = 35.4$), mannerisms ($P < 0.001$, $\chi^2 = 27.2$), and motivation ($P < 0.001$, $\chi^2 = 26.2$) (Figure 3.5).

Subtype 1 is characterized by significantly higher RRB ($P = 0.02$, $\chi^2 = 28.2$), FIQ ($P = 0.009$, $\chi^2 = 13.1$) and VIQ scores ($P = 0.007$, $\chi^2 = 32.3$) compared to subtype 3. Subtype 2 is characterized by deficits in all clinical features across ADI-R and SRS scales, as indicated by significantly higher scores than subtype 1 across ADI-R social ($P < 0.01$, $\chi^2 = -53.2$), ADI-R verbal ($P < 0.01$, $\chi^2 = -71.2$), SRS awareness ($P = 0.007$, $\chi^2 = -36.6$), SRS cognition ($P < 0.001$, $\chi^2 = -73.2$), SRS communication ($P < 0.001$, $\chi^2 = -62.5$), SRS mannerisms ($P < 0.001$, $\chi^2 = -49.4$), and SRS motivation ($P < 0.001$, $\chi^2 = -59.6$) symptoms. Subtype 2 exhibited significantly higher scores compared to subtype 3 across ADI-R social ($P = 0.013$, $\chi^2 = 28.3$), ADI-R verbal ($P = 0.004$, $\chi^2 = 32.4$), ADI-R RRB ($P = < 0.001$, $\chi^2 = 53.4$), SRS awareness ($P < 0.001$, $\chi^2 = 51.3$), SRS cognition ($P < 0.001$, $\chi^2 = 67.1$), SRS communication ($P < 0.001$, $\chi^2 = 53.3$), and SRS mannerism ($P < 0.001$ $\chi^2 = 49.8$) symptoms. Subtype 3 is characterized by significantly lower FIQ ($P = 0.009$, $\chi^2 = 31.1$) and VIQ ($P = 0.007$, $\chi^2 = 32.3$) than subtype 1, as well as significant verbal deficits ($P < 0.001$, $\chi^2 = -38.8$) and social motivation deficits ($P < 0.001$, $\chi^2 = -43.2$) compared to subtype 1.

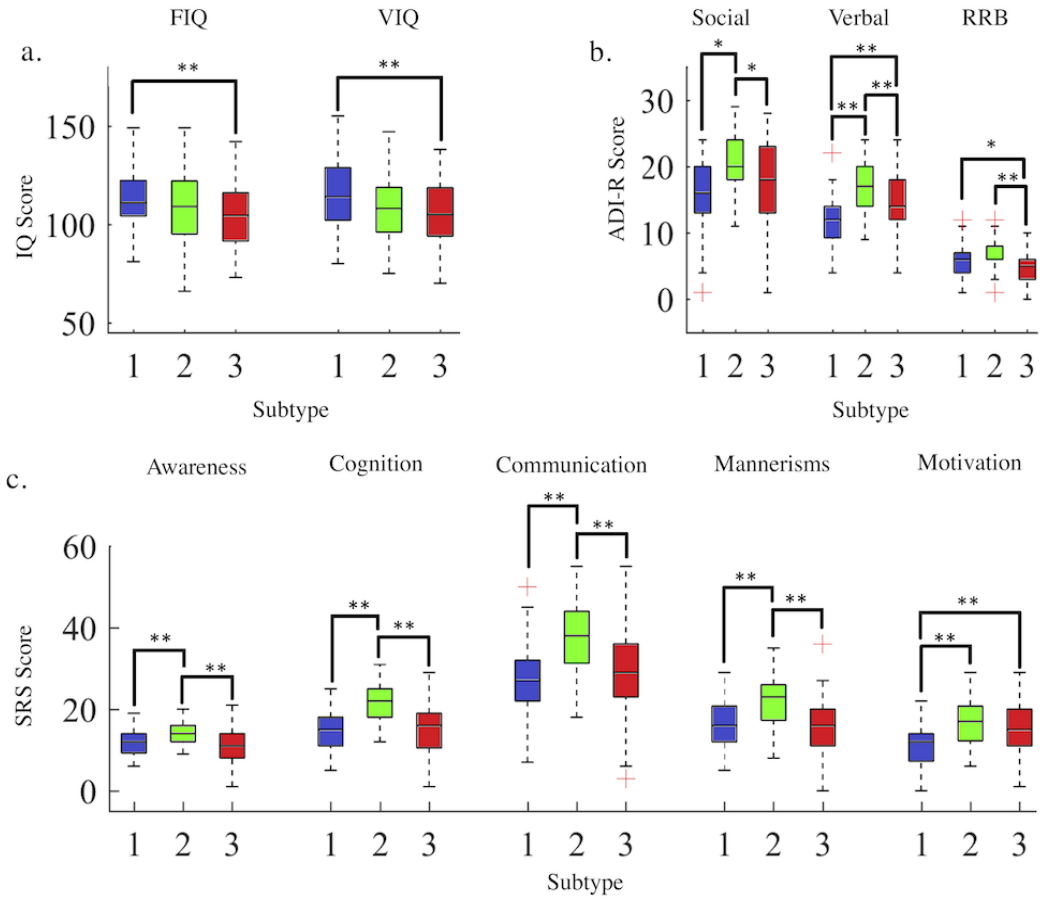

Figure 3.5. Kruskal-Wallis one-way ANOVA boxplots depicting (a) the medians of IQ-related clinical scores of each subtype, (b) the medians of ADI-R clinical scores of each subtype, and (c) the medians of SRS clinical scores of each subtype.
(* = $p < 0.05$, ** = $p < 0.01$, Tukey-Kramer)

A Kruskal-Wallis one-way ANOVA with FDR correction identified the FCs in which the three subtypes differed (Figure 3.6a, Table A7). Wilcoxon rank sum tests with FDR correction were used to identify FC differences between each subtype compared to the other two. Subtype 1 was characterized by overall increased FC, predominantly including nodes in the DMN, CBL and SubC networks, and a single hypoconnected FC feature between the visual and SubC network (Figure 3.6b; Table A8). Subtype 2 was characterized by widespread hypoconnectivity spanning across many networks and six

hyperconnected FC features (Figure 3.6c; Table A9). Subtype 3 was defined by a mix of hyper- and hypoconnectivity, predominantly hypoconnectivity between SubC and DMN nodes and hyperconnectivity involving the DMN (Figure 3.6d; Table A10).

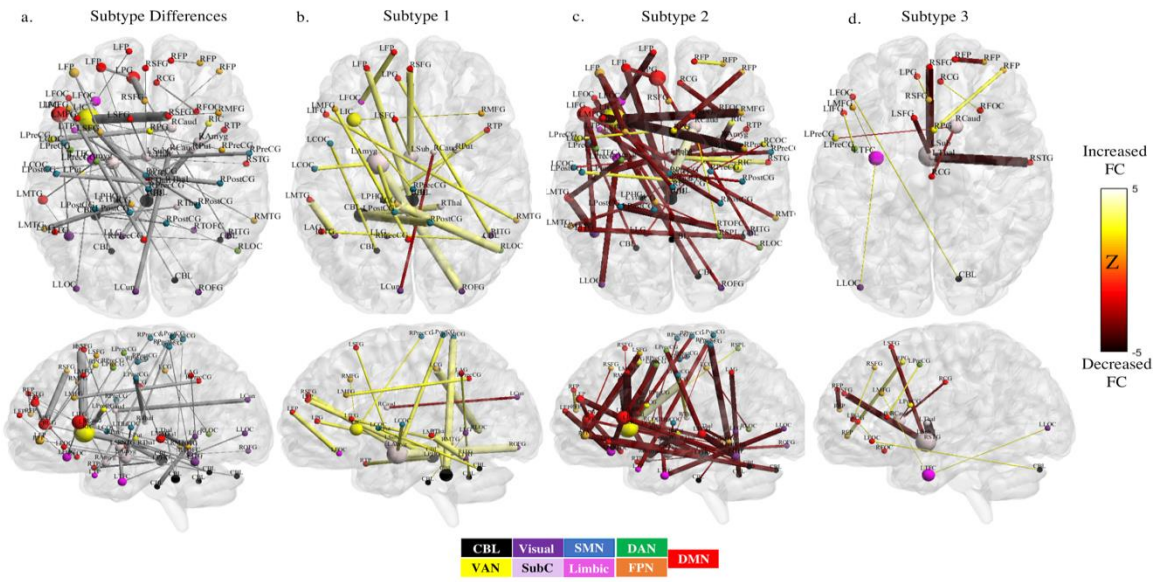

Figure 3.6. FC differences between subtypes. FCs that differ between at least two of three subtypes as determined from a Kruskal-Wallis one-way ANOVA with post-hoc multiple comparisons and FDR correction ($P < 0.05$, FDR corrected) (a). Wilcoxon rank sum tests were used to determine FC values that significantly differed ($P < 0.05$, FDR corrected) between each subtype. The corresponding test statistics (z-value) that significantly differ between one subtype and the other two are depicted for (b) subtype 1, (c) subtype 2, (d) and subtype 3. A positive z-value (light/yellow color) represents an increase in FC compared to the other subtypes, while a negative z-value (dark/red color) represents a decrease in FC compared to the other subtypes. Node size corresponds to the number of significant connections. Edge thickness corresponds to the absolute value of the z-value. ROI network membership is denoted by the colored legend. See Tables A7-10 for full names, acronym labels, and MNI coordinates for ROIs in Figure 3.6a-d.
Abbreviations: Right/Left Lateral Occipital Cortex (R/L LOC), Right/Left Putamen (R/L Put), Cerebellum (CBL), Right/Left Middle Temporal Gyrus (R/L MTG), Right/Left Paracingulate Gyrus (R/L PCG), Right/Left Insular Cortex (R/L IC), Right/Left Postcentral Gyrus (R/L PostCG), Right/Left Cingulate Gyrus (R/L CG), Left Temporal Fusiform Cortex (LTFC), Right/Left Thalamus (R/L Thal), Right/Left Middle Frontal Gyrus (R/L MFG), Right/Left Precentral Gyrus (R/L PreCG), Left Cuneal Cortex (LCun), Left Angular Gyrus (LAG), Right/Left Frontal Orbital Cortex (R/L FOC), Right/Left Inferior Temporal Gyrus (R/L ITG), Right/Left Temporal Pole (R/L TP), Right/Left Superior Frontal Gyrus (R/L SFG), Left Amygdala (LAmyg), Right Caudate (RCaud), Left Subcallosal Gyrus (LSub), Left Inferior Frontal Gyrus (LIFG), Right/Left Central Opercular Cortex (R/L COC), Right Superior Temporal Gyrus (RSTG), Right Temporal Occipital Fusiform Cortex (RTOFC), Right Precuneus Cortex (RPCun), Right Occipital Fusiform Gyrus (ROFG), Left Lingual Gyrus (LLG), Right Superior Parietal Lobule (RSPL).

Bonferroni correction revealed significantly different FC features ($P < 0.0007$) in each subtype (Figure 3.7; Tables A11-12). Further information regarding the Bonferroni corrected Kruskal-Wallis ANOVA and corresponding effect size (η^2) can be found in Table A11. An η^2 value of less than 0.01 indicates a small effect, 0.06 is considered to be moderate, and 0.14 is considered to be a large effect (Cohen, 1988). Subtype 1 was defined by eight hyperconnected features involving mainly the DMN, SubC, CBL and visual network (Figure 3.7b; Table A13-14). Subtype 2 was characterized nineteen hypoconnected features (predominantly involving DMN, CBL and FPN) and one hyperconnected feature (Figure 3.7c; Table A15-16). Subtype 3 exhibited four hypoconnected features involving the SubC network and frontal nodes (Figure 3.7d; Table A17-18). In addition, further information regarding the Bonferroni corrected Wilcoxon rank sum tests and corresponding effect size (r) can be found in Tables A13-18. An r value of less than 0.3 is considered to be a small effect, between 0.3 and 0.5 is considered to be moderate, and greater than 0.5 is considered to be a large effect (Cohen, 1988).

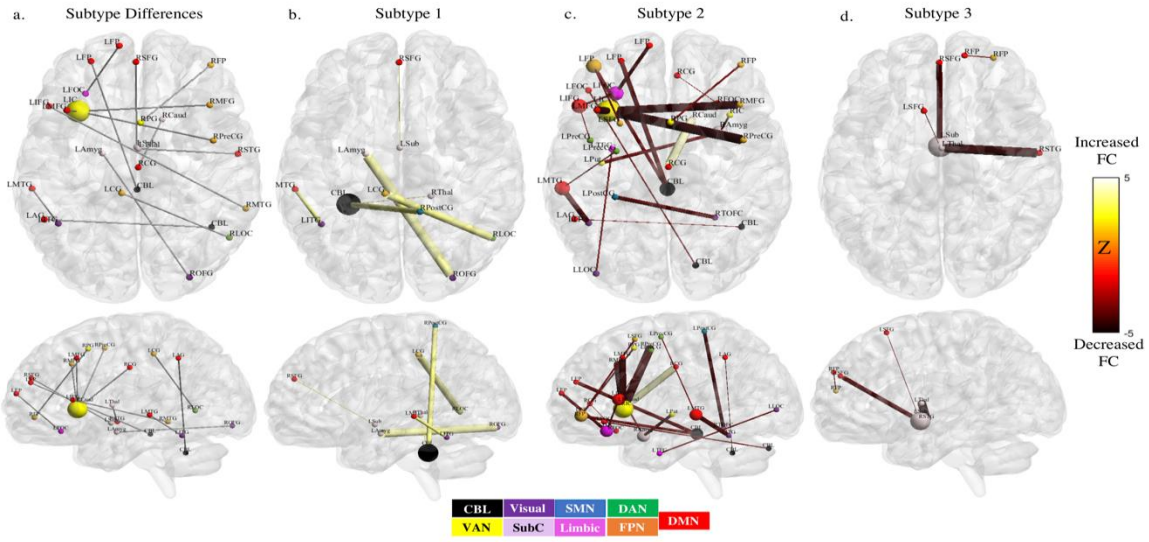

Figure 3.7. Bonferroni corrected ($P < 0.0007$) FC differences between subtypes. (a) FCs that differ between at least two of the three subtypes as determined from a Kruskal-Wallis one-way ANOVA with Bonferroni post-hoc multiple comparisons. (b) Wilcoxon rank sum tests and post-hoc Bonferroni correction were used to determine FC features that significantly differed ($P < 0.0007$) between each subtype. Figure 3.7b depicts the corresponding test statistics (z-value) for FC features that significantly differ between subtype 1 versus subtypes 2 and 3. A positive z-value (light/yellow color) represents an increase in FC compared to the other subtypes, while a negative z-value (dark/red color) represents a decrease in FC compared to the other subtypes. Node size corresponds to the number of significant connections. Edge thickness corresponds to the absolute value of the z-value. ROI network membership is denoted by the colored legend. (c). The test statistics (z-values) for FC features that significantly differ between subtype 2 versus subtypes 1 and 3. (d) The test statistics (z-values) for FC features that significantly differ between subtype 3 versus subtypes 1 and 2.

Abbreviations: Right/Left Middle Temporal Gyrus (R/L MTG), Left Inferior Temporal Gyrus (LITG), Right/Left Thalamus (R/L Thal), Cerebellum (CBL), Right/Left Postcentral Gyrus (R/L PostCG), Right/Left Cingulate Gyrus (R/L CG), Right/Left Lateral Occipital Cortex (R/L LOC), Right/Left Superior Frontal Gyrus (R/L SFG), Left Subcallosal Gyrus (LSub), Right/Left Amygdala (R/L Amyg), Right Occipital Fusiform Gyrus (ROFG), Left Temporal Fusiform Cortex (LTFC), Left Putamen (LPut), Left Angular Gyrus (LAG), Right/Left Precentral Gyrus (R/L PreCG), Right Paracingulate Gyrus (RPG), Right/Left Frontal Pole (R/L FP), Right/Left Insular Cortex (R/L IC), Right/Left Middle Frontal Gyrus (L/R MFG), Right/Left Frontal Orbital Cortex (R/L FOC), Right Caudate (RCaud), Left Inferior Frontal Gyrus (LIFG), Right Temporal Fusiform Occipital Cortex (RTFOC), Right Superior Temporal Gyrus (RSTG).

3.4.5 Subtype Verification

In order to verify subtype assignment, a multiclass SVM classifier with 5-fold cross validation was used to determine if the FC and clinical features used in CCA could predict subtype. The macro-average F1 measure was 71.3% for FC features and 65.2% for clinical features. The sensitivity, specificity, f1-measure, and macro-average f1-measure for the classification system used on FC features and clinical features can be found in Table 3.3.

Table 3.3. Results for SVM classification of subtypes based on FC and clinical features.

	FC Features			Clinical Features		
	Subtype 1	Subtype 2	Subtype 3	Subtype 1	Subtype 2	Subtype 3
Sensitivity	0.656	0.746	0.750	0.771	0.655	0.610
Specificity	0.908	0.877	0.774	0.790	0.859	0.843
F1-measure	0.662	0.712	0.763	0.626	0.636	0.692
Macro-average F1-measure		0.713			0.6517	

3.5 Discussion

The aim of the current study was to define subtypes of ASD using both FC and clinical profiles. ASD is characterized by a wide range of symptoms that vary on a spectrum of severity; however, the underlying connectomic patterns associated with this clinical variation is not clearly understood. By linking FC profiles and clinical symptoms, three distinct subtypes with disparate patterns of connectivity and clinical symptoms were identified: Subtype 1 exhibited high IQ, high RRB scores, and widespread intra-network hyperconnectivity, subtype 2 exhibited increased ADI-R and SRS symptoms and predominantly hypoconnectivity, and subtype 3 was characterized by low IQ, social

motivation deficits, verbal deficits, and mixed connectivity. The resulting subtypes may provide insights into the inconsistencies of previous studies and allow future therapies to be better targeted for specific ASD subtypes.

While studies have shown that ASD is multifaceted in terms of clinical and FC presentation (see Hull et al., 2016), previous work subtyping were based on either clinical (Georgiades et al., 2013) or FC (Easson et al., 2019) domains treated independently. Easson et al. defined two subtypes of ASD based on differences in resting-state fMRI profiles, however, there were no significant differences in terms of clinical scores (IQ, SRS, or ADOS) between subtypes (Easson et al., 2019). FC profiles may not adequately capture all facets of ASD and may explain the lack of correspondence between subtypes derived from FC and clinical features. Therefore, CCA is advantageous to capture the brain-behavior relationships in ASD. To the best of our knowledge, no previous work has been done to subtype ASD based on linked dimensions of FC and clinical features.

3.5.1 Clinical and FC Features Define Three ASD Subtypes

Subtypes differ in terms of associated FC and clinical features. Defining features of subtype 1 include high IQ, more severe RRB symptoms, and intra-network hyperconnectivity (predominantly involving DMN, SubC, CBL, and SMN). Individuals with RRBs may engage in stereotyped and repetitive movements or speech and have an insistence on sameness and routine (American Psychiatric, 2013). While the majority of findings tend to support the hypoconnectivity theory of ASD, several studies report hyperconnectivity in ASD as well (see Hull et al., 2016). Subtype 1 is also consistent with

the findings of previous work showing hyperconnectivity in ASD across brain regions including the DMN, SubC nodes, frontal/occipital regions and the salience network are correlated with RRB severity (Dupong et al., 2020; McKinnon et al., 2019; Monk et al., 2009; Uddin et al., 2013a).

The hypoconnectivity theory of ASD posits that this reduction in connectivity is associated with cognitive deficits (Just et al., 2012). The mechanism underlying the hypoconnectivity theory is that there is reduced function of neural circuitry which is believed to affect cognitive processing, switching tasks, perceptual abilities, and abstraction (Just et al., 2012). This is in accordance with the findings in subtype 1, which is the only subtype that was not characterized by hypoconnectivity and had the highest IQ in comparison to the other two subtypes.

The hypoconnectivity theory also suggests that behavioral features of ASD arise from reduced brain connectivity (Just et al., 2012). This is in accordance with subtype 2 which was defined by decreased whole-brain FC, and more severe deficits across ADI-R and SRS scales. Previous work found that intra-network hypoconnectivity as well as hypoconnectivity within the DMN have been associated with social deficits in ASD (Assaf et al., 2010; Weng et al., 2010; Yerys et al., 2015). Additionally, Verly et al. reported hypoconnectivity between CBL and supratentorial regions and it is suggested that this hypoconnectivity may be responsible for communication deficits in ASD (Verly et al., 2014).

Subtype 3 was defined by mixed connectivity, low FIQ, low VIQ, social motivation deficits, and verbal deficits. Subtype 3 exhibited decreased FC within DMN nodes,

decreased FC between DMN and SubC regions, and increased FC between intra-network regions (predominantly including the DMN). Hypoconnectivity has been associated with cognitive deficits (Just et al., 2012), and social deficits (Assaf et al., 2010; Weng et al., 2010; Yerys et al., 2015). Conversely, other studies have suggested that hyperconnectivity across long- and short-range connections, as well as DMN hyperconnectivity, predicted social deficits in children with ASD (Lynch et al., 2013; Supekar et al., 2013). The findings of subtype 3 are in line with previous work that has found a combination of hyper- and hypoconnectivity in ASD between several DMN nodes and visual, SubC, SMN, salience, VAN and CBL regions (Olivito et al., 2017; Yerys et al., 2015).

It has been suggested that the inconsistencies in ASD literature may be due to age-related differences in the participants included in these studies (Uddin et al., 2013b). Studies including children under the age of 12 have reported predominantly hyperconnectivity in ASD as compared to healthy controls, while studies demonstrating hypoconnectivity have mostly included individuals over the age of 12 (Uddin et al., 2013b). In addition, comorbidities such as ADHD and depression, as well as medication status have been found to play a role in FC results (Reiser et al., 2012; Tomasi et al., 2012). However, there were no significant effects of age, medication status, comorbidities, site, or sex in subtypes. Nevertheless, additional work is needed to fully assess the role of age, comorbidity and medication in ASD subtypes.

After Bonferroni correction ($P < 0.0007$), subtype 1 exhibited six significant hyperconnected FC features (Figure 3.7b; Table A13), subtype 2 exhibited nineteen significant hypoconnected FC features and a single hyperconnected FC feature (Figure

3.7c; Table A15), and subtype 3 was defined by four significant hypoconnected FC features (Figure 3.7d; Table A17). Interestingly, only the hypoconnected FC features in subtype 3 were significant after Bonferroni correction which suggests that subtype 3 is largely driven by the hypoconnected features. The significant FC features across all three subtypes include regions in the SubC and DMN. However, the nodes and direction of connectivity (increase or decrease) differ between subtypes. The DMN is the most commonly implicated network in ASD and is involved in a wide range of cognitive and social tasks (Padmanabhan et al., 2017), however the FC literature involving the DMN has been widely inconsistent (see Hull et al., 2016). In addition, the SubC network is implicated in reward processing, social motivation, social behaviors and RRBs (Abbott et al., 2018; Clements et al., 2018). The social motivation hypothesis suggests that individuals with ASD have aberrant processing in subcortical regions involved in reward processing, resulting in unrewarding social interactions which can lead to abnormal social behaviors (Clements et al., 2018). However, there are also mixed results regarding subcortical regions in literature (Maximo et al., 2014; Woodward et al., 2017). It is possible that the mixed results in ASD in regard to these two networks may be explained by subtypes of ASD.

3.5.2 Subtype Verification

In our work, a multiclass SVM classifier was able to classify subjects with 71.3% accuracy for FC features, and 65.2% accuracy for clinical features. Both are significantly higher than chance (33.3%), indicating that there are distinct clinical and FC differences associated with each subtype.

3.5.3 Limitations and Future Work

While this work increases our understanding of the associations between clinical profiles of ASD and aberrant FC, there are several limitations of this study that must be considered. Although data from sites with similar scanning procedures and inclusion criteria were used in this study, and further age, sex and site related factors were regressed out of the data prior to analysis, replication of our findings in an independent, single-site dataset with small age discrepancies would be necessary to address the limitation of this multi-site sample. Additionally, a more extensive and consistent ASD clinical assessment would be critical for further understanding how brain connectivity relates to ASD symptoms. It would also be beneficial to use clinical and resting-state fMRI data from a much larger population to be able to further characterize the associations between brain connectivity and ASD symptoms. This would be useful for a cluster discovery set of subjects, and for replication of this work. Finally, while NYU sample 1, NYU sample 2, and SDSU did not exclude participants based on FIQ, criteria at ETH, GU, KKI, and TCD limited ASD participants to an FIQ of greater than 70 or 80. Including subjects with low IQs would be important for determining if similar subtypes exist across a wider scope of cognitive deficits.

3.6 Conclusion

The present study identified three ASD subtypes with distinct FC patterns and clinical manifestations using associative analysis of connectomic and clinical profiles. These

findings may provide a perspective for the inconsistent reports in ASD FC studies and suggest the importance of specific treatments and therapies for each ASD subtype.

3.7 Acknowledgements

The authors thank the contributors to the Autism Brain Imaging Data Exchange and Preprocessed Connectomes Project for access to subject data.

3.8 References

Abbott, A. E., Linke, A. C., Nair, A., Jahedi, A., Alba, L. A., Keown, C. L., . . . Müller, R.-A. (2018). Repetitive behaviors in autism are linked to imbalance of corticostriatal connectivity: a functional connectivity MRI study. *Soc. Cogn. Affect. Neurosci., 13*(1), 32-42. doi:10.1093/scan/nsx129

Agcaoglu, O., Wilson, T. W., Wang, Y.-P., Stephen, J., & Calhoun, V. D. (2019). Resting state connectivity differences in eyes open versus eyes closed conditions. *Hum. Brain Mapp., 40*(8), 2488-2498. doi:10.1002/hbm.24539

American Psychiatric, A. (2013). *Diagnostic and Statistical Manual of Mental Disorders (DSM-5®)*: American Psychiatric Pub.

Anderson, J. S., Nielsen, J. A., Froehlich, A. L., DuBray, M. B., Druzgal, T. J., Cariello, A. N., . . . Lainhart, J. E. (2011). Functional connectivity magnetic resonance imaging classification of autism. *Brain, 134*(Pt 12), 3742-3754. doi:10.1093/brain/awr263

Assaf, M., Jagannathan, K., Calhoun, V. D., Miller, L., Stevens, M. C., Sahl, R., . . . Pearlson, G. D. (2010). Abnormal functional connectivity of default mode sub-networks in autism spectrum disorder patients. *Neuroimage, 53*(1), 247-256. doi:10.1016/j.neuroimage.2010.05.067

Belmonte, M. K., Allen, G., Beckel-Mitchener, A., Boulanger, L. M., Carper, R. A., & Webb, S. J. (2004). Autism and abnormal development of brain connectivity. *J. Neurosci., 24*(42), 9228-9231. doi:10.1523/JNEUROSCI.3340-04.2004

Booker, K. W., & Starling, L. (2011). *Test Review: Social Responsiveness Scale by J. N. Constantino and C. P. Gruber. *Assess. Eff. Interv., 36*(3), 192-194. doi:10.1177/1534508410380134

Brady, R. O., Jr., Gonsalvez, I., Lee, I., Öngür, D., Seidman, L. J., Schmahmann, J. D., . . . Halko, M. A. (2019). Cerebellar-Prefrontal Network Connectivity and Negative Symptoms in Schizophrenia. *Am. J. Psychiatry, 176*(7), 512-520. doi:10.1176/appi.ajp.2018.18040429

Chang, C.-C., & Lin, C.-J. (2011). LIBSVM: A Library for Support Vector Machines.

Clements, C. C., Zoltowski, A. R., Yankowitz, L. D., Yerys, B. E., Schultz, R. T., & Herrington, J. D. (2018). Evaluation of the Social Motivation Hypothesis of Autism: A Systematic Review and Meta-analysis. *JAMA Psychiatry, 75*(8), 797-808. doi:10.1001/jamapsychiatry.2018.1100

Cody. (2012). Multi Class SVM - File Exchange - MATLAB Central.

Cohen, J. (1988). *Statistical Power Analysis for the Behavioral Sciences, Second Edition*.

Craddock, R. C., James, G. A., Holtzheimer, P. E., 3rd, Hu, X. P., & Mayberg, H. S. (2012). A whole brain fMRI atlas generated via spatially constrained spectral clustering. *Hum. Brain Mapp., 33*(8), 1914-1928. doi:10.1002/hbm.21333

Di Martino, A., Yan, C. G., Li, Q., Denio, E., Castellanos, F. X., Alaerts, K., . . . Milham, M. P. (2014). The autism brain imaging data exchange: towards a large-scale evaluation of the intrinsic brain architecture in autism. *Mol. Psychiatry, 19*(6), 659-667. doi:10.1038/mp.2013.78

Drysdale, A., Grosenick, L., Downar, J., Dunlop, K., Mansouri, F., Meng, Y., . . . Liston, C. (2017). Resting-state connectivity biomarkers define neurophysiological subtypes of depression. *Natural Medicine*.

Dupong, I., & Di Martino, A. (2020). Hyper-connectivity of the striatum related to restricted and repetitive behaviors' severity in children with ASD. *Cold Spring Harbor Laboratory*. doi:10.1101/2020.02.21.957993

Easson, A. K., Fatima, Z., & McIntosh, A. R. (2019). Functional connectivity-based subtypes of individuals with and without autism spectrum disorder. *Netw Neurosci, 3*(2), 344-362. doi:10.1162/netn_a_00067

Feczko, E., Balba, N. M., Miranda-Dominguez, O., Cordova, M., Karalunas, S. L., Irwin, L., . . . Fair, D. A. (2018). Subtyping cognitive profiles in Autism Spectrum Disorder using a Functional Random Forest algorithm. *Neuroimage, 172*, 674-688. doi:10.1016/j.neuroimage.2017.12.044

Gareth, J., Daniela, W., Trevor, H., & Robert, T. (2013). An introduction to statistical learning: with applications in R.

Georgiades, S., Szatmari, P., Boyle, M., Hanna, S., Duku, E., Zwaigenbaum, L., . . . Pathways in, A. S. D. S. T. (2013). Investigating phenotypic heterogeneity in children with autism spectrum disorder: a factor mixture modeling approach: ASD factor mixture model. *J. Child Psychol. Psychiatry, 54*(2), 206-215. doi:10.1111/j.1469-7610.2012.02588.x

Hong, S.-J., Valk, S. L., Di Martino, A., Milham, M. P., & Bernhardt, B. C. (2018). Multidimensional Neuroanatomical Subtyping of Autism Spectrum Disorder. *Cereb. Cortex, 28*(10), 3578-3588. doi:10.1093/cercor/bhx229

Hotelling, H. (1992). Relations Between Two Sets of Variates. In S. Kotz & N. L. Johnson (Eds.), *Breakthroughs in Statistics: Methodology and Distribution* (pp. 162-190). New York, NY: Springer New York.

Hrdlicka, M., Dudova, I., Beranova, I., Lisy, J., Belsan, T., Neuwirth, J., . . . Urbanek, T. (2005). Subtypes of autism by cluster analysis based on structural MRI data. *Eur. Child Adolesc. Psychiatry, 14*(3), 138-144. doi:10.1007/s00787-005-0453-z

Hull, J. V., Dokovna, L. B., Jacokes, Z. J., Torgerson, C. M., Irimia, A., & Van Horn, J. D. (2016). Resting-State Functional Connectivity in Autism Spectrum Disorders: A Review. *Front. Psychiatry, 7*, 205. doi:10.3389/fpsyt.2016.00205

Just, M. A., Keller, T. A., Malave, V. L., Kana, R. K., & Varma, S. (2012). Autism as a neural systems disorder: a theory of frontal-posterior underconnectivity. *Neurosci. Biobehav. Rev., 36*(4), 1292-1313. doi:10.1016/j.neubiorev.2012.02.007

Lord, C., Rutter, M., & Le Couteur, A. (1994). Autism Diagnostic Interview-Revised: a revised version of a diagnostic interview for caregivers of individuals with possible pervasive developmental disorders. *J. Autism Dev. Disord., 24*(5), 659-685. doi:10.1007/BF02172145

Lynch, C. J., Uddin, L. Q., Supekar, K., Khouzam, A., Phillips, J., & Menon, V. (2013). Default mode network in childhood autism: posteromedial cortex heterogeneity and relationship with social deficits. *Biol. Psychiatry, 74*(3), 212-219. doi:10.1016/j.biopsych.2012.12.013

Maenner, M. J., Shaw, K. A., Baio, J., Washington, A., Patrick, M., DiRienzo, M., . . . PhD. (2020). Prevalence of Autism Spectrum Disorder Among Children Aged 8 Years — Autism and Developmental Disabilities Monitoring Network, 11 Sites, United States, 2016. *MMWR. Surveillance Summaries, 69*(4), 1-12. doi:10.15585/mmwr.ss6904a1

Maximo, J. O., Cadena, E. J., & Kana, R. K. (2014). The implications of brain connectivity in the neuropsychology of autism. *Neuropsychol. Rev., 24*(1), 16-31. doi:10.1007/s11065-014-9250-0

McKinnon, C. J., Eggebrecht, A. T., Todorov, A., Wolff, J. J., Elison, J. T., Adams, C. M., . . . Network, I. (2019). Restricted and Repetitive Behavior and Brain Functional Connectivity in Infants at Risk for Developing Autism Spectrum Disorder. *Biol Psychiatry Cogn Neurosci Neuroimaging, 4*(1), 50-61. doi:10.1016/j.bpsc.2018.09.008

Monk, C. S., Peltier, S. J., Wiggins, J. L., Weng, S.-J., Carrasco, M., Risi, S., & Lord, C. (2009). Abnormalities of intrinsic functional connectivity in autism spectrum disorders. *Neuroimage, 47*(2), 764-772. doi:10.1016/j.neuroimage.2009.04.069

Oksanen, J., Kindt, R., Legendre, P., O'Hara, B., Stevens, M. H. H., Oksanen, M. J., & Suggests, M. (2007). The vegan package. *Community ecology package, 10*(631-637), 719.

Olivito, G., Clausi, S., Laghi, F., Tedesco, A. M., Baiocco, R., Mastropasqua, C., . . . Leggio, M. (2017). Resting-State Functional Connectivity Changes Between Dentate Nucleus and Cortical Social Brain Regions in Autism Spectrum Disorders. *Cerebellum, 16*(2), 283-292. doi:10.1007/s12311-016-0795-8

Padmanabhan, A., Lynch, C. J., Schaer, M., & Menon, V. (2017). The Default Mode Network in Autism. *Biol Psychiatry Cogn Neurosci Neuroimaging, 2*(6), 476-486. doi:10.1016/j.bpsc.2017.04.004

Plitt, M., Barnes, K. A., Wallace, G. L., Kenworthy, L., & Martin, A. (2015). Resting-state functional connectivity predicts longitudinal change in autistic traits and adaptive functioning in autism. *Proc. Natl. Acad. Sci. U. S. A., 112*(48), E6699-6706. doi:10.1073/pnas.1510098112

Reiser, E. M., Schulter, G., Weiss, E. M., Fink, A., Rominger, C., & Papousek, I. (2012). Decrease of prefrontal-posterior EEG coherence: loose control during social-emotional stimulation. *Brain Cogn., 80*(1), 144-154. doi:10.1016/j.bandc.2012.06.001

Sánchez, J. (1982). Multivariate Analysis. Academic Press, London-New York-Toronto-Sydney-San Francisco 1979. xv, 518 pp., $ 61.00. *Biom. J., 24*(5), 502-502. doi:10.1002/bimj.4710240520

Simonoff, E., Pickles, A., Charman, T., Chandler, S., Loucas, T., & Baird, G. (2008). Psychiatric Disorders in Children With Autism Spectrum Disorders: Prevalence, Comorbidity, and Associated Factors in a Population-Derived Sample. *Journal of the American Academy of Child & Adolescent Psychiatry, 47*(8), 921-929. doi:10.1097/chi.0b013e318179964f

Supekar, K., Uddin, L. Q., Khouzam, A., Phillips, J., Gaillard, W. D., Kenworthy, L. E., . . . Menon, V. (2013). Brain hyperconnectivity in children with autism and its links to social deficits. *Cell Rep., 5*(3), 738-747. doi:10.1016/j.celrep.2013.10.001

Tomasi, D., & Volkow, N. D. (2012). Abnormal functional connectivity in children with attention-deficit/hyperactivity disorder. *Biol. Psychiatry, 71*(5), 443-450. doi:10.1016/j.biopsych.2011.11.003

Uddin, L. Q., Supekar, K., Lynch, C. J., Khouzam, A., Phillips, J., Feinstein, C., . . . Menon, V. (2013a). Salience network-based classification and prediction of symptom severity in children with autism. *JAMA Psychiatry, 70*(8), 869-879. doi:10.1001/jamapsychiatry.2013.104

Uddin, L. Q., Supekar, K., & Menon, V. (2013b). Reconceptualizing functional brain connectivity in autism from a developmental perspective. *Front. Hum. Neurosci., 7*, 458. doi:10.3389/fnhum.2013.00458

Verly, M., Verhoeven, J., Zink, I., Mantini, D., Peeters, R., Deprez, S., . . . Sunaert, S. (2014). Altered functional connectivity of the language network in ASD: role of classical language areas and cerebellum. *Neuroimage Clin, 4*, 374-382. doi:10.1016/j.nicl.2014.01.008

Weng, S.-J., Wiggins, J. L., Peltier, S. J., Carrasco, M., Risi, S., Lord, C., & Monk, C. S. (2010). Alterations of resting state functional connectivity in the default network in adolescents with autism spectrum disorders. *Brain Res., 1313*, 202-214. doi:10.1016/j.brainres.2009.11.057

Woodward, N. D., Giraldo-Chica, M., Rogers, B., & Cascio, C. J. (2017). Thalamocortical dysconnectivity in autism spectrum disorder: An analysis of the Autism Brain Imaging Data Exchange. *Biol Psychiatry Cogn Neurosci Neuroimaging, 2*(1), 76-84. doi:10.1016/j.bpsc.2016.09.002

Xia, C. H., Ma, Z., Ciric, R., Gu, S., Betzel, R. F., Kaczkurkin, A. N., . . . Satterthwaite, T. D. (2018). Linked dimensions of psychopathology and connectivity in functional brain networks. *Nat. Commun., 9*(1), 3003. doi:10.1038/s41467-018-05317-y

Xia, M., Wang, J., & He, Y. (2013). BrainNet Viewer: a network visualization tool for human brain connectomics. *PLoS One, 8*(7), e68910. doi:10.1371/journal.pone.0068910

Yan, J., Xu, Y., Sui, J., Li, X., Wang, H., & Zhang, B. (2017). Long-term variation of the macrobenthic community and its relationship with environmental factors in the Yangtze River estuary and its adjacent area. *Mar. Pollut. Bull., 123*(1-2), 339-348. doi:10.1016/j.marpolbul.2017.09.023

Yeo, B. T. T., Krienen, F. M., Sepulcre, J., Sabuncu, M. R., Lashkari, D., Hollinshead, M., . . . Buckner, R. L. (2011). The organization of the human cerebral cortex estimated by intrinsic functional connectivity. *J. Neurophysiol., 106*(3), 1125-1165. doi:10.1152/jn.00338.2011

Yerys, B. E., Gordon, E. M., Abrams, D. N., Satterthwaite, T. D., Weinblatt, R., Jankowski, K. F., . . . Vaidya, C. J. (2015). Default mode network segregation and social deficits in autism spectrum disorder: Evidence from non-medicated children. *NeuroImage: Clinical, 9*, 223-232. doi:10.1016/j.nicl.2015.07.018

Yu, M., Linn, K. A., Cook, P. A., Phillips, M. L., McInnis, M., Fava, M., . . . Sheline, Y. I. (2018). Statistical harmonization corrects site effects in functional connectivity measurements from multi-site fMRI data. *Hum. Brain Mapp., 39*(11), 4213-4227. doi:10.1002/hbm.24241

Zuo, X.-N., Xu, T., Jiang, L., Yang, Z., Cao, X.-Y., He, Y., . . . Milham, M. P. (2013). Toward reliable characterization of functional homogeneity in the human brain: preprocessing, scan duration, imaging resolution and computational space. *Neuroimage, 65*, 374-386. doi:10.1016/j.neuroimage.2012.10.017

Zuur, A. F., Ieno, E. N., & Smith, G. M. (2007). Principal component analysis and redundancy analysis *Analysing Ecological Data* (pp. 193-224). New York, NY: Springer New York.

Chapter 4

4.1 Overview

FMRI is a useful tool in studying neurodevelopmental and psychiatric disorders. Resting-state fMRI data can assess changes in the brain that allow for a better understanding of the relationships between brain connectivity and clinical symptoms associated with various disorders. Large-scale fMRI databases are becoming increasingly common to increase the understanding of the resting brain in diseased populations, however site-effects introduce heterogeneity to fMRI data aggregated from different sites, in addition to the heterogeneity associated with individuals with neurodevelopmental and psychiatric disorders. Elucidating the heterogeneity associated with these disorders, and reducing the heterogeneity introduced by multi-site databases is crucial to gain a better understanding of connectomic features in these populations.

The first study reduced site-effects in ABIDE and B-SNIP multi-site consortiums, while improving the between-group effect size of brain features known to be affected in

ASD and SZ. The second study aimed to identify novel subtypes of ASD based on linked connectomic and clinical profiles thus providing insights into the inconsistencies in resting-state fMRI literature. Together, these studies reduce site-effects in multi-site consortiums without a reduction of the effect size in consistent FC alterations in patients vs controls, and allow a greater understanding of the clinical-connectomic relationships of ASD.

4.2 Summary of Research Contributions and Implications

Multi-site databases introduce site bias due to the use of different hardware, parameters, and protocols. Multi-site harmonization methods have been known to reduce site bias, however the effect of important FC information is often loss in the process. Here, we reduced site bias associated with multi-site fMRI databases through the use of a site de-meaning algorithm, and improve the effect size of brain features known to be affected in ASD and SZ. This method resulted in 2.9-7.9% improvement in effect size compared to the original data, and up to 42.6% improvement compared to previous harmonization methods (ComBat and GLM). This method can be applied to various other multi-site databases and preserve important FC features associated with neurodevelopmental and psychiatric disorders.

Previous studies reported inconsistent and mixed results in terms of the connectomic profiles associated with ASD (see Hull et al., 2016). Some studies posit that ASD is characterized by hypoconnectivity, others found hyperconnectivity to be associated with ASD, and combinations of hypo- and hyperconnectivity have also been found in ASD individuals (see Hull et al., 2016). The three novel subtypes of ASD identified through

CCA and hierarchical clustering revealed that hyperconnectivity, hypoconnectivity and mixed connectivity are associated with distinct symptoms of ASD, thus advancing our understanding of previous reports of FC in ASD. Previous work subtyping ASD has focused on unimodal (i.e. brain anatomy, clinical symptoms, resting-state fMRI) methods, and this work is the first to define subtypes of ASD based on linked brain and behavior relationships. These methods are applicable to other heterogeneous neurodevelopmental and psychiatric disorders to identify distinct subtypes based on clinical and connectomic profiles. The identification of subtypes based on linked brain-behavior relationships allows a better understanding of the inconsistencies in previous ASD FC literature, neural processes underlying this disorder, and can lead to more specified diagnosis and better targeted therapies for these individuals.

4.3 Limitations and Future Directions

There are also several limitations that should be noted in this work. In terms of the SWD algorithm for improved effect size of case vs control subjects, a ground truth FC neuromarker does not exist. Here, we used commonly reported features across multiple studies, utilizing multiple different case vs control cohorts, however these are not universally accepted neuromarkers of ASD or SZ. In addition, while this method has been tested on two multi-site disorders, additional testing would be necessary on other diseased populations to ensure this method is useful across various other disorders. Future work would also benefit from applying the SWD method prior to subtyping to reduce the site-

effects associated with multi-site consortiums while preserving the meaningful FC information in the subjects.

For subtyping ASD, the use of a greater number of subjects with a wide variety of consistent clinical measures should be used in future work. In addition, many sites from ABIDE used cut-off FIQs which limit our understanding of lower-functioning ASD individuals and where they fit into this subtyping model. It would also be beneficial to use a more homogeneous cohort in terms of age, medication status, and comorbidity to limit any confounding effects that these variables could have on results.

4.4 References

Hull, J. V., Dokovna, L. B., Jacokes, Z. J., Torgerson, C. M., Irimia, A., & Van Horn, J. D. (2016). Resting-State Functional Connectivity in Autism Spectrum Disorders: A Review. *Front. Psychiatry, 7*, 205. doi:10.3389/fpsyt.2016.00205

Appendix A

Table A1. Medication and comorbidity status of participants.

Site	Medication Status	Off stimulants at time of scan	Comorbidities
ETH	100% unknown	100% unknown	100% unknown
GU	37.5% on medication	100% off stimulants	100% unknown
KKI	40.8% on medication	100% off stimulants	91.8% comorbid ADHD (65.3%), GAD (10.2%), OCD (12.2%), ODD (26.5%), simple phobia (30.6%)
NYU 1	20.5% on medication	100% off stimulants	54.6% comorbid ADHD (50.0%), GAD (6.8%), ODD (13.6%)
NYU 2	13% on medication	100% off stimulants	60.9% comorbid ADHD (39.1%), GAD (13.0%), OCD (4.35%), ODD (4.4%), simple phobia (8.7%)
SDSU	45.2% on medication	74.2% off stimulants	100% unknown
TCD	0% on medication	100% off stimulants	100% unknown

Abbreviations: ETH Zurich (ETH), Georgetown University (GU), Kennedy Krieger Institute (KKI), New York University Langone Medical Center Sample 1 (NYU 1), New York University Langone Medical Center Sample 2 (NYU 2), San Diego State University (SDSU), Trinity Center for Health Sciences (TCD), Attention Deficit/Hyperactive Disorder (ADHD), Generalized Anxiety Disorder (GAD), Obsessive Compulsive Disorder (OCD), Oppositional Defiance Disorder (ODD).
Notes: Unknown refers to information that was not present on the ABIDE phenotypic assessments.

Table A2. MNI coordinates (mm) of ROIs associated with the 72 FC features identified from Spearman's rank correlation coefficient with the highest correlation to clinical variables and VIF < 5 in Figure 3.2b.

		MNI Coordinates		
ROI	Network	x	y	z
Left Lateral Occipital Cortex	Visual	-39.6	-85.4	1.4
Left Angular Gyrus	DMN	-49.7	-60.8	23.2
Left Putamen/ Insular Cortex	VAN	-36.6	-13.9	-2.3
Left Paracingulate Gyrus	DMN	-6.8	45.7	7.8
Cerebellum	CBL	-19.3	-62.1	-26.1
Cerebellum	CBL	43.3	-55.2	-32.2
Left Middle Temporal Gyrus	DMN	-58.9	-30.2	-2.4
Right Paracingulate Gyrus	VAN	2.8	12.4	49.4
Right Putamen	SubC	13.5	12.3	-7
Right Thalamus	SubC	11.6	-20	9.5
Left Insular Cortex	VAN	-32.7	19.7	2
Left Postcentral Gyrus	SMN	-8.8	-38	69.3
Right Cingulate Gyrus	DMN	6.7	42.6	6.1
Left Temporal Fusiform Cortex	Limbic	-30.5	-5.1	-32.6
Right Postcentral Gyrus	SMN	30.4	-33.7	63.4
Right Cingulate Gyrus	DMN	1.6	-16.5	34.8
Cerebellum	CBL	2.9	-28	-36
Right Superior Parietal Lobule	DAN	29.7	-54.6	59.7
Left Supramarginal Gyrus	VAN	-56.5	-43.3	26.5
Right Insular Cortex	SMN	41	-4.7	10.8
Left Thalamus	SubC	-13.4	-32.3	0.8
Right Middle Frontal Gyrus	FPN	42.4	23.8	37.6
Right Middle Temporal Gyrus	FPN	62.9	-43	-7.8
Right Thalamus	SubC	18.5	-34.6	-1.8
Left Precentral Gyrus	DAN	-28.2	-6.3	58
Left Cuneal Cortex	Visual	-5.4	-87.2	25
Left Angular Gyrus	DMN	-51.9	-50.2	42.1
Left Frontal Orbital Cortex	Limbic	-28.4	31.1	-15.3
Right Insular Cortex	VAN	36.7	17.2	3.6
Right Postcentral Gyrus	SMN	43.3	-19.9	53.7
Left Middle Frontal Gyrus	DMN	-39.1	20.3	42.2
Left Inferior Temporal Gyrus	Visual	-43.9	-52.7	-18.6
Right Superior Frontal Gyrus	DAN	28.8	-0.3	56.8
Right Postcentral Gyrus	SMN	12.3	-44.8	67.7

Right Thalamus	SubC	1.6	-20.8	-7.6
Right Frontal Orbital Cortex	DMN	29.6	24.6	-15.1
Left Precentral Gyrus	DAN	-43	0.8	47.6
Left Frontal Orbital Cortex	DMN	-44	33	-8.1
Right Frontal Pole	FPN	31.7	54.8	14.9
Left Cingulate Gyrus	FPN	-7.9	-33.1	45.5
Cerebellum	CBL	17.2	-80.1	-28.7
Left Temporal Pole	Limbic	-40.6	12.9	-28.2
Left Lateral Occipital Cortex	DMN	-42.9	-67	40.7
Right Temporal Fusiform Cortex	Limbic	37.8	-12.8	-26
Right Superior Frontal Gyrus	DMN	0.3	51.6	26.5
Left Amygdala	SubC	-18.7	-7.4	-15.9
Right Caudate	SubC	14.2	-0.5	17.5
Left Superior Frontal Gyrus	FPN	-26	11.7	56.2
Left Postcentral Gyrus	SMN	-28.8	-35.9	62.4
Right Precentral Gyrus	SMN	60.1	-1.3	25
Left Middle Temporal Gyrus	FPN	-58	-48.3	-8.1
Right Inferior Temporal Gyrus	Visual	48	-52.7	-16.7
Cerebellum	CBL	-28.4	-40	-30.7
Left Frontal Pole	DMN	-9.2	62	14.2
Right Temporal Pole	SubC	30.9	5.8	-19
Right Precentral Gyrus	SMN	2.1	-23.6	68.5
Left Frontal Orbital Cortex	DMN	-28.9	12.1	-16.6
Right Frontal Pole	FPN	42.9	49.6	-4.4
Right Precentral Gyrus	FPN	44.4	0.9	50
Right Central Opercular Cortex	VAN	55.8	3.8	5.8
Cerebellum	CBL	-17.3	-81.3	-30.9
Left Temporal Fusiform Cortex	DMN	-27.6	-38	-11.4
Right Precentral Gyrus	SMN	0.4	-15.1	51.8
Cerebellum	CBL	35.7	-73	-30.6
Right Supramarginal Gyrus	VAN	61.2	-31.4	26.6
Left Subcallosal Gyrus	SubC	0.7	-3.4	-8.7
Right Precentral Gyrus	SMN	24.6	-13.5	67
Right Caudate	SubC	15.3	14.6	7
Right Insular Cortex	VAN	40.7	-11.3	-3.9
Left Inferior Frontal Gyrus	DMN	-49.2	22.9	9.3
Right Lateral Occipital Cortex	DAN	53.5	-61.8	1
Left Central Opercular Cortex	SMN	-56	-10.9	5.6

Right Thalamus	SubC	1.7	-4.4	5.3
Right Superior Frontal Gyrus	FPN	-0.2	31.1	45.5
Left Lateral Occipital Cortex	Visual	-46.1	-72.1	12.1
Left Middle Frontal Gyrus	FPN	-44	26.5	26.6
Cerebellum	CBL	1.7	-56.9	-12.7
Right Superior Temporal Gyrus	DMN	58.4	-7.8	-7.8
Left Postcentral Gyrus	SMN	-51.2	-14.1	40.4
Right Subcallosal Cortex	Limbic	0.1	20.4	-8
Right Precuneus Cortex	DAN	10.3	-63.5	56.2
Right Inferior Frontal Gyrus	FPN	51.9	21	21.1
Left Precentral Gyrus	VAN	-54.1	7.2	18.2
Right Lateral Occipital Cortex	DMN	44.9	-65.5	39.3
Left Frontal Pole	DMN	-25.3	52	22.9
Left Frontal Pole	FPN	-40.9	48.7	-3.4
Right Temporal Occipital Fusiform Cortex	Visual	28.1	-49.1	-13
Left Superior Frontal Gyrus	DMN	-8.6	19.9	60.4
Right Precuneus Cortex	DMN	-0.7	-55.1	38.3
Right Occipital Fusiform Gyrus	Visual	30.8	-87.5	-10.9
Right Putamen	SubC	27.2	0.8	-0.1
Left Lingual Gyrus	Visual	-13.3	-52.9	-0.7
Right Temporal Pole	DMN	45.7	13.3	-22.7
Left Central Opercular Cortex	SMN	-46.7	5	2.8
Right Superior Frontal Gyrus	DMN	13.5	21.7	59.8
Right Frontal Pole	DMN	15	56.3	29.4
Cerebellum	CBL	1	-30.8	-17.5
Right Temporal Fusiform Cortex	Limbic	30.8	-1.4	-36.2
Left Parahippocampal Gyrus	CBL	-15	-30.8	-18.3

Table A3. MNI coordinates (mm) of ROIs associated with CV1 positive (Figure 3.3b).

			MNI Coordinates		
ROI Label	Full ROI Name	Network	x	y	z
LITG	Left Inferior Temporal Gyrus	Visual	-43.9	-52.7	-18.6
LPostCG	Left Postcentral Gyrus	SMN	-8.8	-38	69.3
RPreCG	Right Precentral Gyrus	SMN	60.1	-1.3	25
RSFG	Right Superior Frontal Gyrus	DAN	28.8	-0.3	56.8
LSMG	Left Supramarginal Gyrus	VAN	-56.5	-43.3	26.5
RSMG	Right Supramarginal Gyrus	VAN	61.2	-31.4	26.6
LAmyg	Left Amygdala	SubC	-18.7	-7.4	-15.9
LSub	Left Subcallosal Gyrus	SubC	0.7	-3.4	-8.7
RThal	Right Thalamus	SubC	1.7	-4.4	5.3
LTFC	Left Temporal Fusiform Cortex	Limbic	-30.5	-5.1	-32.6
LFOC	Left Frontal Orbital Cortex	Limbic	-28.4	31.1	-15.3
RCG	Right Cingulate Gyrus	DMN	6.7	42.6	6.1
LAG	Left Angular Gyrus	DMN	-51.9	-50.2	42.1
RFOC	Right Frontal Orbital Cortex	DMN	29.6	24.6	-15.1
LIFG	Left Inferior Frontal Gyrus	DMN	-49.2	22.9	9.3
RSTG	Right Superior Temporal Gyrus	DMN	58.4	-7.8	-7.8
RLOC	Right Lateral Occipital Cortex	DMN	44.9	-65.5	39.3
LSFG	Left Superior Frontal Gyrus	DMN	-8.6	19.9	60.4

Table A4. MNI coordinates (mm) of ROIs associated with CV1 negative (Figure 3.3c).

			MNI Coordinates		
ROI Label	Full ROI Name	Network	x	y	z
CBL	Cerebellum	CBL	-28.4	-40	-30.7
LLOC	Left Lateral Occipital Cortex	Visual	-39.6	-85.4	1.4
RIC	Right Insular Cortex	SMN	41	-4.7	10.8
LPostCG	Left Postcentral Gyrus	SMN	-51.2	-14.1	40.4
RSPL	Right Superior Parietal Lobule	DAN	29.7	-54.6	59.7
RPcun	Right Precuneus Cortex	DAN	10.3	-63.5	56.2
LIC	Left Insular Cortex	VAN	-32.7	19.7	2
LPreCG	Left Precentral Gyrus	VAN	-54.1	7.2	18.2
RThal	Right Thalamus	SubC	11.6	-20	9.5
RThal	Right Thalamus	SubC	18.5	-34.6	-1.8
RThal	Right Thalamus	SubC	1.6	-20.8	-7.6
LSubC	Left Subcallosal Gryus	SubC	0.7	-3.4	-8.7
RCaud	Right Caudate	SubC	15.3	14.6	7
LTFC	Left Temporal Fusiform Cortex	Limbic	-30.5	-5.1	-32.6
RMTG	Right Middle Temporal Gyrus	FPN	62.9	-43	-7.8
LMFG	Left Middle Frontal Gyrus	FPN	-44	26.5	26.6
RSFG	Right Superior Frontal Gyrus	DMN	0.3	51.6	26.5
LIFG	Left Inferior Frontal Gyrus	DMN	-49.2	22.9	9.3

Table A5. MNI coordinates (mm) of ROIs associated with CV2 positive (Figure 3.3e).

			MNI Coordinates		
ROI Label	Full ROI Name	Network	x	y	z
CBL	Cerebellum	CBL	43.3	-55.2	-32.2
CBL	Cerebellum	CBL	17.2	-80.1	-28.7
LITG	Left Inferior Temporal Gyrus	Visual	-43.9	-52.7	-18.6
LPreCG	Left Precentral Gyrus	DAN	-43	0.8	47.6
LIC	Left Insular Cortex	VAN	-32.7	19.7	2
LSMG	Left Supramarginal Gyrus	VAN	-56.5	-43.3	26.5
RIC	Right Insular Cortex	VAN	36.7	17.2	3.6
RAmyg	Right Amygdala/Temporal Pole	SubC	30.9	5.8	-19
LSubC	Left Subcallosal Gyrus	SubC	0.7	-3.4	-8.7
LTFC	Left Temporal Fusiform Cortex	Limbic	-30.5	-5.1	-32.6
LMFG	Left Middle Frontal Gyrus	FPN	-44	26.5	26.6
LMTG	Left Middle Temporal Gyrus	DMN	-58.9	-30.2	-2.4
LAG	Left Angular Gyrus	DMN	-51.9	-50.2	42.1
LMFG	Left Middle Frontal Gyrus	DMN	-39.1	20.3	42.2
LFOC	Left Frontal Orbital Cortex	DMN	-44	33	-8.1
LIFG	Left Inferior Frontal Gyrus	DMN	-49.2	22.9	9.3
LSFG	Left Superior Frontal Gyrus	DMN	-8.6	19.9	60.4
RSFG	Right Superior Frontal Gyrus	DMN	13.5	21.7	59.8

Table A6. MNI coordinates (mm) of ROIs associated with CV2 negative (Figure 3.3f).

			MNI Coordinates		
ROI Label	Full ROI Name	Network	x	y	z
CBL	Cerebellum	CBL	-19.3	-62.1	-26.1
CBL	Cerebellum	CBL	-28.4	-40	-30.7
CBL	Cerebellum	CBL	-17.3	-81.3	-30.9
CBL	Cerebellum	CBL	35.7	-73	-30.6
LLOC	Left Lateral Occipital Cortex	Visual	-39.6	-85.4	1.4
LPostCG	Left Postcentral Gyrus	SMN	-8.8	-38	69.3
RPostCG	Right Postcentral Gyrus	SMN	12.3	-44.8	67.7
LCOC	Left Central Opercular Cortex	SMN	-46.7	5	2.8
RSMG	Right Supramarginal Gyrus	VAN	61.2	-31.4	26.6
RThal	Right Thalamus	SubC	1.6	-20.8	-7.6
LAmyg	Left Amygdala	SubC	-18.7	-7.4	-15.9
RCaud	Right Caudate	SubC	15.3	14.6	7
RThal	Right Thalamus	SubC	1.7	-4.4	5.3
LTFC	Left Temporal Fusiform Cortex	Limbic	-30.5	-5.1	-32.6
RSubC	Right Subcallosal Cortex	Limbic	0.1	20.4	-8
RCG	Right Cingulate Gyrus	DMN	1.6	-16.5	34.8
LFP	Left Frontal Pole	DMN	-9.2	62	14.2
RSTG	Right Superior Temporal Gyrus	DMN	58.4	-7.8	-7.8

Table A7. MNI coordinates (mm) of the nodes associated with subtype differences in Figure 3.6a.

			MNI Coordinates		
ROI Label	Full ROI Name	Network	x	y	z
LLOC	Left Lateral Occipital Cortex	Visual	-39.6	-85.4	1.4
LPut	Left Putamen/ Insular Cortex	VAN	-36.6	-13.9	-2.3
LPG	Left Paracingulate Gyrus	DMN	-6.8	45.7	7.8
CBL	Cerebellum	CBL	-19.3	-62.1	-26.1
CBL	Cerebellum	CBL	43.3	-55.2	-32.2
LMTG	Left Middle Temporal Gyrus	DMN	-58.9	-30.2	-2.4
RPG	Right Paracingulate Gyrus	VAN	2.8	12.4	49.4
RThal	Right Thalamus	SubC	11.6	-20	9.5
LIC	Left Insular Cortex	VAN	-32.7	19.7	2
LPostCG	Left Postcentral Gyrus	SMN	-8.8	-38	69.3
RCG	Right Cingulate Gyrus	DMN	6.7	42.6	6.1
LTFC	Left Temporal Fusiform Cortex	Limbic	-30.5	-5.1	-32.6
RPostCG	Right Postcentral Gyrus	SMN	30.4	-33.7	63.4
RCG	Right Cingulate Gyrus	DMN	1.6	-16.5	34.8
CBL	Cerebellum	CBL	2.9	-28	-36
LThal	Left Thalamus	SubC	-13.4	-32.3	0.8
RMFG	Right Middle Frontal Gyrus	FPN	42.4	23.8	37.6
RMTG	Right Middle Temporal Gyrus	FPN	62.9	-43	-7.8
RThal	Right Thalamus	SubC	18.5	-34.6	-1.8
LPrecCG	Left Precentral Gyrus	DAN	-28.2	-6.3	58
LCun	Left Cuneal Cortex	Visual	-5.4	-87.2	25
LAG	Left Angular Gyrus	DMN	-51.9	-50.2	42.1
LFOC	Left Frontal Orbital Cortex	Limbic	-28.4	31.1	-15.3
RIC	Right Insular Cortex	VAN	36.7	17.2	3.6
RPostCG	Right Postcentral Gyrus	SMN	43.3	-19.9	53.7
LMFG	Left Middle Frontal Gyrus	DMN	-39.1	20.3	42.2
LITG	Left Inferior Temporal Gyrus	Visual	-43.9	-52.7	-18.6
RPostCG	Right Postcentral Gyrus	SMN	12.3	-44.8	67.7
RThal	Right Thalamus	SubC	1.6	-20.8	-7.6

RFOC	Right Frontal Orbital Cortex	DMN	29.6	24.6	-15.1
LPreCG	Left Precentral Gyrus	DAN	-43	0.8	47.6
LFOC	Left Frontal Orbital Cortex	DMN	-44	33	-8.1
RFP	Right Frontal Pole	FPN	31.7	54.8	14.9
LCG	Left Cingulate Gyrus	FPN	-7.9	-33.1	45.5
CBL	Cerebellum	CBL	17.2	-80.1	-28.7
LTP	Left Temporal Pole	Limbic	-40.6	12.9	-28.2
RSFG	Right Superior Frontal Gyrus	DMN	0.3	51.6	26.5
LAmyg	Left Amygdala	SubC	-18.7	-7.4	-15.9
RCaud	Right Caudate	SubC	14.2	-0.5	17.5
LSFG	Left Superior Frontal Gyrus	FPN	-26	11.7	56.2
LPostCG	Left Postcentral Gyrus	SMN	-28.8	-35.9	62.4
RPreCG	Right Precentral Gyrus	SMN	60.1	-1.3	25
LMTG	Left Middle Temporal Gyrus	FPN	-58	-48.3	-8.1
RITG	Right Inferior Temporal Gyrus	Visual	48	-52.7	-16.7
CBL	Cerebellum	CBL	-28.4	-40	-30.7
LFP	Left Frontal Pole	DMN	-9.2	62	14.2
RAmyg	Right Amygdala/Temporal Pole	SubC	30.9	5.8	-19
RPrecCG	Right Precentral Gyrus	SMN	2.1	-23.6	68.5
RFP	Right Frontal Pole	FPN	42.9	49.6	-4.4
RPreCG	Right Precentral Gyrus	FPN	44.4	0.9	50
RPreCG	Right Precentral Gyrus	SMN	0.4	-15.1	51.8
LSub	Left Subcallosal Gyrus	SubC	0.7	-3.4	-8.7
RCaud	Right Caudate	SubC	15.3	14.6	7
LIFG	Left Inferior Frontal Gyrus	DMN	-49.2	22.9	9.3
RLOC	Right Lateral Occipital Cortex	DAN	53.5	-61.8	1
LCOC	Left Central Opercular Cortex	SMN	-56	-10.9	5.6
RThal	Right Thalamus	SubC	1.7	-4.4	5.3
RSFG	Right Superior Frontal Gyrus	FPN	-0.2	31.1	45.5
LMFG	Left Middle Frontal Gyrus	FPN	-44	26.5	26.6
RSTG	Right Superior Temporal Gyrus	DMN	58.4	-7.8	-7.8

LPostCG	Left Postcentral Gyrus	SMN	-51.2	-14.1	40.4
LPreCG	Left Precentral Gyrus	VAN	-54.1	7.2	18.2
LFP	Left Frontal Pole	DMN	-25.3	52	22.9
LFP	Left Frontal Pole	FPN	-40.9	48.7	-3.4
RTOFC	Right Temporal Occipital Fusiform Cortex	Visual	28.1	-49.1	-13
LSFG	Left Superior Frontal Gyrus	DMN	-8.6	19.9	60.4
RPcun	Right Precuneus Cortex	DMN	-0.7	-55.1	38.3
ROFG	Right Occipital Fusiform Gyrus	Visual	30.8	-87.5	-10.9
RPut	Right Putamen	SubC	27.2	0.8	-0.1
LLG	Left Lingual Gyrus	Visual	-13.3	-52.9	-0.7
RTP	Right Temporal Pole	DMN	45.7	13.3	-22.7
LCOC	Left Central Opercular Cortex	SMN	-46.7	5	2.8
RSFG	Right Superior Frontal Gyrus	DMN	13.5	21.7	59.8
RFP	Right Frontal Pole	DMN	15	56.3	29.4
CBL	Cerebellum	CBL	1	-30.8	-17.5
LPHG	Left Parahippocampal Gyrus	CBL	-15	-30.8	-18.3

Table A8. MNI coordinates (mm) of the nodes associated with subtype 1 in Figure 3.6b.

			MNI Coordinates		
ROI Label	Full ROI Name	Network	x	y	z
LPG	Left Paracingulate Gyrus	DMN	-6.8	45.7	7.8
CBL	Cerebellum	CBL	-19.3	-62.1	-26.1
CBL	Cerebellum	CBL	43.3	-55.2	-32.2
LMTG	Left Middle Temporal Gyrus	DMN	-58.9	-30.2	-2.4
LIC	Left Insular Cortex	VAN	-32.7	19.7	2
LPostCG	Left Postcentral Gyrus	SMN	-8.8	-38	69.3
CBL	Cerebellum	CBL	2.9	-28	-36
RMFG	Right Middle Frontal Gyrus	FPN	42.4	23.8	37.6
RMTG	Right Middle Temporal Gyrus	FPN	62.9	-43	-7.8
RThal	Right Thalamus	SubC	18.5	-34.6	-1.8
LCun	Left Cuneal Cortex	Visual	-5.4	-87.2	25
LAG	Left Angular Gyrus	DMN	-51.9	-50.2	42.1
LFOC	Left Frontal Orbital Cortex	Limbic	-28.4	31.1	-15.3
LITG	Left Inferior Temporal Gyrus	Visual	-43.9	-52.7	-18.6
RPostCG	Right Postcentral Gyrus	SMN	12.3	-44.8	67.7
LCG	Left Cingulate Gyrus	FPN	-7.9	-33.1	45.5
RSFG	Right Superior Frontal Gyrus	DMN	0.3	51.6	26.5
LAmyg	Left Amygdala	SubC	-18.7	-7.4	-15.9
RCaud	Right Caudate	SubC	14.2	-0.5	17.5
RITG	Right Inferior Temporal Gyrus	Visual	48	-52.7	-16.7
CBL	Cerebellum	CBL	-28.4	-40	-30.7
LFP	Left Frontal Pole	DMN	-9.2	62	14.2
RPrecCG	Right Precentral Gyrus	SMN	2.1	-23.6	68.5
LSub	Left Subcallosal Gyrus	SubC	0.7	-3.4	-8.7
LIFG	Left Inferior Frontal Gyrus	DMN	-49.2	22.9	9.3
RLOC	Right Lateral Occipital Cortex	DAN	53.5	-61.8	1
LCOC	Left Central Opercular Cortex	SMN	-56	-10.9	5.6
LMFG	Left Middle Frontal Gyrus	FPN	-44	26.5	26.6
LFP	Left Frontal Pole	DMN	-25.3	52	22.9
LSFG	Left Superior Frontal Gyrus	DMN	-8.6	19.9	60.4

RPcun	Right Precuneus Cortex	DMN	-0.7	-55.1	38.3
ROFG	Right Occipital Fusiform Gyrus	Visual	30.8	-87.5	-10.9
RPut	Right Putamen	SubC	27.2	0.8	-0.1
LLG	Left Lingual Gyrus	Visual	-13.3	-52.9	-0.7
RTP	Right Temporal Pole	DMN	45.7	13.3	-22.7
LCOC	Left Central Opercular Cortex	SMN	-46.7	5	2.8
CBL	Cerebellum	CBL	1	-30.8	-17.5
LPHG	Left Parahippocampal Gyrus	CBL	-15	-30.8	-18.3

Table A9. MNI coordinates (mm) of the nodes associated with subtype 2 in Figure 3.6c.

			MNI Coordinates		
ROI Label	Full ROI Name	Network	x	y	z
LLOC	Left Lateral Occipital Cortex	Visual	-39.6	-85.4	1.4
LPut	Left Putamen/Insular Cortex	VAN	-36.6	-13.9	-2.3
LPG	Left Paracingulate Gyrus	DMN	-6.8	45.7	7.8
CBL	Cerebellum	CBL	-19.3	-62.1	-26.1
CBL	Cerebellum	CBL	43.3	-55.2	-32.2
LMTG	Left Middle Temporal Gyrus	DMN	-58.9	-30.2	-2.4
RPG	Right Paracingulate Gyrus	VAN	2.8	12.4	49.4
RThal	Right Thalamus	SubC	11.6	-20	9.5
LIC	Left Insular Cortex	VAN	-32.7	19.7	2
LPostCG	Left Postcentral Gyrus	SMN	-8.8	-38	69.3
RCG	Right Cingulate Gyrus	DMN	6.7	42.6	6.1
LTFC	Left Temporal Fusiform Cortex	Limbic	-30.5	-5.1	-32.6
RPostCG	Right Postcentral Gyrus	SMN	30.4	-33.7	63.4
RCG	Right Cingulate Gyrus	DMN	1.6	-16.5	34.8
CBL	Cerebellum	CBL	2.9	-28	-36
RSPL	Right Superior Parietal Lobule	DAN	29.7	-54.6	59.7
LThal	Left Thalamus	SubC	-13.4	-32.3	0.8
RMFG	Right Middle Frontal Gyrus	FPN	42.4	23.8	37.6
RMTG	Right Middle Temporal Gyrus	FPN	62.9	-43	-7.8
LPrecCG	Left Precentral Gyrus	DAN	-28.2	-6.3	58
LAG	Left Angular Gyrus	DMN	-51.9	-50.2	42.1
LFOC	Left Frontal Orbital Cortex	Limbic	-28.4	31.1	-15.3
RIC	Right Insular Cortex	VAN	36.7	17.2	3.6
RPostCG	Right Postcentral Gyrus	SMN	43.3	-19.9	53.7
LMFG	Left Middle Frontal Gyrus	DMN	-39.1	20.3	42.2
LITG	Left Inferior Temporal Gyrus	Visual	-43.9	-52.7	-18.6
RThal	Right Thalamus	SubC	1.6	-20.8	-7.6
RFOC	Right Frontal Orbital Cortex	DMN	29.6	24.6	-15.1
LPreCG	Left Precentral Gyrus	DAN	-43	0.8	47.6
LFOC	Left Frontal Orbital Cortex	DMN	-44	33	-8.1
RFP	Right Frontal Pole	FPN	31.7	54.8	14.9
LCG	Left Cingulate Gyrus	FPN	-7.9	-33.1	45.5
CBL	Cerebellum	CBL	17.2	-80.1	-28.7
LTP	Left Temporal Pole	Limbic	-40.6	12.9	-28.2
LAmyg	Left Amygdala	SubC	-18.7	-7.4	-15.9

LSFG	Left Superior Frontal Gyrus	FPN	-26	11.7	56.2
LPostCG	Left Postcentral Gyrus	SMN	-28.8	-35.9	62.4
RPreCG	Right Precentral Gyrus	SMN	60.1	-1.3	25
LMTG	Left Middle Temporal Gyrus	FPN	-58	-48.3	-8.1
RITG	Right Inferior Temporal Gyrus	Visual	48	-52.7	-16.7
LFP	Left Frontal Pole	DMN	-9.2	62	14.2
RAmyg	Right Amygdala/Temporal Pole	SubC	30.9	5.8	-19
RPreCG	Right Precentral Gyrus	SMN	2.1	-23.6	68.5
RFP	Right Frontal Pole	FPN	42.9	49.6	-4.4
RPreCG	Right Precentral Gyrus	FPN	44.4	0.9	50
RCOC	Right Central Opercular Cortex	VAN	55.8	3.8	5.8
RPreCG	Right Precentral Gyrus	SMN	0.4	-15.1	51.8
LSub	Left Subcallosal Gyrus	SubC	0.7	-3.4	-8.7
RPreCG	Right Precentral Gyrus	SMN	24.6	-13.5	67
RCaud	Right Caudate	SubC	15.3	14.6	7
RIC	Right Insular Cortex	VAN	40.7	-11.3	-3.9
LIFG	Left Inferior Frontal Gyrus	DMN	-49.2	22.9	9.3
RLOC	Right Lateral Occipital Cortex	DAN	53.5	-61.8	1
LCOC	Left Central Opercular Cortex	SMN	-56	-10.9	5.6
RThal	Right Thalamus	SubC	1.7	-4.4	5.3
RSFG	Right Superior Frontal Gyrus	FPN	-0.2	31.1	45.5
CBL	Cerebellum	CBL	1.7	-56.9	-12.7
RSTG	Right Superior Temporal Gyrus	DMN	58.4	-7.8	-7.8
LPostCG	Left Postcentral Gyrus	SMN	-51.2	-14.1	40.4
LPreCG	Left Precentral Gyrus	VAN	-54.1	7.2	18.2
LFP	Left Frontal Pole	DMN	-25.3	52	22.9
LFP	Left Frontal Pole	FPN	-40.9	48.7	-3.4
RTOFC	Right Temporal Occipital Fusiform Cortex	Visual	28.1	-49.1	-13
ROFG	Right Occipital Fusiform Gyrus	Visual	30.8	-87.5	-10.9
RPut	Right Putamen	SubC	27.2	0.8	-0.1
LLG	Left Lingual Gyrus	Visual	-13.3	-52.9	-0.7
RTP	Right Temporal Pole	DMN	45.7	13.3	-22.7
LCOC	Left Central Opercular Cortex	SMN	-46.7	5	2.8
RSFG	Right Superior Frontal Gyrus	DMN	13.5	21.7	59.8
RFP	Right Frontal Pole	DMN	15	56.3	29.4

CBL	Cerebellum	CBL	1	-30.8	-17.5
LPHG	Left Parahippocampal Gyrus	CBL	-15	-30.8	-18.3

Table A10. MNI coordinates (mm) of the nodes associated with subtype 3 in Figure 3.6d.

			MNI Coordinates		
ROI Label	Full ROI Name	Network	x	y	z
LLOC	Left Lateral Occipital Cortex	Visual	-39.6	-85.4	1.4
LPG	Left Paracingulate Gyrus	DMN	-6.8	45.7	7.8
RPG	Right Paracingulate Gyrus	VAN	2.8	12.4	49.4
RCG	Right Cingulate Gyrus	DMN	6.7	42.6	6.1
LTFC	Left Temporal Fusiform Cortex	Limbic	-30.5	-5.1	-32.6
RCG	Right Cingulate Gyrus	DMN	1.6	-16.5	34.8
RFOC	Right Frontal Orbital Cortex	DMN	29.6	24.6	-15.1
LPreCG	Left Precentral Gyrus	DAN	-43	0.8	47.6
LFOC	Left Frontal Orbital Cortex	DMN	-44	33	-8.1
RFP	Right Frontal Pole	FPN	31.7	54.8	14.9
CBL	Cerebellum	CBL	17.2	-80.1	-28.7
RSFG	Right Superior Frontal Gyrus	DMN	0.3	51.6	26.5
RFP	Right Frontal Pole	FPN	42.9	49.6	-4.4
LSub	Left Subcallosal Gyrus	SubC	0.7	-3.4	-8.7
RCaud	Right Caudate	SubC	15.3	14.6	7
LIFG	Left Inferior Frontal Gyrus	DMN	-49.2	22.9	9.3
RThal	Right Thalamus	SubC	1.7	-4.4	5.3
RSFG	Right Superior Frontal Gyrus	FPN	-0.2	31.1	45.5
LMFG	Left Middle Frontal Gyrus	FPN	-44	26.5	26.6
RSTG	Right Superior Temporal Gyrus	DMN	58.4	-7.8	-7.8
LPreCG	Left Precentral Gyrus	VAN	-54.1	7.2	18.2
LSFG	Left Superior Frontal Gyrus	DMN	-8.6	19.9	60.4
RFP	Right Frontal Pole	DMN	15	56.3	29.4

Table A11. Kruskal-Wallis ANVOA, χ^2, and effect sizes for ROI pairs that were significant after Bonferroni post-hoc test ($P < 0.0007$) (Figure 3.7a).

ROI Pair	Test Statistic (χ^2)	Effect Size (η^2)	Subtypes Implicated
CBL - LAG	45.7	0.21	1-2
LMTG - LITG	56.8	0.26	1-2
RPG – RFP	-38.7	-0.20	2-3
LIC – RMFG	-38.1	-0.19	2-3
	50.2	0.23	1-2
LIC – LMFG	-39.9	-0.20	2-3
LIC – RPreCG	-42.3	-0.21	2-3
	45.9	0.21	1-2
RCG – RCaud	43.4	0.20	2-3
RMTG – LIFG	45.4	0.21	1-2
LFOC – LFP	52.3	0.24	1-2
LCG – RLOC	48.0	0.22	1-2
RSFG – LSub	43.7	0.20	1-3
LAmyg – ROFG	52.0	0.24	1-2
RSTG – RSTG	41.7	0.19	2-3
LFP - CBL	53.8	0.25	1-2

Abbreviations: Cerebellum (CBL), Left Angular Gyrus (LAG), Right/Left Middle Temporal Gyrus (R/L MTG), Left Inferior Temporal Gyrus (LITG), Right Paracingulate Gyrus (LPG), Left Insular Cortex (LIC), Right/Left Middle Frontal Gyrus (R/L MFG), Right Precentral Gyrus (RPreCG), Right/Left Cingulate Gyrus (R/L CG), Right Caudate (RCaud), Left Inferior Frontal Gyrus (LIFG), Left Frontal Pole (LFP), Right Superior Frontal Gyrus (RSFG), Left Subcallosal Gyrus (LSub), Left Amygdala (LAmyg), Right Superior Temporal Gyrus (RSTG), Right Lateral Occipital Cortex (RLOC), Left Frontal Orbital Cortex (LFOC), Right Occipital Fusiform Gyrus (ROFG).

Table A12. MNI coordinates (mm) of ROIs associated with the FC features in Figure 3.7a and Table A11.

		MNI Coordinates		
ROI	Network	x	y	z
CBL	CBL	43.3	-55.2	-32.2
LMTG	DMN	-58.9	-30.2	-2.4
RPG	VAN	2.8	12.4	49.4
LIC	VAN	-32.7	19.7	2.0
RCG	DMN	1.6	-16.5	34.8
RMFG	FPN	42.4	23.8	37.6
RMTG	FPN	62.9	-43	-7.8
LAG	DMN	-51.9	-50.2	42.1
LFOC	Limbic	-28.4	31.1	-15.3
LMFG	DMN	-39.1	20.3	42.2
LITG	Visual	-43.9	-52.7	-18.6
LCG	FPN	-7.9	-33.1	45.5
RSFG	DMN	0.3	51.6	26.5
LAmyg	SubC	-18.7	-7.4	-15.9
LFP	DMN	-9.2	62	14.2
RFP	FPN	42.9	49.6	-4.4
RPreCG	FPN	44.4	0.9	50.0
LSub	SubC	0.7	-3.4	-8.7
RCaud	SubC	15.3	14.6	7.0
LIFG	DMN	-49.2	22.9	9.3
RLOC	DAN	53.5	-61.8	1.0
RThal	SubC	1.7	-4.4	5.3
RSTG	DMN	58.4	-7.8	-7.8
LFP	DMN	-25.3	52	22.9
ROFG	Visual	30.8	-87.5	-10.9
CBL	CBL	1.0	-30.8	-17.5

Table A13. Wilcoxon rank sum test z-value and effect sizes for FC features that were significant after Bonferroni post-hoc test ($P < 0.0007$) for subtype 1 (Figure 3.7b).

ROI Pair	**z-value**	**Effect size (r)**
LMTG – LITG	3.67	0.25
RThal - CBL	3.47	0.24
RPostCG - CBL	3.79	0.26
LCG - RLOC	3.92	0.27
RSFG - LSub	3.47	0.24
LAmyg - ROFG	4.03	0.28

Abbreviations: Left Middle Temporal Gyrus (LMTG), Left Inferior Temporal Gyrus (LITG), Right Thalamus (RThal), Cerebellum (CBL), Right Postcentral Gyrus (RPostCG), Left Cingulate Gyrus (LCG), Right Lateral Occipital Cortex (RLOC), Right Superior Frontal Gyrus (RSFG), Left Subcallosal Gyrus (LSub), Left Amygdala (LAmyg), Right Occipital Fusiform Gyrus (ROFG).

Table A14. MNI coordinates (mm) of ROIs associated with the FC features in Figure 3.7b and Table A13.

		MNI Coordinates		
ROI	Network	x	y	z
LMTG	DMN	-58.9	-30.2	-2.4
RThal	SubC	18.5	-34.6	-1.8
LITG	Visual	-43.9	-52.7	-18.6
RPostCG	SMN	12.3	-44.8	67.7
LCG	FPN	-7.9	-33.1	45.5
RSFG	DMN	0.3	51.6	26.5
LAmyg	SubC	-18.7	-7.4	-15.9
CBL	CBL	-28.4	-40	-30.7
LSub	SubC	0.7	-3.4	-8.7
RLOC	SMN	53.5	-61.8	1.0
ROFG	Visual	30.8	-87.5	-10.9

Table A15. Wilcoxon rank sum test z-value and effect sizes for ROI pairs that were significant after Bonferroni post-hoc test ($P < 0.0007$) for subtype 2 (Figure 3.7c).

ROI Pair	z-value	Effect Size (r)
LLOC – LTFC	-3.54	-0.24
LPut – RAmyg	-3.77	-0.26
CBL – LAG	-3.42	-0.24
LMTG – LPreCG	-3.49	-0.24
LMTG – LITG	-3.99	-0.28
RPG – RFP	-3.58	-0.25
LIC – RMFG	-4.38	-0.30
LIC – LMFG	-4.29	-0.30
LIC – PreCG	-4.54	-0.31
RCG – RFOC	-3.42	-0.24
RCG – RCaud	4.40	0.30
LFOC – LFP	-3.78	-0.26
LFOC – LIFG	-3.58	-0.25
RIC – RAmyg	-3.57	-0.25
LPreCG – LIFG	-3.44	-0.24
LFOC – CBL	-3.51	-0.24
LSFG – LFP	-3.57	-0.25
LPostCG – RTOFC	-3.85	-0.25
LFP – CBL	-3.88	-0.27
LFP - CBL	-3.77	-0.26

Abbreviations: Left Lateral Occipital Cortex (LLOC), Left Temporal Fusiform Cortex (LTFC), Left Putamen (LPut), Right Amygdala (RAmyg), Cerebellum (CBL), Left Angular Gyrus (LAG), Left Middle Temporal Gyrus (LMTG), Left Precentral Gyrus (LPreCG), Left Inferior Temporal Gyrus (LITG), Right Paracingulate Gyrus (RPG), Right/Left Frontal Pole (R/L FP), Right/Left Insular Cortex (R/L IC), Right/Left Middle Frontal Gyrus (L/R MFG), Right Cingulate Gyrus (RCG), Right/Left Frontal Orbital Cortex (R/L FOC), Right Caudate (RCaud), Left Inferior Frontal Gyrus (LIFG), Left Superior Frontal Gyrus (LSFG), Left Postcentral Gyrus (LPostCG), Right Temporal Fusiform Occipital Cortex (RTFOC).

Table A16. MNI coordinates (mm) of ROIs associated with the FC features in Figure 3.7c and Table A15.

		MNI Coordinates		
ROI	Network	x	y	z
LLOC	Visual	-39.6	-85.4	1.4
LPut	VAN	-36.6	-13.9	-2.3
CBL	CBL	43.3	-55.2	-32.2
LMTG	DMN	-58.9	-30.2	-2.4
RPG	VAN	2.8	12.4	49.4
LIC	VAN	-32.7	19.7	2.0
RCG	DMN	6.7	42.6	6.1
LTFC	Limbic	-30.5	-5.1	-32.6
RCG	DMN	1.6	-16.5	34.8
RMFG	FPN	42.4	23.8	37.6
LPreCG	DAN	-28.2	-6.3	58.0
LAG	DMN	-51.9	-50.2	42.1
LFOC	Limbic	-28.4	31.1	-15.3
RIC	VAN	36.7	17.2	3.6
LMFG	DMN	-39.1	20.3	42.2
LITG	Visual	-43.9	-52.7	-18.6
RFOC	DMN	29.6	24.6	-15.1
LPreCG	DAN	-43.0	0.8	47.6
LFOC	DMN	-44.0	33	-8.1
CBL	CBL	17.2	-80.1	-28.7
LSFG	FPN	-26.0	11.7	56.2
LPostCG	SMN	-28.8	-35.9	62.4
LFP	DMN	-9.2	62	14.2
RAmyg	SubC	30.9	5.8	-19.0
RFP	FPN	42.9	49.6	-4.4
RPreCG	FPN	44.4	0.9	50.0
RCaud	SubC	15.3	14.6	7.0
LIFG	DMN	-49.2	22.9	9.3
LFP	DMN	-25.3	52	22.9
LFP	FPN	-40.9	48.7	-3.4
RTOFC	Visual	28.1	-49.1	-13.0

Table A17. Wilcoxon rank sum test z-value and effect sizes for ROI pairs that were significant after Bonferroni post-hoc test ($P < 0.0007$) for subtype 3 (Figure 3.7d).

ROI pair	**z-value**	**Effect size (r)**
RFP – RFP	-3.53	-0.24
RSFG – LSub	-4.06	-0.28
LSub – LSFG	-3.48	-0.24
RThal - RSTG	-4.58	-0.32

Abbreviations: Right Frontal Pole (RFP), Right/Left Superior Frontal Gyrus (R/L SFG), Left Subcallosal Gyrus (LSub), Right Thalamus (RThal), Right Superior Temporal Gyrus (RSTG).

Table A18. MNI coordinates (mm) of ROIs associated with the FC features in Figure 3.7d and Table A17.

		MNI Coordinates		
ROI	Network	x	y	z
RFP	FPN	31.7	54.8	14.9
RSFG	DMN	0.3	51.6	26.5
LSub	SubC	0.7	-3.4	-8.7
RThal	SubC	1.7	-4.4	5.3
RSTG	DMN	58.4	-7.8	-7.8
LSFG	DMN	-8.6	19.9	60.4
RFP	DMN	15.0	56.3	29.4